

SUPPORTING INFORMATION for:

[Ir(COD)Cl]₂ as a Catalyst Precursor for the Intramolecular Hydroamination of Unactivated Alkenes with Primary Amines and Secondary Alkyl- or Arylamines: A Combined Catalytic, Mechanistic, and Computational Investigation

Kevin D. Hesp,^a Sven Tobisch,^{*,b} and Mark Stradiotto^{*,a}

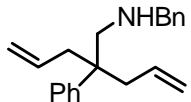
^aDalhousie University, Department of Chemistry, Halifax, Nova Scotia B3H 4J3 (Canada).

^bUniversity of St Andrews, School of Chemistry, St Andrews, KY16 9ST (UK).

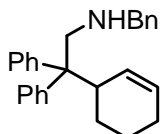
Contents of experimental section:

- 1. Synthetic Details and Characterization Data**
- 2. Catalyst Optimization and Kinetic Experiments**
- 3. Computational Analysis, Details, and Tabulated Data**
- 4. NMR Spectra for Isolated Compounds**

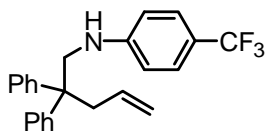
1. Synthetic Details and Characterization Data



Preparation of *N*-Benzyl-2-Phenyl-2-(2-propenyl)-1-amino-4-pentene. The indicated compound was obtained in 80 % yield as a colorless oil by using the same procedure as was used for the preparation of *N*-benzyl-2,2-diphenylpent-4-en-1-amine.¹ The compound was purified by flash column chromatography on silica gel (hexane:ethyl acetate = 10:1). ¹H NMR (CDCl₃): δ 7.45-7.27 (m, 10H), 5.70 (m, 2H), 5.18-5.07 (m, 4H), 3.81 (s, 2H), 2.92 (s, 2H), 2.72-2.65 (m, 2H), 2.62-2.55 (m, 2H), 1.17 (s, 1H); ¹³C{¹H} NMR (CDCl₃): δ 144.9, 140.7, 134.6, 128.2, 128.1, 127.9, 126.8, 126.7, 125.9, 117.4, 55.9, 54.3, 44.9, 40.3. HRMS (ESI/[M+H]⁺) calcd. for C₂₁H₂₆N: 292.2060. Found: 292.2053.

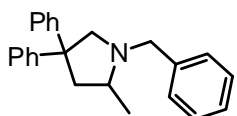


Preparation of *N*-Benzyl-2,2-diphenyl-2-cyclohex-3-en-1-amine. The indicated compound was obtained in 95 % yield as a colorless oil by using the same procedure as was used for the preparation of *N*-benzyl-2,2-diphenylpent-4-en-1-amine.¹ The compound was purified by flash column chromatography on silica gel (hexane:ethyl acetate = 20:1). ¹H NMR (CDCl₃): δ 7.37-7.20 (m, 15H), 5.90 (m, 1H), 5.67 (m, 1H), 3.80-3.71 (m, 2H), 3.55 (m, 1H), 3.32 (m, 1H), 3.25 (m, 1H), 1.93 (m, 1H), 1.85-1.68 (m, 2H), 1.65-1.56 (m, 2H), 1.17-0.82 (m, 2H); ¹³C{¹H} NMR (CDCl₃): δ 145.2, 143.5, 140.6, 129.6, 129.5, 129.4, 128.5, 128.1, 127.8, 127.7, 127.0, 126.7, 125.9, 125.8, 56.2, 54.9, 54.0, 39.4, 25.0, 24.7, 22.4. HRMS (ESI/[M+H]⁺) calcd. for C₂₇H₂₉N: 368.2373. Found: 368.2380.

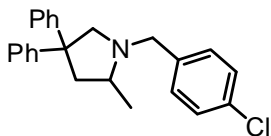


Preparation of *N*-(4-Trifluoromethylphenyl)-2,2-diphenylpent-4-en-1-amine. [Pd(cinnamyl)Cl]₂ (4.1 mg, 0.008 mmol) and 2-(di-*tert*-butylphosphino)-*N,N*-dimethylaniline (8.3 mg, 0.031 mmol) were mixed in 4.200 mL toluene for 10 minutes. From this stock solution, 2.000 mL was added to a vial containing NaOtBu (173 mg, 1.8 mmol), followed by the addition of 2,2-diphenylpent-4-en-1-amine (380 mg, 1.58 mmol), 1.5 mmol of *p*-bromo-trifluoromethylbenzene and 1 mL of additional toluene. The vial was sealed with a cap containing a PTFE septum, heated at 110 °C and the reaction was periodically monitored by TLC. Upon completion of the reaction, products were purified by column chromatography on silica gel (hexanes:EtOAc = 20:1) as a colorless oil that solidified as a white solid upon standing (0.17 g, 0.44 mmol, 75 %). ¹H NMR (CDCl₃): δ 7.44-7.35 (m,

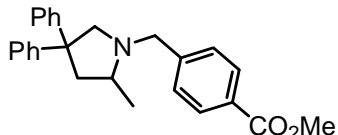
6H), 7.34-7.26 (m, 6H), 6.59 (d, J = 10.0 Hz, 2H), 5.43 (m, 1H), 5.09-5.02 (m, 2H), 3.82 (s, 2H), 3.63 (br s, 1H), 3.05 (d, J = 10.0 Hz, 2H); $^{13}\text{C}\{\text{H}\}$ NMR (CDCl_3): δ 150.7, 145.3, 134.0, 128.4, 127.9, 126.6, 126.5, 126.4, 118.7, 112.1, 50.0, 49.6, 42.1. HRMS (ESI/[M+H] $^+$) calcd. for $\text{C}_{24}\text{H}_{23}\text{F}_3\text{N}$: 382.1777. Found: 382.1746.



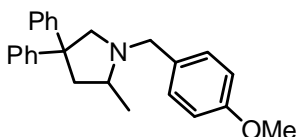
1-Benzyl-2-methyl-4,4-diphenylpyrrolidine. The indicated compound was purified by flash chromatography on silica gel (hexanes:EtOAc = 20:1) in a 88 % yield (72 mg) as a white solid.¹ ^1H NMR (CDCl_3): 7.53-7.19 (m, 15H), 4.21 (d, J = 13.5 Hz, 1H), 3.77 (d, J = 9.5 Hz, 1H), 3.38 (d, J = 13.5 Hz, 1H), 3.07-2.89 (m, 3H), 2.34 (d of d, J = 13.0, 8.0 Hz, 1H), 1.29 (d, J = 6.5 Hz, 3H); $^{13}\text{C}\{\text{H}\}$ NMR (CDCl_3): 150.6, 148.7, 140.1, 128.6, 128.2, 128.1, 127.8, 127.4, 127.2, 126.7, 125.8, 125.4, 66.4, 59.6, 58.0, 52.5, 48.0, 19.5.



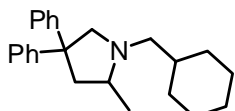
1-(4-Chlorobenzyl)-2-methyl-4,4-diphenylpyrrolidine. The indicated compound was purified by flash chromatography on silica gel (pentane:Et₂O = 30:1) in an 85 % yield (77 mg) as a white solid.² ^1H NMR (CDCl_3): δ 7.43-7.17 (m, 14H), 4.12 (d, J = 13.5 Hz, 1H), 3.71 (d, J = 10.0 Hz, 1H), 3.33 (d, J = 13.5 Hz, 1H), 3.05-2.89 (m, 2H), 2.87 (d, J = 9.5 Hz, 1H), 2.33 (d of d, J = 12.5, 7.9 Hz, 1H), 1.26 (d, J = 6.5 Hz, 3H); $^{13}\text{C}\{\text{H}\}$ NMR (CDCl_3): δ 150.4, 148.6, 138.6, 132.4, 129.8, 128.3, 128.1, 127.8, 127.3, 127.1, 125.8, 125.5, 66.3, 59.6, 57.2, 52.5, 47.8, 19.5.



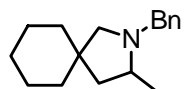
Methyl 4-(2-methyl-4,4-diphenylpyrrolidin-1-ylmethyl)-benzoate. The indicated compound was purified by flash chromatography on silica gel (pentane:Et₂O = 8:1) in a 87 % yield (84 mg) as a colorless oil.¹ ^1H NMR (CDCl_3): δ 8.07 (d, J = 8.0 Hz, 2H), 7.50 (d, J = 8.5 Hz, 2H), 7.35-7.15 (m, 10H), 4.16 (d, J = 14.0 Hz, 1H), 3.98 (s, 3H), 3.68 (d, J = 10.0 Hz, 1H), 3.39 (d, J = 13.5 Hz, 1H), 3.02-2.88 (m, 2H), 2.86 (d, J = 10.0 Hz, 1H), 2.31 (d of d, J = 13.0, 7.5 Hz, 1H), 1.23 (d, J = 5.5 Hz, 3H); $^{13}\text{C}\{\text{H}\}$ NMR (CDCl_3): δ 167.1, 150.3, 148.5, 145.7, 129.6, 128.7, 128.4, 128.1, 127.8, 127.3, 127.1, 125.8, 125.5, 66.4, 59.7, 57.7, 52.6, 51.9, 47.8, 19.5.



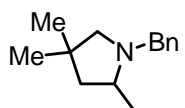
1-(4-Methoxybenzyl)-2-methyl-4,4-diphenylpyrrolidine. The indicated compound was purified by flash chromatography on silica gel (pentane:Et₂O = 15:1) in a 89 % yield (80 mg) as a colorless oil.² ¹H NMR (CDCl₃): δ 7.29 (m, 1H), 7.00-6.95 (m, 2H), 4.13 (d, *J* = 13.0 Hz, 1H), 3.90 (s, 3H), 3.74 (d, *J* = 10.0 Hz, 1H), 3.30 (d, *J* = 13.0 Hz, 1H), 3.02 (d of d, *J* = 13.0, 7.5 Hz, 1H), 2.96-2.85 (m, 2H), 2.30 (d of d, *J* = 13.0, 7.5 Hz, 1H), 1.27 (d, *J* = 6.0 Hz, 3H); ¹³C{¹H} NMR (CDCl₃): δ 158.5, 150.6, 148.7, 132.0, 129.6, 128.1, 127.8, 127.4, 127.2, 125.7, 125.3, 113.5, 66.3, 59.5, 57.2, 55.2, 52.4, 48.0, 19.5.



1-Cyclohexylmethyl-2-methyl-4,4-diphenylpyrrolidine. The indicated compound was purified by flash chromatography on silica gel (hexanes:EtOAc = 8:1) in a 88 % yield (73 mg) as a white solid.³ ¹H NMR (CDCl₃): 7.38-7.21 (m, 9H), 7.16 (m, 1H), 3.87 (d, *J* = 9.5 Hz, 1H), 2.87 (d of d, *J* = 13.0, 7.5 Hz, 1H), 2.82 (d, *J* = 10.0 Hz, 1H), 2.66 (m, 1H), 2.56 (m, 1H), 2.18-2.03 (m, 3H), 1.82-1.63 (m, 4H), 1.53 (m, 1H), 1.36-1.15 (m, 3H), 1.10 (d, *J* = 6.0 Hz, 3H), 1.02-0.87 (m, 2H); ¹³C{¹H} NMR (CDCl₃): δ 151.3, 148.9, 128.1, 127.8, 127.6, 127.3, 125.7, 125.4, 67.6, 61.4, 60.3, 52.8, 48.1, 37.3, 32.2, 31.9, 26.9, 26.3, 26.1, 19.6.

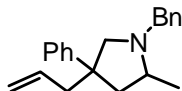


2-Benzyl-3-methyl-2-aza-spiro[4,5]decane. The indicated compound was purified by flash chromatography on silica gel (hexanes:EtOAc = 20:1) in a 86 % yield (52 mg) as a colorless oil.¹ ¹H NMR (CDCl₃): δ 7.40-7.24 (m, 5H), 4.06 (d, *J* = 13.0 Hz, 1H), 3.14 (d, *J* = 13.5 Hz, 1H), 2.82 (d, *J* = 9.5 Hz, 1H), 2.54 (m, 1H), 1.91 (d, *J* = 9.5 Hz, 1H), 1.80 (d of d, *J* = 12.0, 7.0 Hz, 1H), 1.56-1.27 (m, 11H), 1.19 (d, *J* = 6.0 Hz, 3H); ¹³C{¹H} NMR (CDCl₃): δ 140.0, 128.6, 128.0, 126.5, 66.6, 59.0, 58.0, 47.0, 39.3, 39.2, 38.5, 26.1, 23.6, 23.5, 19.3.

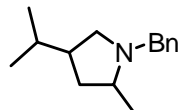


1-Benzyl-2,4,4-trimethylpyrrolidine. The indicated compound was purified by flash chromatography on silica gel (hexanes:EtOAc = 20:1) in a 84 % yield (42 mg) as a colorless oil.¹ ¹H NMR (CDCl₃): δ 7.39-7.23 (m, 5H), 4.05 (d, *J* = 14.5 Hz, 1H), 3.15 (d, *J* = 13.5 Hz, 1H), 2.67 (d, *J* = 9.0 Hz, 1H), 2.59 (m, 1H), 1.98 (d, *J* = 9.0 Hz, 1H), 1.76 (d of d, *J* = 12.0, 7.5 Hz, 1H), 1.35 (d of d, *J* = 12.5, 9.0 Hz, 1H), 1.19 (d, *J* = 6.0 Hz, 3H), 1.11 (s,

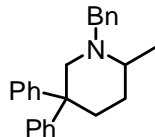
3H), 1.01 (s, 3H); $^{13}\text{C}\{\text{H}\}$ NMR (CDCl_3): δ 140.1, 128.7, 128.0, 126.5, 68.4, 59.7, 58.0, 49.1, 35.4, 30.9, 29.2, 19.4.



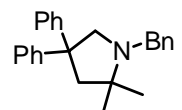
1-Benzyl-4-Allyl-2-methyl-4-phenyl-pyrrolidine. The indicated compound was purified by flash chromatography on silica gel (hexanes:EtOAc = 10:1) in a 86 % yield (67 mg) as a colorless oil. The diastereomeric ratio was determined to be 1.7:1 on the basis of ^1H NMR integration of the crude product mixture prior to purification; the spectra provided correspond to the major diastereomer with minor impurities of the other diastereomer. ^1H NMR (CDCl_3): δ 7.51-7.38 (m, 4H), 7.36-7.30 (m, 3H), 7.26-7.15 (m, 3H), 5.48 (m, 1H), 5.02-4.94 (m, 2H), 4.17 (d, J = 13.4 Hz, 1H), 3.25 (d of d, J = 13.1, 9.1 Hz, 2H), 2.74-2.65 (m, 2H), 2.61-2.53 (m, 1H), 2.51-2.42 (m, 2H), 1.91 (d of d, J = 12.5, 7.7 Hz, 1H), 1.34 (d, J = 6.0 Hz, 3H); $^{13}\text{C}\{\text{H}\}$ NMR (CDCl_3): δ 148.0, 140.2, 135.5, 128.4, 128.1, 127.9, 126.8, 126.6, 125.5, 117.1, 63.9, 59.4, 57.8, 48.5, 47.4, 45.2, 20.2. HRMS (ESI/[M+H] $^+$) calcd. for $\text{C}_{21}\text{H}_{26}\text{N}$: 292.2060. Found: 292.2046.



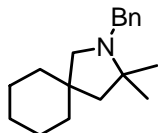
1-Benzyl-2-methyl-4-isopropylpyrrolidine. The indicated compound was obtained in 81 % yield with a diastereomeric ratio of 1.5:1 on the basis of ^1H NMR using 1,4-bis(trifluoromethyl)benzene as an internal standard.¹



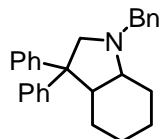
1-Benzyl-2-methyl-5,5-diphenylpiperidine. The indicated compound was purified by flash chromatography on silica gel (hexanes:EtOAc = 20:1) in a 72 % yield (62 mg) as a colorless oil.³ ^1H NMR (CDCl_3): δ 7.46-7.14 (m, 15H), 4.13 (d, J = 13.5 Hz, 1H), 3.43 (d, J = 12.5 Hz, 1H), 3.21 (d, J = 13.5 Hz, 1H), 3.60-2.50 (m, 3H), 2.25 (m, 1H), 1.70 (m, 1H), 1.45 (m, 1H), 1.21 (d, J = 6.0 Hz, 3H); $^{13}\text{C}\{\text{H}\}$ NMR (CDCl_3): δ 148.6, 146.7, 139.4, 129.5, 128.4, 128.0, 127.9, 127.6, 127.0, 126.9, 125.6, 125.3, 61.0, 58.9, 56.1, 46.5, 34.2, 31.0, 18.6.



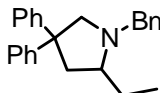
1-Benzyl-2-2-dimethyl-4,4-diphenylpyrrolidine. The indicated compound was purified by flash chromatography on silica gel (hexanes:EtOAc = 20:1) in a 88 % yield (75 mg) as a white solid.⁴ ^1H NMR (CDCl_3): δ 7.52-7.20 (m, 15H), 3.73 (s, 2H), 3.41 (s, 2H), 2.74 (s, 2H), 1.26 (s, 6H); $^{13}\text{C}\{\text{H}\}$ NMR (CDCl_3): δ 149.7, 140.9, 128.5, 128.1, 127.8, 127.2, 126.7, 125.4, 6.1, 60.4, 54.4, 52.4, 51.6, 25.1.



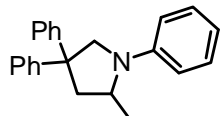
2-benzyl-3,3-dimethyl-2-azaspiro[4.5]decane. The indicated compound was purified by flash chromatography on silica gel (hexanes:EtOAc = 10:1) in a 74 % yield (48 mg) as a pale yellow oil. ^1H NMR (CDCl_3): δ 7.47-7.20 (m, 5H), 3.56 (s, 2H), 2.46 (s, 2H), 1.60 (m, 10H), 1.14 (s, 6H); $^{13}\text{C}\{\text{H}\}$ NMR (CDCl_3): δ 141.6, 128.0, 127.9, 126.3, 62.7, 59.9, 53.7, 52.1, 39.1, 29.7, 26.0, 24.7, 23.7.



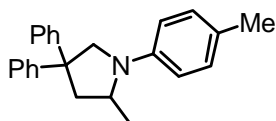
3,3-Diphenyl-1-benzyl-octahydro-indole. The indicated compound was purified by flash column chromatography on silica gel (hexanes:EtOAc = 20:1) in a 88 % yield (81 mg) as a colorless oil. ^1H NMR (CDCl_3): δ 7.47-7.37 (m, 6H), 7.34-7.27 (m, 3H), 7.24-7.16 (m, 5H), 7.11 (m, 1H), 4.08-3.95 (m, 2H), 3.38 (d, J = 15.0 Hz, 1H), 3.31 (d, J = 15.0 Hz, 1H), 3.21 (m, 1H), 3.05 (m, 1H), 1.82 (m, 1H), 1.73-1.62 (m, 2H), 1.56 (m, 1H), 1.49-1.39 (m, 2H), 1.38-1.18 (m, 2H); $^{13}\text{C}\{\text{H}\}$ NMR (CDCl_3): δ 149.0, 146.0, 141.3, 128.3, 128.3, 128.2, 128.1, 127.7, 127.2, 126.6, 125.6, 125.3, 62.6, 62.1, 58.5, 57.1, 45.1, 27.2, 25.9, 25.0, 20.2. HRMS (ESI/[M+H] $^+$) calcd. for $\text{C}_{27}\text{H}_{29}\text{N}$: 368.2373. Found: 368.2372.



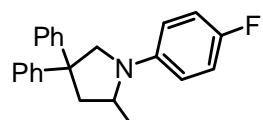
2-Ethyl-1-benzyl-4,4-diphenylpyrrolidine. The indicated compound was obtained in 52 % yield on the basis of ^1H NMR using 1,4-bis(trifluoromethyl)benzene as an internal standard. The identity of the pyrrolidine was confirmed by use of GC-MS methods, as well as by comparison of ^1H NMR data for this product to data reported for an N-Me analog.³



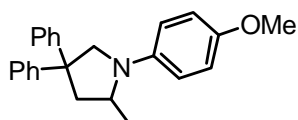
1-Phenyl-2-methyl-4,4-diphenylpyrrolidine. The indicated compound was purified by flash chromatography on silica gel (hexanes:EtOAc) = 10:1) in a 95 % yield (74 mg) as a colorless oil that solidified to white solid upon standing.⁵ ^1H NMR (CDCl_3): δ 7.45-7.36 (m, 6H), 7.35-7.26 (m, 3H), 7.25-7.15 (m, 3H), 6.85 (m, 1H), 6.82-6.78 (m, 2H), 4.21-4.14 (m, 2H), 3.88 (m, 1H), 2.91 (m, 1H), 2.61 (m, 1H), 1.32 (d, J = 6.0 Hz, 3H); $^{13}\text{C}\{\text{H}\}$ NMR (CDCl_3): δ 147.0, 146.9, 146.6, 129.1, 128.3, 128.2, 127.1, 126.7, 126.3, 126.0, 116.1, 113.0, 60.1, 52.8, 52.4, 46.8, 19.6.



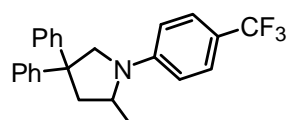
1-(4-Methylphenyl)-2-methyl-4,4-diphenylpyrrolidine. The indicated compound was purified by flash column chromatography on silica gel (hexanes:EtOAc = 10:1) in a 96 % yield (79 mg) as a white solid.⁵ ¹H NMR (CDCl₃): δ 7.40-7.35 (m, 4H), 7.31-7.22 (m, 3H), 7.20-7.10 (m, 5H), 6.70-6.66 (m, 2H), 4.12-4.07 (m, 2H), 3.80 (m, 1H), 2.84 (d of d, *J* = 11.5, 7.0 Hz, 1H), 2.55 (d of d, *J* = 12.0, 8.0 Hz, 1H), 2.36 (s, 3H), 1.25 (d, *J* = 5.5 Hz, 3H); ¹³C{¹H} NMR (CDCl₃): δ 147.1, 146.8, 144.9, 129.6, 128.3, 128.2, 127.2, 126.8, 126.3, 126.0, 125.1, 113.0, 60.4, 52.8, 52.5, 46.9, 20.3, 19.6.



1-(4-Fluorophenyl)-2-methyl-4,4-diphenylpyrrolidine. The indicated compound was purified by flash column chromatography on silica gel (hexanes:EtOAc = 10:1) in a 95 % yield (79 mg) as a colorless oil that solidified as a white solid upon standing.⁵ ¹H NMR (CDCl₃): δ 7.41-7.34 (m, 4H), 7.31-7.22 (m, 3H), 7.19 (m, 1H), 7.13-7.09 (m, 2H), 7.08-7.02 (m, 2H), 6.68-6.63 (m, 2H), 4.11-4.08 (m, 2H), 3.75 (m, 1H), 2.84 (d of d, *J* = 12.0, 6.0 Hz, 1H), 2.57 (d of d, *J* = 12.0, 8.0 Hz, 1H), 1.25 (d, *J* = 6.0 Hz, 3H); ¹³C{¹H} NMR (CDCl₃): δ 155.1 (d, *J* = 234.0 Hz), 146.9, 146.5, 143.7, 128.4, 128.3, 127.1, 126.7, 126.4, 126.1, 115.5 (d, *J* = 21.6 Hz), 113.5 (d, *J* = 7.2 Hz), 60.8, 52.9, 52.7, 46.9, 19.5.

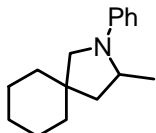


1-(4-Methoxyphenyl)-2-methyl-4,4-diphenylpyrrolidine. The indicated compound was purified by flash column chromatography on silica gel (hexanes:EtOAc = 6:1) in a 94 % yield (81 mg) as a colorless oil.⁵ ¹H NMR (CDCl₃): δ 7.38-7.32 (m, 4H), 7.31-7.14 (m, 4H), 7.11-7.07 (m, 2H), 6.95-6.90 (m, 2H), 6.71-6.66 (m, 2H), 4.11-4.02 (m, 2H), 3.84 (s, 3H), 3.74 (m, 1H), 2.80 (d of d, *J* = 12.5, 7.0 Hz, 1H), 2.53 (d of d, *J* = 12.0, 8.0 Hz, 1H), 1.22 (d, *J* = 6.0 Hz, 3H); ¹³C{¹H} NMR (CDCl₃): δ 151.1, 147.2, 146.8, 141.9, 128.3, 128.2, 127.2, 126.8, 126.3, 126.0, 114.9, 113.9, 61.0, 55.8, 52.9, 52.7, 46.9, 19.7.

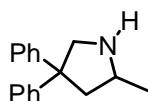


1-(4-Trifluoromethyl)-2-methyl-4,4-diphenylpyrrolidine. The indicated compound was obtained in 67 % yield on the basis of ¹H NMR using 1,4-bis(trifluoromethyl)benzene as an internal standard. The identity of the

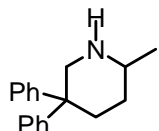
pyrrolidine was confirmed by comparison of ^1H NMR data for this product to data reported for an N-Ph analog.⁵



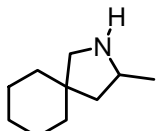
2-Phenyl-3-methyl-2-aza-spiro[4,5]decane. The indicated compound was purified by flash column chromatography on silica gel (hexanes:EtOAc = 20:1) in a 95 % yield (54 mg) as a colorless oil. ^1H NMR (CDCl_3): δ 7.34-7.25 (m, 2H), 6.76-6.64 (m, 3H), 3.95 (m, 1H), 3.30 (m, 2H), 2.18 (d of d, J = 12.8, 6.5 Hz, 1H), 1.72-1.37 (m, 11H), 1.32 (d, J = 6.2 Hz, 3H); $^{13}\text{C}\{\text{H}\}$ NMR (CDCl_3): δ 148.0, 128.9, 115.3, 112.6, 60.3, 52.4, 46.4, 41.1, 37.3, 36.2, 26.2, 23.9, 23.3, 20.3. HRMS (ESI/[M+H] $^+$) calcd. for $\text{C}_{16}\text{H}_{24}\text{N}$: 230.1903. Found: 230.1902.



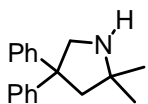
2-Methyl-4,4-diphenylpyrrolidine. The indicated compound was purified by flash column chromatography on silica gel ($\text{CH}_2\text{Cl}_2:\text{MeOH} = 10:1$) in a 89 % yield (53 mg) as a colorless oil.³ ^1H NMR (CDCl_3): δ 7.34-7.26 (m, 8H), 7.23-7.18 (m, 2H), 3.73 (d, J = 11.0 Hz, 1H), 3.52 (d, J = 11.0 Hz, 1H), 3.42 (m, 1H), 2.79 (d of d, J = 10.0, 6.5 Hz, 1H), 2.19-2.03 (m, 2H), 1.26 (d, J = 6.0 Hz, 3H); $^{13}\text{C}\{\text{H}\}$ NMR (CDCl_3): δ 147.8, 147.1, 128.3, 128.2, 127.0, 126.9, 126.0, 125.9, 57.9, 57.3, 53.1, 47.1, 22.3.



2-Methyl-5,5-diphenylpiperidine. The indicated compound was purified by flash column chromatography on silica gel ($\text{CH}_2\text{Cl}_2:\text{MeOH} = 10:1$) in a 84 % yield (53 mg) as a colorless oil.³ ^1H NMR (CDCl_3): δ 7.50-7.44 (m, 2H), 7.43-7.36 (m, 2H), 7.33-7.13 (m, 6H), 3.97 (d of d, J = 13.7, 3.1 Hz, 1H), 3.17 (d, J = 13.7 Hz, 1H), 2.83 (m, 1H), 2.76 (m, 1H), 2.27 (d of t, J = 13.4, 3.8 Hz, 1H), 1.69 (m, 1H), 1.38 (s, 1H), 1.21 (m, 1H), 1.07 (d, J = 6.3 Hz, 3H); $^{13}\text{C}\{\text{H}\}$ NMR (CDCl_3): δ 148.8, 144.7, 128.6, 128.2, 128.1, 126.4, 125.7, 125.6, 55.8, 52.3, 45.2, 35.4, 31.7, 22.4.



2,3-Dimethyl-2-aza-spiro[4,5]decane. The indicated compound was obtained in 75 % yield on the basis of ^1H NMR using 1,4-bis(trifluoromethyl)benzene as an internal standard.³



2,2-Methyl-4,4-diphenylpyrrolidine. The indicated compound was purified by flash column chromatography on silica gel ($\text{CH}_2\text{Cl}_2:\text{MeOH} = 10:1$) in a 84 % yield (53 mg) as a faint yellow oil.³ ^1H NMR (CDCl_3): δ 7.37-7.28 (m, 8H), 7.22-7.16 (m, 2H), 3.69 (s, 2H), 2.59 (s, 2H), 1.95 (br s, 1H), 1.20 (s, 6H); $^{13}\text{C}\{\text{H}\}$ NMR (CDCl_3): δ 147.5, 128.4, 126.9, 125.9, 59.3, 58.3, 57.2, 52.0, 30.7.

References to Experimental Section

- (1) Bender, C. F.; Widenhoefer, R. A. *J. Am. Chem. Soc.* **2005**, *127*, 1070.
- (2) Ackermann, L.; Kaspar, L. T.; Althammer, A. *Org. Biomol. Chem.* **2007**, *5*, 1975.
- (3) Liu, Z.; Hartwig, J. F. *J. Am. Chem. Soc.* **2008**, *130*, 1570.
- (4) Dochwahl, M.; Pissarek, J.-W.; Blechert, S.; Löhnwitz, K.; Roesky, P. W. *Chem. Commun.* **2006**, 3405.
- (5) Hesp, K. D.; Stradiotto, M. *Org. Lett.* **2009**, *11*, 1449.

2. Catalyst Optimization and Kinetic Experiments

Table S1: Optimization of the intramolecular hydroamination of **1a** employing $[\text{Ir}(\text{COD})\text{Cl}]_2$ as a pre-catalyst.^a

entry	mol% Ir	time (h)	Temp (°C)	conversion to 2a ^b
S1-1	0.1	24	110	<50
S1-2	0.25	3	110	>95
S1-3	2.5	7	80	>95
S1-4	5.0	16	40	15
S1-5	2.5	7	80	61 ^c
S1-6	2.5	7	80	76 ^d
S1-7	2.5	7	80	45 ^e

^a Reaction Conditions: 0.25 mmol **1a** and $[\text{Ir}(\text{COD})\text{Cl}]_2$ in 0.5 mL 1,4-dioxane unless otherwise noted. ^b On the basis of ^1H NMR data (average of two runs); **2a** was observed as the only reaction product. ^c In 1,2-dichloroethane. ^d In 1,2-dimethoxyethane. ^e In toluene.

Representative procedure for determining the effect of added salts. To five screw-capped vials containing **1a** (41 mg, 0.125 mmol) and a stir-bar was added 0.25 mL of a stock solution of $[\text{Ir}(\text{COD})\text{Cl}]_2$ (3.4 mg, 0.005 mmol) and LiOTf (1.6 mg, 0.010 mmol) in 4.000 mL of 1,4-dioxane ($[\text{Ir}] = [\text{LiOTf}] = 0.0025 \text{ mM}$). The vials were sealed under N_2 with a cap containing a PTFE septum and, once all the material had dissolved, were removed from the glovebox and were placed in a temperature-controlled aluminum heating block set at 110 °C. A vial was removed from the heating block every 20 min (0.33 – 1.66 h) followed by rapid cooling in an ice bath, removal of the solvent under reduced pressure, and dissolution into CDCl_3 . The consumption of substrate **1a** and the appearance of the product **2a** were quantified by integration of the alkene resonances of the ^1H NMR spectrum relative to 1,4-bis(trifluoromethyl)benzene as an internal standard. The % conversion to **2a** was plotted as a function of time (Figure S1).

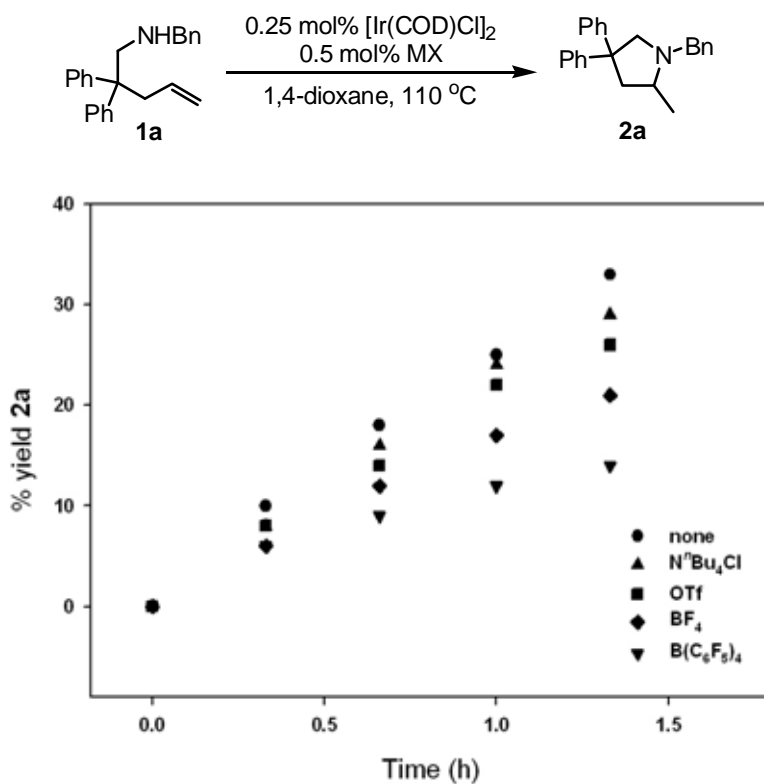
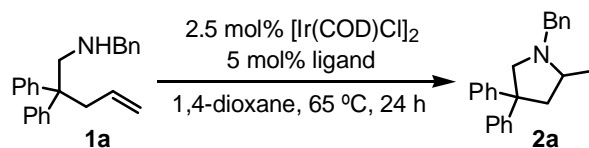


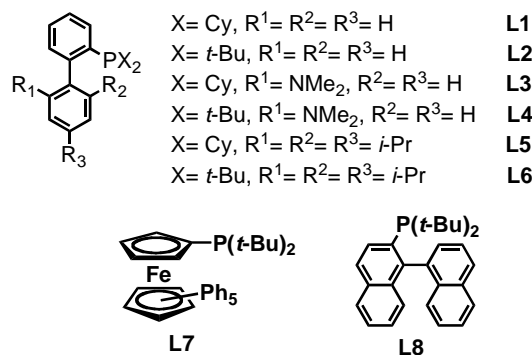
Figure S1. Relationship between the conversion to **2a** upon addition of salts in the $[\text{Ir}(\text{COD})\text{Cl}]_2$ catalyzed hydroamination of **1a**. The reactions were conducted at the following concentrations: $[\mathbf{1a}] = 5.0 \times 10^{-4} \text{ M}$, $[\text{Ir}] = 2.5 \times 10^{-6} \text{ M}$, $[\text{MX}] = 2.5 \times 10^{-6} \text{ M}$.

Table S2: Effect of added ligands on the hydroamination of **1a** using $[\text{Ir}(\text{COD})\text{Cl}]_2$.^a



Entry	Ligand	% Conversion ^b (% Yield 2a)
S2-1	-	60
S2-2	2,2'-bipyridine	<5
S2-3	Terpyridine	<5
S2-4	PPh_3	<5
S2-5	PCy_3	34
S2-6	$\text{P}(t\text{-Bu})_3$	62
S2-7	DPPE ^c	>95 (<5)
S2-8	DCPE ^d	90 (<5)
S2-9	DPPB ^e	<5
S2-10	Xantphos ^f	<5
S2-11	DPEphos ^g	<5
S2-12	DPPF ^h	>95 (<5)
S2-13	DiPPP ⁱ	45 (<5)
S2-14	L1	<5
S2-15	L2	>95
S2-16	L3	7
S2-17	L4	>95
S2-18	L5	6
S2-19	L6	58
S2-20	L7	>95
S2-21	L8	>95

^aReaction Conditions: 0.125 mmol **1a**, 2.5 mol % $[\text{Ir}(\text{COD})\text{Cl}]_2$ and 5 mol % ligand in 0.25 mL 1,4-dioxane. ^bOn the basis of ^1H NMR data; **2a** was observed as the only reaction product unless noted. ^c 1,2-Bis(diphenylphosphino)ethane. ^d 1,2-Bis(dicyclohexylphosphino)ethane. ^e 1,4-Bis(diphenylphosphino)butane. ^f 4,5-Bis(diphenylphosphino)-9,9-dimethylxanthene. ^g Bis(2-diphenylphosphinophenyl)ether. ^h 1,1'-Bis(diphenylphosphino)ferrocene. ⁱ 1,1'-Bis(diisopropylphosphino)ferrocene.



Determination of reaction order in (*t*-Bu)-Johnphos (L2**) for $[\text{Ir}(\text{COD})\text{Cl}]_2$ -catalyzed hydroamination.** To five screw-capped vials containing **1a** (41 mg, 0.125 mmol) and a stir-bar was added 0.25 mL of a stock solution of $[\text{Ir}(\text{COD})\text{Cl}]_2$ (12.7 mg, 0.0189 mmol) and **L2** (33.8 mg, 0.113 mmol) in 1.512 mL of 1,4-dioxane ($[\text{Ir}] = 0.025 \text{ mM}$; $[\text{L2}] = 3[\text{Ir}]$). The vials were sealed under N_2 with a cap containing a PTFE septum and, once all the material had dissolved, were removed from the glovebox and were placed in a temperature-controlled aluminum heating block set at 65 °C. A vial was removed from the heating block every 1.5–2 h (0–8 h) followed by rapid cooling in an ice bath, removal of the solvent under reduced pressure, and dissolution into CDCl_3 . The consumption of substrate **1a** and the appearance of the product **2a** were quantified by integration of the alkene resonances of the ^1H NMR spectrum relative to 1,4-bis(trifluoromethyl)benzene as an internal standard. Pseudo-first order rate constants were obtained by plotting $[\text{1a}]_t$ vs. time (in all cases these gave linear plots). The k_{obs} values obtained in these experiments were plotted versus $[\text{L2}]$ to determine the reaction order in added phosphine ligand at 65 °C (Figure S2). According to Figure S2(b), an inverse-order in **L2** was determined at 65 °C. Given that when 2.5 mol% $[\text{Ir}(\text{COD})\text{Cl}]_2$ was used at 110 °C the reaction rates were difficult to measure reproducibly, the reaction order in **L2** was determined using 0.5 mol% $[\text{Ir}(\text{COD})\text{Cl}]_2$ to be zero-order with varied **[L2]** (Figure S2(a)).

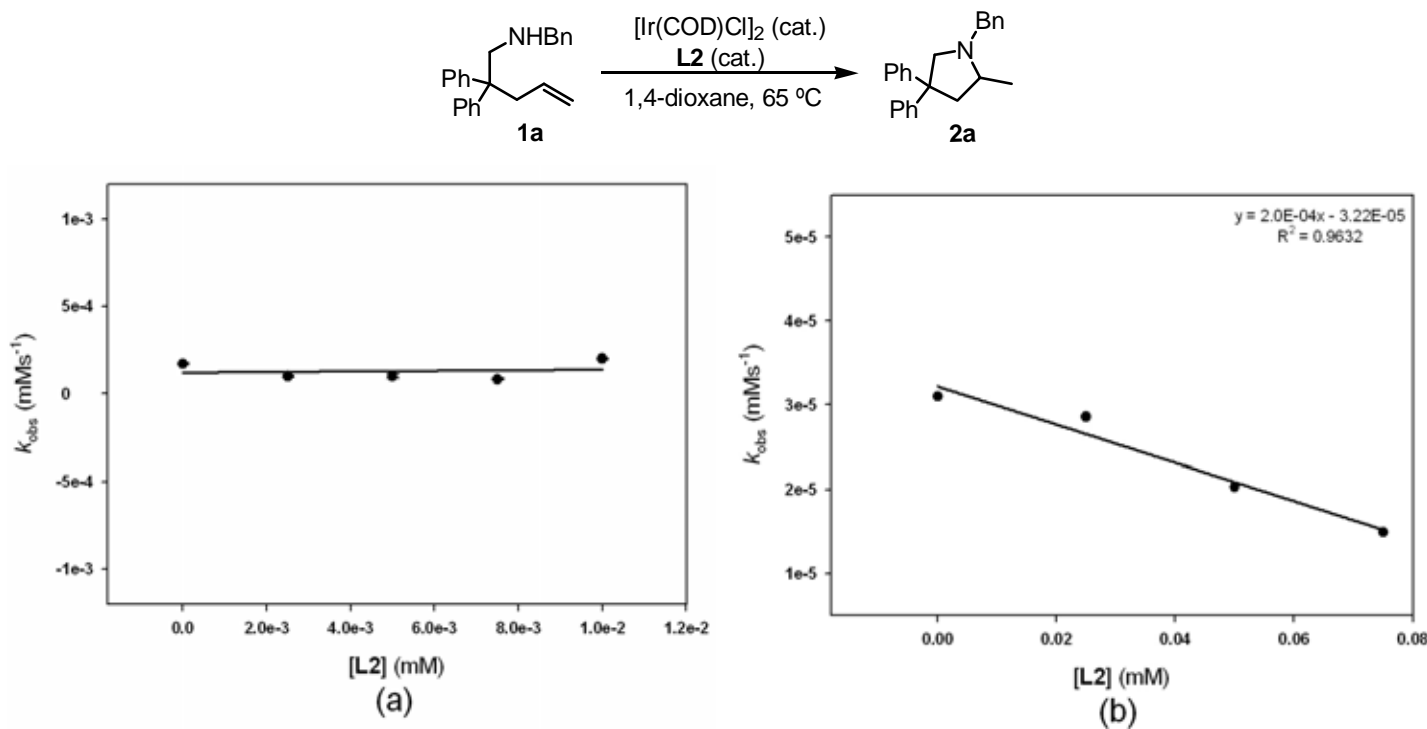


Figure S2. Relationship between k_{obs} and $[\text{L2}]$. (a) The reactions were conducted in 1,4-dioxane at 110 °C at the following concentrations: $[\text{1a}] = 5.0 \times 10^{-4} \text{ M}$, $[\text{Ir}] = 5.0 \times 10^{-6} \text{ M}$ and $[\text{L2}]$ was varied from 0 M to $1.0 \times 10^{-5} \text{ M}$. (b) The reactions were conducted in 1,4-dioxane at 65 °C at the following concentrations: $[\text{1a}] = 5.0 \times 10^{-4} \text{ M}$, $[\text{Ir}] = 2.5 \times 10^{-5} \text{ M}$ and $[\text{L2}]$ was varied from 0 M to $7.5 \times 10^{-5} \text{ M}$.

Representative procedure for the determination of the rate of reaction (k_{obs}) for the hydroamination of **1a with $[\text{Ir}(\text{COD})\text{Cl}]_2$.** To eight screw-capped vials containing **1a** (41 mg, 0.125 mmol) and a stir-bar was added 0.25 mL of a stock solution of $[\text{Ir}(\text{COD})\text{Cl}]_2$ (7.1 mg, 0.011 mmol) in 4.227 mL of 1,4-dioxane ($[\text{Ir}] = 0.005$ mM). The vials were sealed under N_2 with a cap containing a PTFE septum and, once all the material had dissolved, were removed from the glovebox and were placed in a temperature-controlled aluminum heating block set at 110 °C. A vial was removed from the heating block every 20 min (0.33 – 2.33 h) followed by rapid cooling in an ice bath, removal of the solvent under reduced pressure, and dissolution into CDCl_3 . The consumption of substrate **1a** and the appearance of the product **2a** were quantified by integration of the alkene resonances of the ^1H NMR spectrum relative to 1,4-bis(trifluoromethyl)benzene as an internal standard. The rate of reaction (k_{obs}) was obtained through plots of $[\text{1a}]_t$ versus time (Figure S3).

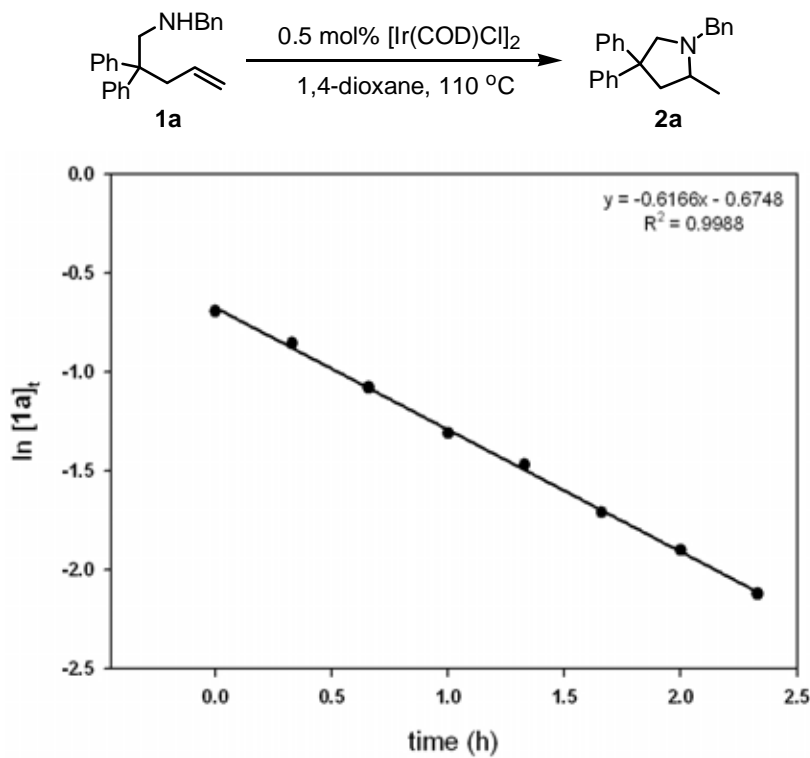


Figure S3. Representative first order plot for the hydroamination of **1a** with $[\text{Ir}(\text{COD})\text{Cl}]_2$. The reactions were conducted at the following concentrations: $[\text{Ir}] = 5.0 \times 10^{-6}$ M and $[\text{1a}] = 5.0 \times 10^{-4}$ M.

Determination of reaction order in catalyst for $[\text{Ir}(\text{COD})\text{Cl}]_2$ -catalyzed hydroamination. Using the general procedure outlined on page S14, pseudo-first order rate constants were obtained by plotting $[\text{1a}]_t$ vs. time (in all cases these gave linear plots) for a series of experiments with varied $[\text{Ir}]$ ($0.001 - 0.00475 \text{ mM}$). The k_{obs} values obtained in these experiments were plotted versus $[\text{Ir}(\text{COD})\text{Cl}]_2$ to determine the reaction order in catalyst (Figure S4(a)). According to Figure S4(a), a pseudo first-order in catalyst was determined. This was confirmed by a non-linear least squares fit of the data to the equation: $f(x) = a[\text{Ir}]^n$. As shown in Figure S4(b), this afforded a reaction order (n) of $1.15(9)$.

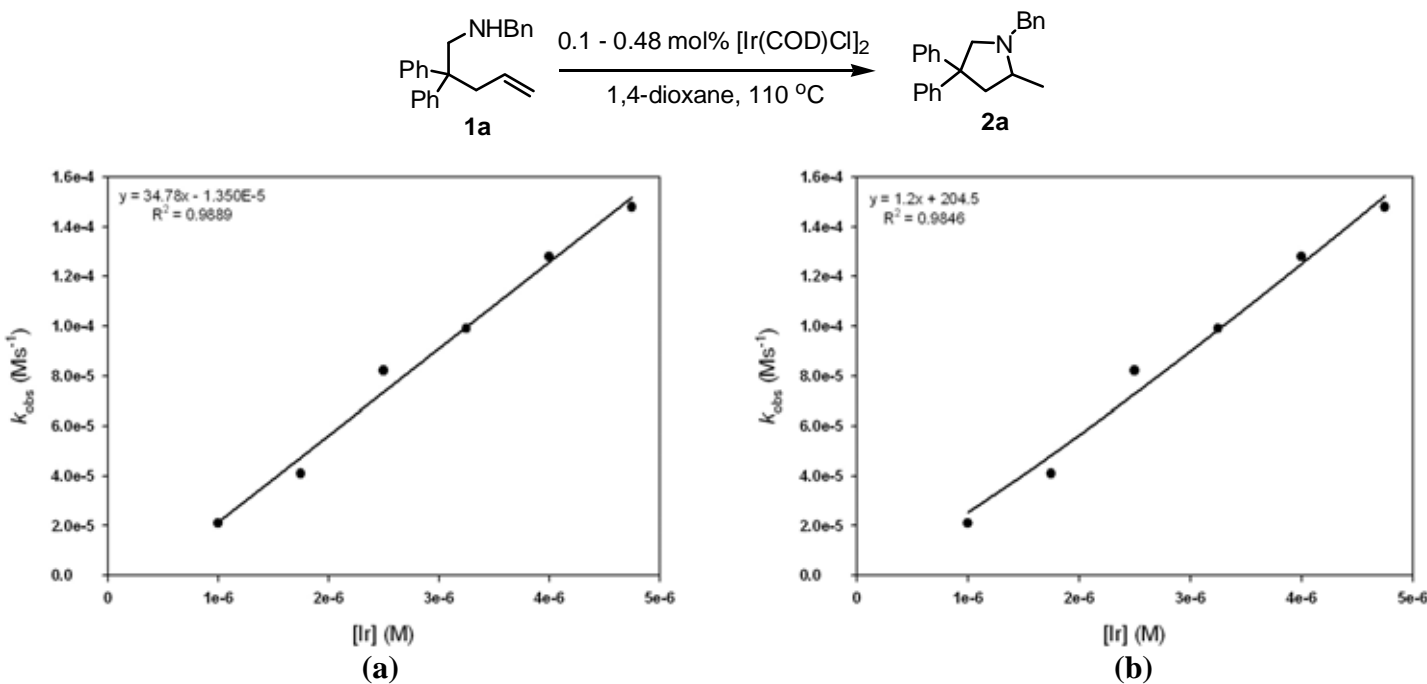


Figure S4. Relationship between k_{obs} and $[\text{Ir}]$. The reactions were conducted at the following concentrations: $[\text{1a}] = 5.0 \times 10^{-4} \text{ M}$ and $[\text{Ir}]$ was varied from $1.0 \times 10^{-6} \text{ M}$ to $4.75 \times 10^{-6} \text{ M}$.

Determination of reaction order in substrate (1a**) for $[\text{Ir}(\text{COD})\text{Cl}]_2$ -catalyzed hydroamination.** Using the general procedure outlined on page S14, pseudo-first order rate constants were obtained by plotting $[\text{1a}]_t$ vs. time (in all cases these gave linear plots) for a series of experiments with varied **[1a]** (0.02 – 0.15 mM). The k_{obs} values obtained in these experiments were plotted vs. **[1a]** to determine the reaction order in substrate (**1a**) (Figure S5). According to Figure S5, an inverse-order in substrate was determined.

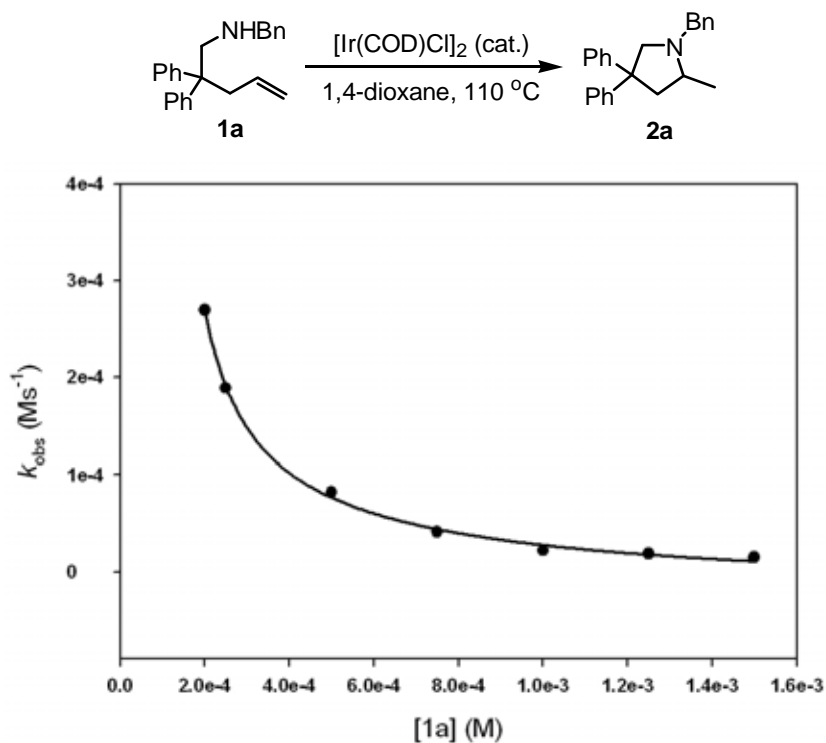


Figure S5. Relationship between k_{obs} and **1a**. The reactions were conducted at the following concentrations: $[\text{Ir}] = 2.5 \times 10^{-6}$ M and **[1a]** was varied from 2.0×10^{-4} M to 1.5×10^{-3} M.

General procedure for the Hammett study with *para*-substituted arylamine substrates. To five screw-capped vials containing substrate (**3a-e**) (0.125 mmol) and a stir-bar was added 0.25 mL of a stock solution of $[\text{Ir}(\text{COD})\text{Cl}]_2$ in 1,4-dioxane ($[\text{Ir}] = 0.005 \text{ mM}$). The vials were sealed under N_2 with a cap containing a PTFE septum and, once all the material had dissolved, were removed from the glovebox and were placed in a temperature-controlled aluminum heating block set at 110 °C. A vial was removed from the heating block every 20 min (0.33 – 1.66 h) followed by rapid cooling in an ice bath, removal of the solvent under reduced pressure, and dissolution into CDCl_3 . The consumption of substrate (**3a-e**) and the appearance of the product (**4a-e**) were quantified by integration of the alkene resonances of the ^1H NMR spectrum relative to 1,4-bis(trifluoromethyl)benzene as an internal standard. The rate of reaction (k_{obs}) was obtained through plots of $[\mathbf{3a-e}]_t$ versus time (in all cases gave linear plots). A plot of $\log(k_{\text{obsX}}/k_{\text{obsH}})$ versus σ_p generated a linear plot and a ρ value of -2.4(2) (Figure S6).

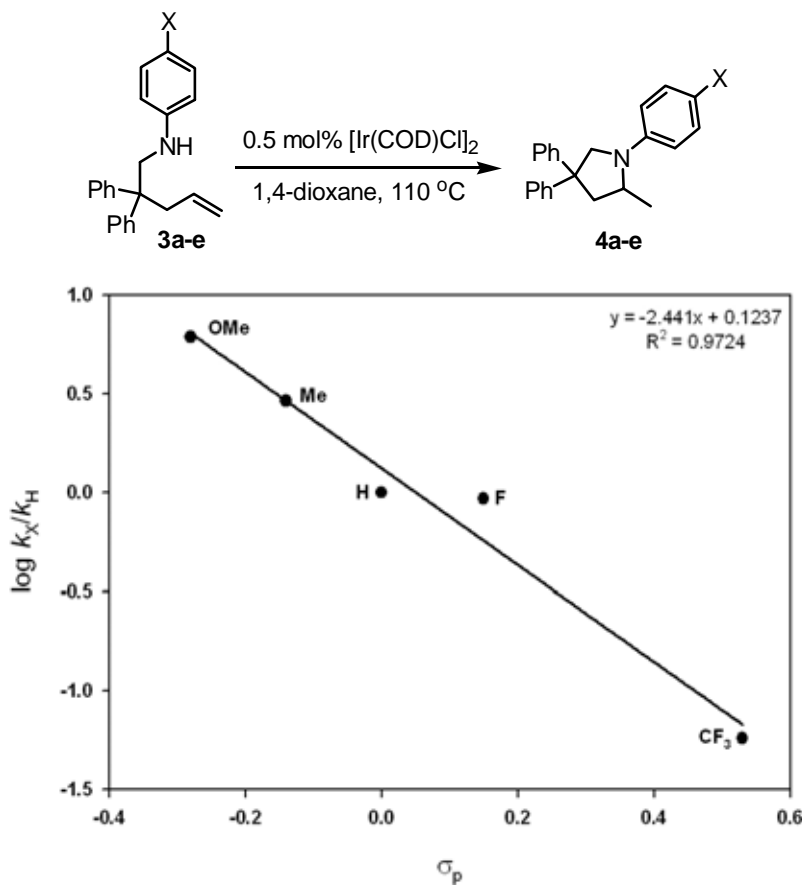


Figure S6. Hammett plot for the $[\text{Ir}(\text{COD})\text{Cl}]_2$ catalyzed hydroamination of arylamino-alkene substrates **3a-e**. The reactions were conducted at the following concentrations: $[\mathbf{3a-e}] = 5.0 \times 10^{-4} \text{ M}$, $[\text{Ir}] = 5.0 \times 10^{-6} \text{ M}$.

Determination of kinetic isotope effect (KIE) for $[\text{Ir}(\text{COD})\text{Cl}]_2$ -catalyzed hydroamination of **1a.** Using the general procedure outlined on page S14, pseudo-first order rate constants were obtained by plotting $[\mathbf{1a}]_t$ vs. time (or $[\mathbf{1a-d}_1]_t$ vs. time); in all cases these gave linear plots. The k_{obs} values obtained in these experiments were used to determine the H/D KIE (Figure S7). According to Figure S7, a H/D KIE of 3.4(3) was determined.

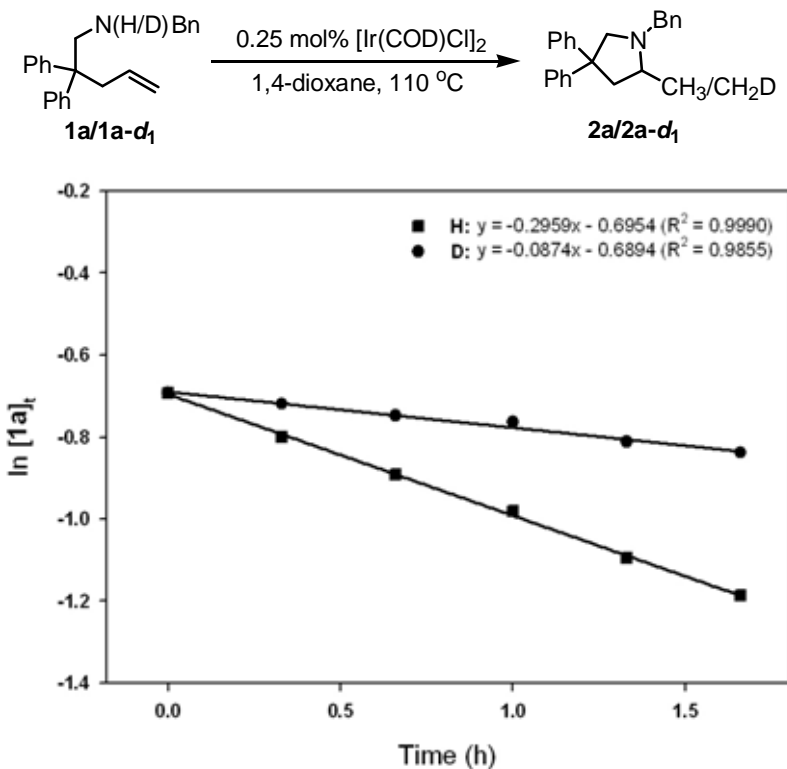


Figure S7. H/D kinetic isotope effect for the $[\text{Ir}(\text{COD})\text{Cl}]_2$ catalyzed hydroamination of **1a**. The reaction conditions were conducted at the following concentrations: $[\mathbf{1a}/\mathbf{1a-d}_1] = 5.0 \times 10^{-4} \text{ M}$ and $[\text{Ir}] = 2.5 \times 10^{-6} \text{ M}$. The kinetic isotope effect is $k_{\text{H}}/k_{\text{D}} = 3.4(3)$.

General procedure for the determination of activation parameters for the hydroamination of **1a employing $[\text{Ir}(\text{COD})\text{Cl}]_2$ as a precatalyst.** To five screw-capped vials containing **1a** (0.125 mmol) and a stir-bar was added 0.25 mL of a stock solution of $[\text{Ir}(\text{COD})\text{Cl}]_2$ in 1,4-dioxane ($[\text{Ir}] = 0.005 \text{ mM}$). The vials were sealed under N_2 with a cap containing a PTFE septum and, once all the material had dissolved, were removed from the glovebox and were placed in a temperature-controlled aluminum heating block set at desired temperature (90–130 °C). A vial was removed from the heating block every 20 min (0.33 – 1.66 h) followed by rapid cooling in an ice bath, removal of the solvent under reduced pressure, and dissolution into CDCl_3 . The consumption of substrate **1a** and the appearance of the product **2a** were quantified by integration of the alkene resonances of the ^1H NMR spectrum relative to 1,4-bis(trifluoromethyl)benzene as an internal standard. Pseudo-first order rate constants were obtained by plotting $[\text{1a}]_t$ vs. time (in all cases these gave linear plots). The k_{obs} values obtained in these experiments were used in Eyring and Arrhenius plots to determine the activation parameters for the hydroamination of **1a** with $[\text{Ir}(\text{COD})\text{Cl}]_2$ (Figure S8).

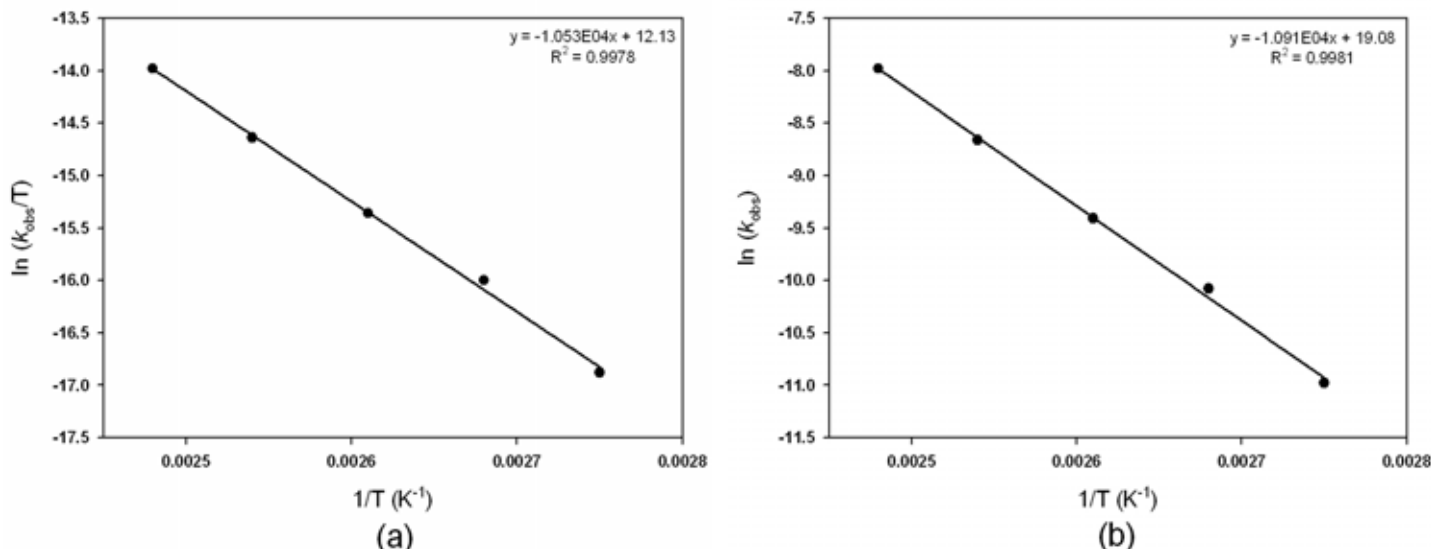
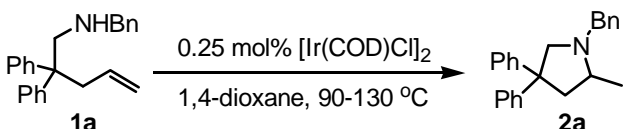


Figure S8. (a) Eyring plot for the hydroamination of **1a** catalyzed by $[\text{Ir}(\text{COD})\text{Cl}]_2$. The reactions were conducted in 1,4-dioxane over a temperature range of 90–130 °C at the following concentrations: $[\text{1a}] = 5.0 \times 10^{-4} \text{ M}$ and $[\text{Ir}] = 2.5 \times 10^{-6} \text{ M}$ ($\Delta H^\ddagger = 20.9(3) \text{ kcal/mol}$, $\Delta S^\ddagger = -23.1(8) \text{ cal/K}\cdot\text{mol}$). (b) Arrhenius plot for the hydroamination of **1a** catalyzed by $[\text{Ir}(\text{COD})\text{Cl}]_2$. The reactions were conducted in 1,4-dioxane over a temperature range of 90–130 °C at the following concentrations: $[\text{1a}] = 5.0 \times 10^{-4} \text{ M}$ and $[\text{Ir}] = 2.5 \times 10^{-6} \text{ M}$ ($E_a = 21.6(3) \text{ kcal/mol}$).

3. Computational Analysis, Details, and Tabulated Data

Detailed Computational Characterization of Important Elementary Steps

(A) *Nature of the Catalytically Competent Compound.* Several possible equilibria for fragmentation of precatalyst $[\text{Ir}(\text{COD})\text{Cl}]_2 \textbf{M0}$ in the presence of substrate **5a** and 1,4-dioxane have been examined (Figure S9). Fragmentation via eq 1 is endergonic ($\Delta G = 7.5 \text{ kcal mol}^{-1}$, while eq 3 is moderately exergonic ($\Delta G = -3.1 \text{ kcal mol}^{-1}$). 1,4-Dioxane association to $[\text{Ir}(\text{COD})\text{Cl}(\text{dioxane})]$ is unfavorable by another $12.1 \text{ kcal mol}^{-1}$ (eq 2). Analogously, $[\text{Ir}(\text{COD})\text{Cl}(\text{substrate})_2]$ species are unlikely to be present in appreciable concentrations, as amine association to the $[\text{Ir}(\text{COD})\text{Cl}(\text{substrate})]$ **M1a** is strongly uphill ($\Delta G = 27.7 \text{ kcal mol}^{-1}$, eq 4). DFT predicts that the $[\text{Ir}(\text{COD})\text{Cl}(\text{substrate})]$ complex **M1** is the prevalent species generated through fragmentation of **M0** in the presence of substrate and solvent.

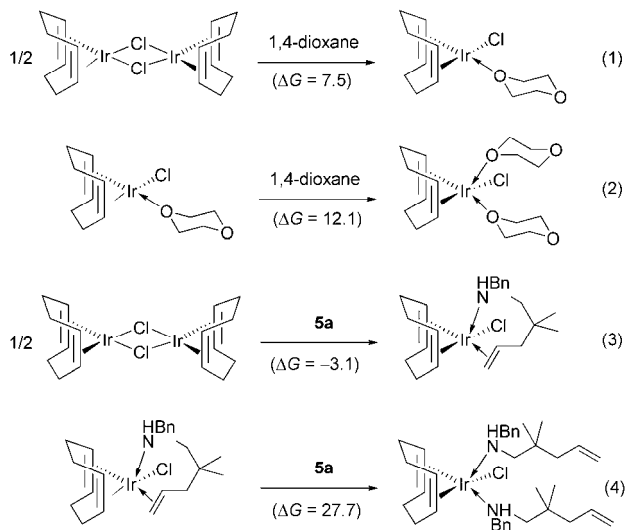


Figure S9. Fragmentation of $[\text{Ir}(\text{COD})\text{Cl}]_2$ precatalyst **M0**. The thermodynamic force is given in kcal mol^{-1} .

Several forms are conceivable for **M1**, which are distinguished by the mode in which the substrate complexes to the Ir^{I} center (Figure S10). Of the various forms, a substrate chelate through amine and olefin functionalities is most stable (**M1a**), while substrate association in a mono-hapto fashion through amine (**M1b**, $\Delta G = 3.3 \text{ kcal mol}^{-1}$) and olefin (**M1c**, $\Delta G = 7.3 \text{ kcal mol}^{-1}$) units is somewhat less favorable. Nevertheless, isomers **M1a–M1c** are all present in a rapid equilibrium, with **M1a** being prevalent. The $[\text{Ir}(\text{COD})\text{Cl}(\text{dioxane})]$ compound is found to be $10.6 \text{ kcal mol}^{-1}$ above **M1a**.

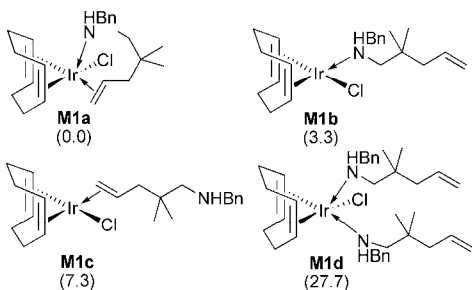


Figure S10. Various forms of the catalytically competent $[\text{Ir}(\text{COD})\text{Cl}(\text{substrate})]$ compound **M1** (free energies in kcal mol^{-1} relative to **M1a**)

Another intriguing aspect is as to whether $[\text{Ir}(\text{COD})\text{Cl}(\text{substrate})]$ compound **M1** or alternatively a solvent-separated $[\text{Ir}(\text{COD})(\text{dioxane})(\text{substrate})]^+ \text{Cl}^-$ ion pair **M1-IP** represents the catalytically competent species. Comparable performance observed for $[\text{Ir}(\text{COD})\text{Cl}]_2$ and $[\text{Ir}(\text{COD})\text{Cl}]_2/2\text{AgBF}_4$ may suggest that **M1-IP** triggers hydroamination catalysis. The propensity of dioxane to displace the chloride from the immediate vicinity of the Ir center has been gauged computationally by employing a microsolvation approach. To this end, an ensemble of three explicit dioxane molecules have been placed closely around the Cl center in **M1** and **M1-IP**, respectively, thereby simulating specific solvation effects adequately. As revealed from Figure S11, **M1-IP** is distinctly separated energetically from **M1** being more than 28 kcal mol⁻¹ uphill, irrespective of the substrate's association mode. Thus, **M1a** is almost exclusively present, because exchange of chloride for dioxane is energetically challenging. Moreover, the assessed gap between **M1** and **M1-IP** is larger than the turnover-limiting barrier for the productive hydroamination cycle that commences from **M1** (see below), thereby indicating that **M1-IP** with an outer-sphere chloride is unlikely to play any significant role for the herein described catalyst system under the reported reaction conditions. These computational results complement conductivity measurements (see manuscript) and both collectively provide compelling evidence that neutral **M1** is the catalytically competent compound.

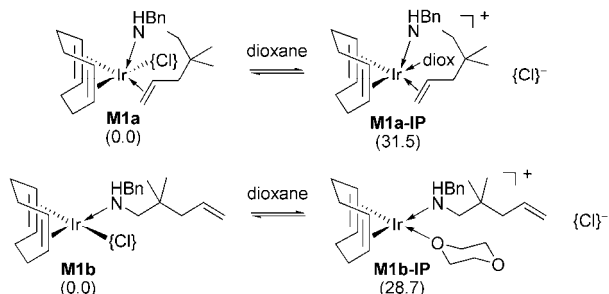


Figure S11. Thermodynamic force (in kcal mol⁻¹) for ion-pair separation in **M1**.

(B) Hydroamination via C=C Activation.

(B1) Ring Closure by Amine Attack on the Ir–Olefin Linkage. Ring closure by nucleophilic attack of the amine functionality on the Ir-coordinated, hence activated, C=C bond can proceed along distinct trajectories constituting frontside (i.e., amine approach *cis*(*syn*) to the metal) and backside (i.e.; amine approach *trans*(*anti*) to the metal) approaches. Figure S12 shows three conformers of the resulting zwitterionic $\text{Ir}^{\text{l}}\text{-cycloammonio-alkyl}$ intermediate **M2**. Frontside amine attack leads initially to **M2a**, which has the hydrogen of the quarternised ammonium center placed closely to the electron-rich metal center. Intermediate **M2a** converts readily into the more stable conformer **M2c**, featuring a positively charged ammonium unit that points towards the negatively polarized chloride. Transient **M2b** that is first generated along the backside trajectory relaxes almost instantaneously into **M2c**, which represents the minimum energy conformer of the $\text{Ir}^{\text{l}}\text{-cycloammonio-alkyl}$ intermediate.

The most stable form **M1a** of the catalytically competent $[\text{Ir}(\text{COD})\text{Cl}(\text{substrate})]$ compound featuring a chelating aminoalkene does not represent the direct precursor for cyclization. The most accessible pathways for frontside and backside amine approach are found to commence instead from **M1c**. Hence, the amine group must first disconnect from the Ir center in the prevalent **M1a** before ring closure can occur.

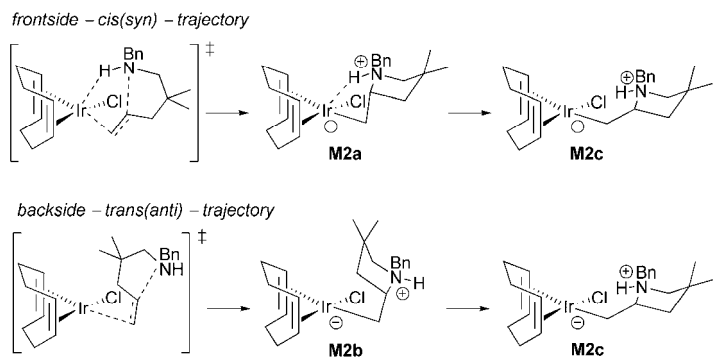


Figure S12. Cyclization via nucleophilic attack of the amine on the Ir–olefin linkage proceeding through frontside and backside trajectories.

Table S3. Free-energy profile for nucleophilic attack of the amine on the Ir–olefin linkage (in kcal mol⁻¹, relative to **M1a**)

	precursor	TS	product
frontside approach <i>cis</i> (<i>syn</i>) to Ir	7.3 (M1c)	20.9	13.0 (M2a) 9.5 (M2c)
backside approach <i>trans</i> (<i>anti</i>) to Ir	7.3 (M1c)	16.9	15.4 (M2b) 9.5 (M2c)

As revealed Table S3, backside amine attack is the dominant pathway for ring closure. This uphill transformation has a moderate activation barrier that amounts to 16.9 kcal mol⁻¹. Passage through the alternative frontside trajectory is kinetically somewhat more demanding ($\Delta\Delta G^\ddagger = 4.0$ kcal mol⁻¹), but nevertheless also viable.

(B2) Cleavage of the Ir–C bond in the zwitterionic intermediate **M2.** Two principal mechanistic scenarios are conceivable, as outlined in Figure S13.

- (A) direct protonolysis of the Ir–C bond by the excess proton available from the ammonium unit
- (B) protonation of the metal center affording a transient Ir^{III}–hydrido intermediate, with subsequent reductive elimination of the cycloamine

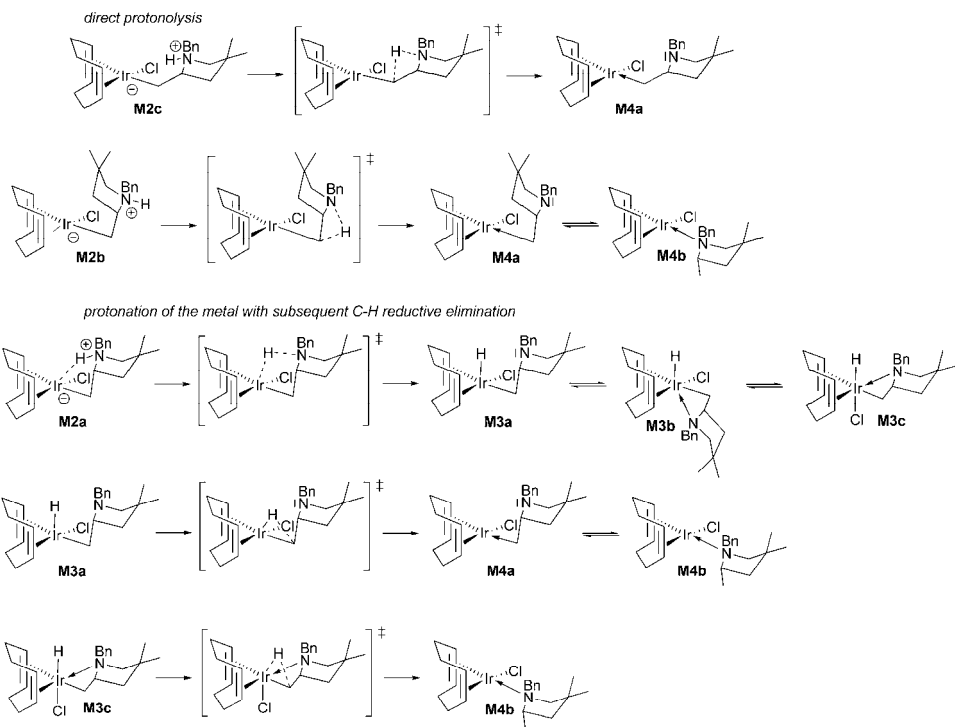


Figure S13. Cleavage of the Ir–C bond in **M2** through (a) direct protonolysis or (b) proton transfer onto the metal and ensuing reductive elimination.

Mechanism A: A first conceivable route for protolytic cleavage of the Ir–C bond in **M2** is an intramolecular process transferring the proton from the ammonium unit directly to the terminal C(α) center of the azacycle's tether (see Figure S13, top). For direct protonolysis to commence from **M2a** and **M2c** all attempts to localize the corresponding TS structure were unsuccessful. The located TS structures were found to be transition states for C–H reductive elimination, rather than Ir–C bond protonolysis. However, a TS structure constituting the protonolysis of the Ir–C bond in **M2b** has been located. The assessed energy profile (**M2b** → **M4a** : $\Delta G^\ddagger = 39.2 \text{ kcal mol}^{-1}$, $\Delta G = -0.5 \text{ kcal mol}^{-1}$, relative to **M2c**), renders this pathway as being almost impossible to be traversed under operating reaction conditions.

Excess amine substrate can be envisioned to accelerate protonolysis. In order to keep the computations affordable, the Me_2NH model substrate **S'** has been used to gauge the effect of excess substrate. As a first scenario, stabilisation of $\text{TS}[\text{M2b} \cdots \text{M4a}]$ by substrate association has been considered, but proven not to be effective, as adducts $\text{TS}[\text{M2b} \cdots \text{M4a}] \cdots \text{S}'$, which are stable relative to $\{\text{TS}[\text{M2b} \cdots \text{M4a}] + \text{S}'\}$ at the ΔH surface, could not be located. In a more probable scenario, the amine may act instead as a mediating agent. The associated TS structures feature the simultaneous protonation/deprotonation of an external molecule **S'** bearing a formally quaternary nitrogen center and reveal a concerted, but asynchronous proton transfer. The enthalpy barrier for such relay mechanism diminishes substantially, but the entropy penalty associated with the involvement of another substrate molecule gives rise to a free energy of activation that amounts to 31.6 kcal mol^{-1} . Although being lower than the barrier for the **M2b** → **M4a** pathway, which does not benefit from the participation of additional substrate molecules, the magnitude of the barrier renders this pathway as being also non-accessible.

To summarize, it is not the direct protolytic cleavage of the Ir–C bond in **M2** that generates [Ir(COD)Cl(cycloamine)] compound **M4**, but rather a two-step process, which involves first the generation of an Ir^{III}–hydrido intermediate **M3a** with ensuing C–H reductive elimination of the cycloamine.

Mechanism B: Intramolecular deprotonation of the ammonium unit in **M2** leads to the Ir^{III}–hydrido-cycloamido intermediate **M3**. The most accessible pathway commences from **M2a**, which has the ammonium unit already suitably orientated towards the Ir center. The proton transfer from the ammonium unit to the metal therefore does not require major structural reorganization. Additionally, the moderate nucleophilicity of the Ir^I center supports the protonation electronically. Indeed, the **M2a** → **M3a** conversion which involves the formal change of the oxidation state of the metal center from Ir^I to Ir^{III} has a small barrier of only 10.8 kcal mol⁻¹ and furnishes directly square-pyramidal **M3a** that has the hydride in an apical position. **M3a** is uphill by 10.4 kcal mol⁻¹ and represents a very shallow minimum on the free-energy surface, as the reverse **M3a** → **M2a** has a minimal barrier of only 0.4 kcal mol⁻¹. It implies an almost negligible stationary population of **M3a**, which should therefore be rather difficult to observe by spectroscopy. Transient **M3a** can undergo skeletal rearrangement to relax into the more stable six-coordinate **M3b** featuring an additional Ir^{III}–N(azacycle) ligation and having Cl and H in trans positions. Alternatively, pyrrolidine can be reductively eliminated from the Ir^{III}–hydrido-cycloamido intermediate. Notably, the TS structure passed through along the most accessible pathway for reductive elimination adopts a ligand arrangement that is similar to **M3b**. However, given the small energy gap between this transition state and **M3a**, it can reasonably be assumed that facile skeletal rearrangement in **M3a** and reductive elimination do occur concomitantly. Accordingly, C–H reductive elimination to commence from five-coordinate **M3a** traverses a highly ordered six-coordinate TS structure and affords the Ir^I–N(pyrrolidine) compound **M4b**. As shown in Table S4 the reductive elimination has the higher barrier of the two consecutive steps and thus discriminates the overall kinetics of the dominant pathway towards pyrrolidine by stepwise cleavage of the Ir–C bond in **M2**. Additional substrate molecules are indicated not to facilitate this pathway.

Table S4. Free-energy profile for stepwise cleavage of the Ir–C bond in **M2** (in kcal mol⁻¹, relative to **M2c**)

	precursor	TS	product
protonation of Ir M2a → M3a	3.5 (M2a)	10.8	10.4 (M3a) 1.9 (M3b)
reductive elimination M3a → M4b		15.1	-6.6 (M4b)

(B3) Displacement of the Cycloamine in **M4 by New Substrate.** An associative mechanism has been considered for the expulsion of pyrrolidine **6a** from **M4b** by incoming substrate **5a**. Two trajectories that lead directly to **M1b** or **M1c** have been scrutinized (Figure S14). Reaction profiles that are almost degenerate energetically have been found for **M4b** + **5a** → **M1b** + **6a** and **M4b** + **5a** → **M1c** + **6a** (Table S5). Thus, both

trajectories are traversable at comparable probabilities to regenerate the catalytically competent compound **M1** (thereby closing the catalytic cycle) in a step that is downhill, hence irreversible.

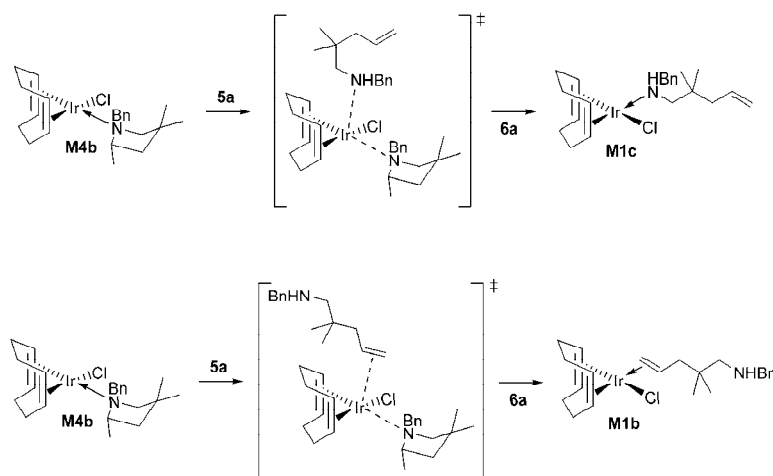


Figure S14. Associative displacement of pyrrolidine by substrate in **M4b**.

Table S5. Free-energy profile for associative product displacement (in kcal mol⁻¹, relative to {**M4b + 5a**})

	precursor	TS	product
M4b + 5a → M1b + 6a	0.0 (M4b)	19.3	-13.2 (M1b)
M4b + 5a → M1c + 6a	0.0 (M4b)	19.7	-9.3 (M1c)

(B4) β -Hydride Elimination from **M2.** In an effort to probe a reaction that could be in competition with the productive hydroamination cycle and may lead to unwanted products, the ability of intermediate **M2** to undergo β -hydride elimination to furnish the Ir-cycloenammoium-hydrido compound **M5** was examined. The most accessible pathway traverses a square-pyramidal (SPY) transition-state structure featuring cis disposed olefin and hydride units, both occupying basal positions. The TS decays thereafter via smooth skeletal rearrangements into trigonal bipyramidal (TBP) **M5a**, in which the H and Cl occupy axial positions (Figure S15).

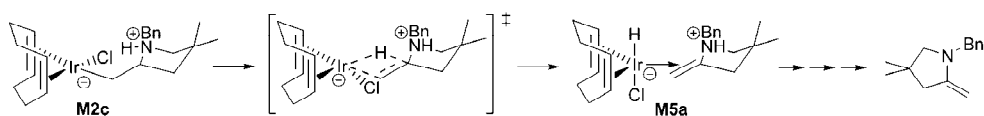


Figure 15. β -Hydride elimination from **M2**.

Table S6. Free-energy profile for β -hydride elimination from **M2c** (in kcal mol⁻¹)

	precursor	TS	product
M2c → M5a	0.0 (M2c)	27.0	11.3 (M5a)

Comparison with the rival hydroamination pathway, namely stepwise **M2a** → **M3a** → **M4b** cleavage of the Ir–C bond, leads us to the following conclusions:

- (1) The **M2a** → **M4b** transformation is connected to a moderate barrier of 15.1 kcal mol⁻¹ overall and is downhill by 6.6 kcal mol⁻¹.
- (2) In contrast, β-hydride elimination is significantly more demanding kinetically (hence substantially slower, if traversable at all, since the kinetic gap is as large as 11.9 kcal mol⁻¹) and also endergonic, such that the reverse olefin insertion into the Ir–H bond is more favorable.
- (3) β-Hydride elimination is not competitive with **M2a** → **M4b** cycloamine formation on either kinetic or thermodynamic grounds and can thus not be traversed. This may serve in rationalizing why cycloamines other than **6a** are not among the observed products.

(C) Hydroamination via N–H Activation.

(C1) Oxidative Addition of the Amine N–H Bond to the Ir^I Center in **M1.** Oxidative addition of the amine N–H bond at the low-valent, coordinatively unsaturated Ir^I(d⁸) center in the 16-electron compound **M1b** produces the five-coordinate Ir^{III}-amido-hydrido complex **M6**. Several positional isomers (diastereomers) are possible for each of the key stationary species; the ones involved along the most accessible pathway are shown in Figure S16. The square-planar (SP) structure of precursor **M1b** remains virtually undisturbed in the TS structure. The TS decays thereafter smoothly into square-pyramidal (SPY) **M6a**, in which the hydrido ligand (as the strongest donor) occupies the axial position. As indicated by the planarity of the amido unit, its lone pair is involved in π-bonding in complex **M6a**.

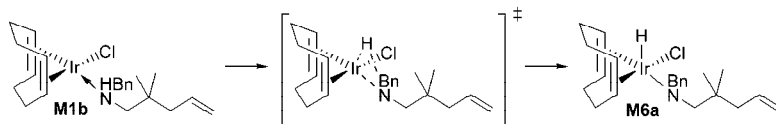


Figure S16. Oxidative addition of the amine N–H bond.

Table S7. Free-energy profile for oxidative addition of the amine N–H bond in **M1** (in kcal mol⁻¹, relative to **M1a**)

	precursor	TS	product
M1b → M6a	3.3 (M1b)	38.3	25.7 (M6a)

Because the Ir^I center in **M1b** is rather electron-deficient (as strong donor ligands, like phosphines, are absent) the huge barrier comes as no surprise. Moreover, this transformation is strongly endergonic seeing **M6a** by 25.7 kcal mol⁻¹ uphill in free energy. Thus, DFT predicts that amine N–H oxidative addition is challenging energetically on both kinetic and thermodynamic considerations. The highly demanding energy profile is not compatible with the observed hydroamination catalysis, thereby leading us to conclude that oxidative amine addition is not viable. This already renders the amine activation route as being almost impossible to traverse by use of [Ir(COD)Cl]₂ as a pre-catalyst.

(C2) Association of the Olefin Unit to the Ir^{III} Center in M6. Commencing from Ir^{III}-amido-hydrido intermediate **M6a** with a $\eta^1(\text{N})$ -Ir ligated amidoalkene, the double bond can approach the metal center at its remaining vacant coordination site, thereby giving rise to the six-coordinate Ir^{III}- $\eta^2(\text{C},\text{N})$ -amido-hydrido intermediate **M6'**. Following this process in a linear-transit approach gave no indication of the existence of a substantial enthalpy barrier. Hence, double bond complexation is likely facile kinetically, but comes at some thermodynamic cost. The various positional isomers are shown in Figure S17, all of which are higher in free energy by $\Delta G = 11.0$ (**M6'a**), 14.8 (**M6'b**) and 4.2 (**M6'c**) kcal mol⁻¹, respectively, relative to **M6a**. All these isomers can be assumed to readily interconvert, since the barriers for interconversion via *Berry* pseudorotation are generally considered to be low.

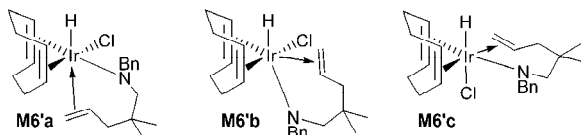


Figure S17. Positional isomers of the six-coordinate Ir^{III}-amido-hydrido intermediate **M6'**.

(C3) Ring Closure by Insertion of the Double Bond into the Ir-N bond in M6' and ensuing C–H Reductive Elimination. Insertion of the double bond into the Ir^{III}-amido bond under ring closure can be achieved for all isomers **M6'a**–**M6'c**, giving rise to the six-coordinate Ir^{III}-azacycle-hydrido intermediate **M7** (Figure S18). Table S8 collects the energy profile for the various pathways. Ring closure in **M6'** through C–N bond formation has a moderate barrier of 10.7 kcal mol⁻¹ and is strongly exergonic. The pathway that involves the thermodynamically favorable precursor **M6'c** is predicted to be most accessible on both thermodynamic and kinetic grounds.

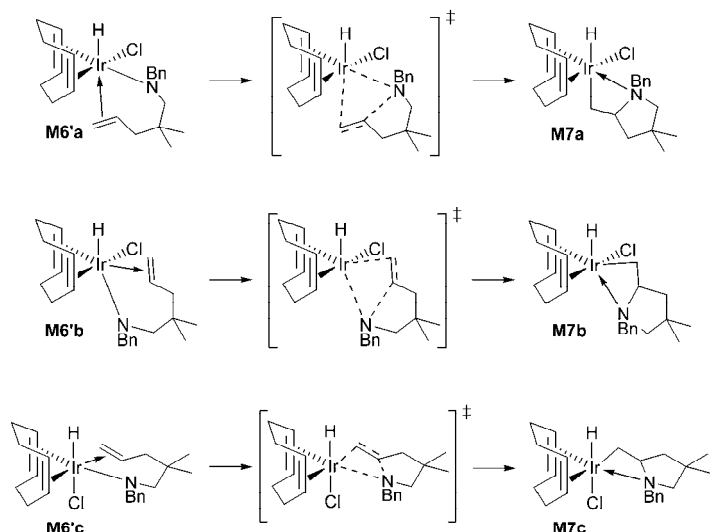
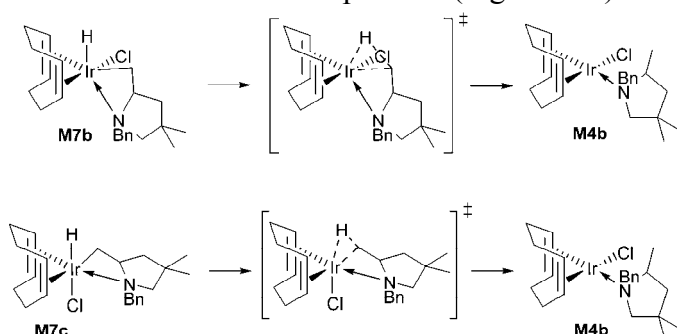


Figure S18. Olefin insertion into the Ir^{III}-N bond in **M6'** with ring closure.

Table S8. Free-energy profile for olefin insertion into the Ir^{III}–N bond of **M6'** (in kcal mol⁻¹, relative to **M6a**)

	precursor	TS	product
M6'a → M7a	11.0 (M6'a)	17.6	-7.3 (M7a)
M6'b → M7b	14.8 (M6'b)	17.4	-10.0 (M7b)
M6'c → M7c	4.2 (M6'c)	10.7	-14.5 (M7c)

Intermediate **M7** undergoes thereafter C–H reductive elimination to furnish the Ir^I–η¹(N)-cycloamine complex **M4b**. Incoming substrate expels the pyrrolidine **6a** from the immediate proximity of the Ir center and regenerates the catalytically competent compound **M1b** (see above). C–H reductive elimination requires that H and tether-C¹ centers are mutually *cis*, which is met for **M7b** and **M7c**. Accordingly, **M7a** needs to undergo ligand interconversion before reductive elimination can proceed (Figure S19).

**Figure S19.** C–H Reductive elimination from **M7**.**Table S9.** Free-energy profile for C–H reductive elimination from **M7** (in kcal mol⁻¹, relative to **M7c**)

	precursor	TS	product
M7b → M4b	4.5 (M7b)	20.1	-9.5 (M4b)
M7c → M4b	0.0 (M7c)	18.9	-9.5 (M4b)

As revealed from Table S9, intermediate **M7c** formed via the most accessible pathway for ring closure also participates in the favourable pathway for subsequent reductive elimination. The latter requires overcoming a barrier of 18.9 kcal mol⁻¹ and formation of **M4b** is driven by a thermodynamic force of 9.5 kcal mol⁻¹. The overall **M6a** → **M4b** transformation to follow the most accessible path via initial C–N bond formation involves the **M6a** → **M6'c** → **M7c** → **M4b** sequence of steps. This conversion is strongly downhill by 24.0 kcal mol⁻¹, thus reflecting that **M6a** is a high-energy intermediate.

(C4) *Insertion of the Double Bond into the Ir–H bond of **M6'** and Subsequent Reductive Elimination under Ring Closure.* The alternative route toward **M4b** starts with the insertion of the double bond into the Ir^{III}–H bond in **M6'**. This can be achieved only from isomers **M6'b** and **M6'c** (Fig. S20), the energy profile of which is summarized in Table S10. The favorable pathway for formation of Ir^{III}-cycloamido(alkyl tether) intermediate

M8 commences from **M6'b** and proceeds through a quasi-planar four-membered TS structure constituting olefin insertion into the Ir–H bond. It possesses a very small intrinsic barrier of only 1.6 kcal mol⁻¹ (relative to **M6'b**) and gives rise to **M8b**, which can convert readily into the more stable **M8a** thereafter. The alternative **M6'c** → **M8c** pathway is seen to be kinetically inaccessible as the involved non-planar TS does not benefit from the optimal overlap between reacting units, as TS[**M6'b**–**M8b**] does. One can expect the barriers for the interconversion of the various positional isomers of **M8** via *Berry* pseudorotation to be small.

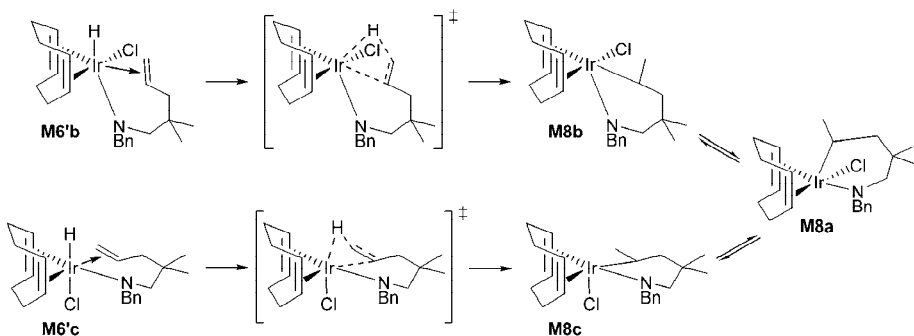


Figure S20. Olefin insertion into the Ir–H bond in **M6'**.

Table S10. Free-energy profile for olefin insertion into the Ir^{III}–H bond in **M6'** (in kcal mol⁻¹, relative to **M6a**)

	precursor	TS	product
M6'b → M8b	14.8 (M6'b)	16.4	10.4 (M8b) -1.1 (M8a)
M6'c → M8c	4.2 (M6'c)	43.3	5.8 (M8c) -1.1 (M8a)

Subsequent ring closure by C–N reductive elimination has been studied for pathways that commence from **M8b** and **M8a** (Figure S21). Examination of the reaction path for **M8c** revealed some positional reorganizations were happening at early stages, such that this TS structure is identical to one traversed along **M8a** → **M4b**. Ring closure via C–N reductive elimination is highly facile when traversing the most accessible **M8a** → **M4b** pathway, giving rise to **M4b** in a transformation that is strongly downhill (Table S11). The alternative route towards **M4b** that starts with olefin insertion into the Ir^{III}–H bond of **M6'** hence involves the **M6a** → **M6'b** → **M8b** → **M8a** → **M4b** sequence of steps.

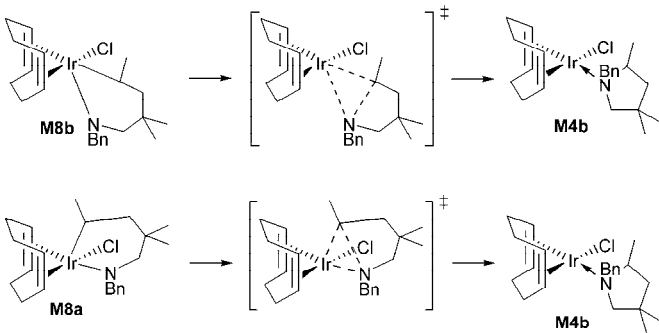


Figure S21. C–H Reductive elimination from **M8**.

Table S11. Free-energy profile for C–N reductive elimination with ring closure from **M8** (in kcal mol^{−1}, relative to **M8a**)

	precursor	TS	product
M8b → M4b	11.5 (M8b)	35.9	−23.0 (M4b)
M8a → M4b	0.0 (M8a)	7.0	−23.0 (M4b)

Comparison of alternative **M6a** → **M6'c** → **M7c** → **M4b** and **M6a** → **M6'b** → **M8b** → **M8a** → **M4b** routes towards Ir^I–cycloamine compound **M4b**, leads us to the following conclusions:

- the first **M6'c** → **M7c** and **M6'b** → **M8b** steps determine at which probability the two routes are traversed
- the double bond inserts preferably into the Ir^{III}–N bond in **M6'** rather than into the Ir^{III}–H bond on both kinetic and thermodynamic grounds
- accordingly, **M6a** → **M6'c** → **M7c** → **M4b** (+ **5a**) → **6a** (+ **M1b**) is the dominant route for the generation of pyrrolidine **6a**, which is almost exclusively traversed ($\Delta\Delta G^\ddagger = 5.7$ kcal mol^{−1})

Computational Details

All calculations have been performed with the program package TURBOMOLE¹ using Kohn-Sham density functional theory² (DFT). The almost nonempirical meta-GGA Tao–Perdew–Staroverov–Scuseria (TPSS)³ was employed within the RI-J approximation⁴ in conjunction with flexible basis sets of triple- ζ quality. For iridium we used the Stuttgart–Dresden scalar-relativistic effective core potential (SDD, 60 core electrons)⁵ in combination with the (8s7p6d1f)/[6s5p3d1f] (def2-TZVP) valence basis set.⁶ All remaining elements were represented by Ahlrich's valence triple- ζ TZVP basis set⁷ with polarization functions on all atoms. The good to excellent performance of the TPSS functional for a wide range of applications, with transition-metal complexes in particular, has been demonstrated previously.⁸ In view of the fact that all species investigated in this study show a large HOMO–LUMO gap, a spin-restricted formalism was used for all the calculations.

All stationary points were located by utilizing analytical gradients/Hessians according to standard algorithms without imposing any symmetry constraints and were identified exactly by the curvature of the potential-energy surface at these points corresponding to the eigenvalues of the Hessian. All reported transition states possess

exactly one negative Hessian eigenvalue, while all other stationary points exhibit exclusively positive eigenvalues. The many isomers that are possible for each of the investigated species were carefully explored. It has been explicitly scrutinized for each of the individual steps as to whether additional substrate molecules, which are present in excess, are likely serving to facilitate the elementary process.

The reaction and activation enthalpies and free energies for gas-phase conditions (ΔH , ΔH^\ddagger and ΔG , ΔG^\ddagger at 298 K and 1 atm) were evaluated according to standard textbook procedures⁹ using computed harmonic frequencies. The frequency analysis was performed for stationary points that were located for gas-phase conditions with an alternative basis set, consisting of the aforementioned basis for Ir and of Ahlrichs' split-valence SV(P) basis set^{7c} with polarisation functions on main group atoms, but not on hydrogen. This level of basis-set quality has been identified as a reliable tool for the assessment of structural parameters and vibrational frequencies,¹⁰ thus this strategy allows an affordable and accurate determination of thermodynamic state functions. Enthalpies were reported as $\Delta E +$ zero point energy corrections at 0 K + thermal motion corrections at 298 K and Gibbs free-energies were obtained as $\Delta G = \Delta H - T\Delta S$ at 298 K.

The influence of nonspecific solute–solvent interactions¹¹ on both geometries and reaction energetics has been estimated for 1,4-dioxane (dielectric constant $\epsilon = 2.2099$ at 298 K)¹² by employing the conductor-like screening model (COSMO) due to Klamt and Schüürmann¹³ as implemented in TURBOMOLE.¹⁴ As aforementioned, the complexation of excess solvent molecules has been probed explicitly for each of the key stationary species. The solvent excluding surface was used along with $\epsilon = 2.21$ and nonelectrostatic contributions to solvation were not considered. The solvation effects were included selfconsistently in the calculations, and all key stationary species were fully optimised in the presence of the bulk solvent. The optimised atomic COSMO radii ($r_H = 1.3$ Å, $r_C = 2.0$ Å, $r_N = 1.83$ Å, $r_{Cl} = 2.05$ Å)¹⁵ have been used, in combination with the a radius of 2.223 Å for Ir. Although the Born energy reported by the COSMO model is, in a strict sense, a free energy, the entropy contributions accounts to only a very small fraction (~2%) of the total energy.¹⁶ The solvation enthalpy was approximated by the difference between the electronic energy computed using the COSMO solvation model and the gas-phase energy. As an alternative, $H_{\text{solution}}(T)$ can be obtained from the same functional form as for $H_{\text{gas}}(T)$, but with the inertia moments and vibrational frequencies modified by solvation.¹⁷ This gave almost identical results with an enthalpy disparity of typically less than 1 kcal mol⁻¹, but at drastically increased computational costs. The entropy contributions for condensed-phase conditions were estimated based on the computed gas-phase entropies by employing the procedure of Wertz.¹⁸ According to this three step procedure, the solute in gas phase is first compressed to the molar volume of the solvent. The associated change in solute entropy is given by $\Delta S = R \ln(V_{m,f}/V_{m,i})$, where $V_{m,i}$ and $V_{m,f}$ are the solute molar volumes at initial and final stage; thus $\Delta S_1 = R \ln(V_{m,lig}/V_{m,gas})$ for the first step. The compressed solute then loses the same fraction of its entropy, which would be lost upon transfer from gas to liquid when the two phases have the same density, namely that of the liquid. The entropy fraction α lost here is given by $\alpha = (S_{\text{liq}}^\circ - S_{\text{gas,ligdens}})/S_{\text{gas,ligdens}}$, where the entropy of gaseous solvent at the same density as the liquid $S_{\text{gas,ligdens}}$ can be obtained from $S_{\text{gas}}^\circ + R \ln(V_{m,lig}/V_{m,gas})$. In a third step, the solute gas is expanded from the molar volume of the liquid solvent to the density of a standard solution of 1.0 L mol⁻¹, with $\Delta S_3 = R \ln(V_{m,1M}/V_{m,lig})$. Taking the experimental data for THF,^{12,19} the entropy fraction lost in the second step amounts to $\alpha = -0.198$. On assumption that all solute molecules lose the same fraction of their entropy when transferred from gas to liquid,

some simple algebraic transformation leads to the solvation entropy as given by the sum of the entropy changes associated with each of the three steps, *viz.* $\Delta S_{\text{solv}} = \Delta S_1 + \alpha(S_{\text{gas}}^\circ + \Delta S_1) + \Delta S_3$. Thus, for THF solvent at 298 K one obtains $\Delta S_{\text{solv}} = -0.198S_{\text{gas}} - 4.105$ eu. Accordingly, the procedure proposed by Wertz gives rise to the following estimate for the total solute entropy (again for benzene solvent at 298 K) as expressed in terms of the gas-phase entropy:

$$S_{\text{sol}} = 0.802 S_{\text{gas}} - 4.105 \text{ eu} \quad (1)$$

Although somehow empirical, the Wertz procedure provides a reasonable estimate of the entropy of a molecule in condensed phase, which is known to be less than its entropy in gaseous phase,^{18,20} that may be used in a somewhat pragmatic way in the absence of reliable alternatives that are affordable. Noteworthy, this procedure has been successfully applied in several cases.²¹ The strict treatment of the free-energy in condensed phase, for instance by applying non-empirical MD simulation techniques, is currently too expensive to be carried out for a mechanistic scenario as diverse as explored herein and taking the size of the employed catalyst model also into account; this is likely to remain so in the foreseeable future.

References to Computational Section

- (1) (a) Ahlrichs, R.; Bär, M.; Häser, M.; Horn, H.; Kölmel, C. *Chem. Phys. Lett.* **1989**, *162*, 165. (b) Treutler, O.; Ahlrichs, R. *J. Chem. Phys.* **1995**, *102*, 346. (c) Ahlrichs, R.; Furche, F.; Hättig, C.; Klopper, W.; Sierka, M.; Weigend, F. *TURBOMOLE, version 6.0*; University of Karlsruhe: Karlsruhe, Germany, 2009; <http://www.turbomole.com>.
- (2) Parr, R. G.; Yang, W. *Density-Functional Theory of Atoms and Molecules*, Oxford University Press, 1989.
- (3) (a) Dirac, P. A. M. *Proc. Royal Soc. (London)* **1929**, *A123*, 714. (b) Slater, J. C. *Phys. Rev.* **1951**, *81*, 385. (c) Perdew, J. P.; Wang, Y. *Phys. Rev.* **1992**, *B45*, 13244. (d) Tao, J.; Perdew, J. P.; Staroverov, V. N.; Scuseria, G. E. *Phys. Rev. Lett.* **2003**, *91*, 146401. (e) Perdew, J. P.; Tao, J.; Staroverov, V. N.; Scuseria, G. E. *J. Chem. Phys.* **2004**, *120*, 6898.
- (4) (a) Vahtras, O.; Almlöf, J.; Feyereisen, M. W. *Chem. Phys. Lett.* **1993**, *213*, 514. (b) Eichkorn, K.; Treutler, O.; Öhm, H.; Häser, M.; Ahlrichs, R. *Chem. Phys. Lett.* **1995**, *242*, 652.
- (5) Andrea, D.; Häußermann, U.; Dolg, M.; Stoll, H.; Preuß, H. *Theor. Chim. Acta* **1990**, *77*, 123.
- (6) (a) Weigend, F.; Ahlrichs, R.; *Phys. Chem. Chem. Phys.* **2005**, *7*, 3297. (b) Weigend, F. *Phys. Chem. Chem. Phys.* **2006**, *8*, 1057.
- (7) (a) Schäfer, A.; Huber, C.; Ahlrichs, R. *J. Chem. Phys.* **1994**, *100*, 5829. (b) Eichkorn, K.; Weigend, F.; Treutler, O.; Ahlrichs, R. *Theor. Chem. Acc.* **1997**, *97*, 119. (c) Schäfer, A.; Huber, C.; Ahlrichs, R. *J. Chem. Phys.* **1992**, *97*, 2571.
- (8) Staroverov, V. N.; Scuseria, G. E.; Tao, J.; Perdew, J. P. *J. Chem. Phys.* **2003**, *119*, 12129. (b) Zao, Y.; Truhlar, D. G. *J. Chem. Theory Comput.* **2005**, *1*, 415. (c) Furche, F.; Perdew, J. P. *J. Chem. Phys.* **2006**, *124*, 044103.
- (9) McQuarrie, D. A. *Statistical Thermodynamics*, Harper & Row, New York, 1973.
- (10) Koch, W.; Holthausen, M. C. *A Chemist's Guide to Density Functional Theory*, 2nd Ed., Wiley-VCH, Weinheim, 2001.
- (11) (a) Tomasi, J.; Persico, M. *Chem. Rev.* **1994**, *94*, 2027. (b) Cramer, C. J.; Truhlar, D. G. *Chem. Rev.* **1999**, *99*, 2161. (c) Cramer, C. J. *Essentials of Computational Chemistry: Theories and Models*; John Wiley & Sons : Chichester, U. K.; U.K., 2002, pp 347–383.
- (12) *CRC Handbook of Chemistry and Physics*, Lide, D. R., Ed. 84th ed. CRC Press, New York, 2003–2004.
- (13) (a) Klamt, A.; Schüürmann, G. *J. Chem. Soc. Perkin Trans. 2* **1993**, 799. (b) Klamt, A. In *Encyclopedia of Computational Chemistry*, Schleyer, P. v. R. et al., Eds.; John Wiley, & Sons: Chichester, 1998; Vol. 1, pp. 604 –615.

- (14) Schäfer, A.; Klamt, A.; Sattel, D.; Lohrenz, J. C. W.; Eckert, F. *Phys. Chem. Chem. Phys.* **2000**, *2*, 2187.
(15) Klamt, A.; Jonas, V.; Bürger, Th.; Lohrenz, J. C. W. *J. Phys. Chem. A* **1998**, *102*, 5074.
(16) Dasent, W. E. *Inorganic Energetics*, Penguin, Middlesex, UK, 1970.
(17) Klamt, A. *J. Phys. Chem.* **1996**, *100*, 3349.
(18) Wertz, D. H. *J. Am. Chem. Soc.* **1980**, *102*, 5316.
(19) Unfortunately, experimental entropy data have not been reported for 1,4-dioxane, but for THF, which can reasonably be regarded as an appropriate substitution.
(20)(a) Cabani, V.; Gianni, P.; Mollica, V.; Lepori, L. *J. Solution Chem.* **1981**, *10*, 563. (b) Wagman, D. D.; Evans, W. H.; Parker, V. B.; Schumm, R. H.; Halow, I.; Bailey, S. M.; Churney, K. L.; Nuttall, R. L. *J. Phys. Ref. Data* **1982**, *11*, Supplement No. 2. (c) Ben-Naim, A.; Marcus, Y. *J. Chem. Phys.* **1984**, *81*, 2016. (d) Okuno, Y. *Chem. Eur. J.* **1997**, *3*, 212. (e) Fawcett, W. R. *J. Phys. Chem. B* **1999**, *103*, 11181.
(21)(a) Williams, I. H.; Spangler, D.; Femec, D. A.; Maggiora, G. M.; Schowen, R. L. *J. Am. Chem. Soc.* **1983**, *105*, 31. (b) Williams, I. H. *J. Am. Chem. Soc.* **1987**, *109*, 6299. (c) Wolfe, S.; Kim, Ch-K.; Yang, K.; Weinberg, N.; Shi, Z. *J. Am. Chem. Soc.* **1995**, *117*, 4240. (d) Cooper, J.; Ziegler, T. *Inorg. Chem.* **2002**, *41*, 6614. (e) Hristov, I. H.; Ziegler, T. *Organometallics* **2003**, *22*, 3515. (f) Lau, J. K.-C.; Deubel, D. V. *Chem. Eur. J.* **2005**, *11*, 2849. (g) Lin, S.-T.; Maiti, P. K.; Goddard, III, W. A. *J. Phys. Chem. B* **2005**, *109*, 8663. (f) Zhu, H.; Ziegler, T. *J. Organomet. Chem.* **2006**, *691*, 4486. (h) Lau, J. K.-C.; Deubel, D. V. *J. Chem. Theory Comp.* **2006**, *2*, 103. (i) Deubel, D. V. *J. Am. Chem. Soc.* **2006**, *128*, 1654.

Optimized structures and total electronic energies (hartree) of all species reported.

M1a			M1b			M1c			
E = -1478.097831 au			E = -1478.088117 au			E = -1478.081283 au			
Ir	-0,0789	-1,1399	-0,1405	Ir	0,2374	0,0155	0,1496	Ir	-0,1465
C	-1,6319	-0,9321	1,3227	C	-1,1825	0,7103	1,5450	C	-1,5755
C	-1,3080	-2,3116	1,1935	C	-1,2854	-0,7158	1,4263	C	-1,6834
C	-2,2309	-3,3245	0,5150	C	-2,4319	-1,4134	0,6897	C	-2,8320
C	-1,8367	-3,5377	-0,9582	C	-2,0610	-1,7056	-0,7824	C	-2,4661
C	-1,1953	-2,2941	-1,5482	C	-1,0919	-0,6821	-1,3486	C	-1,5370
C	-1,7585	-0,9653	-1,4681	C	-1,2312	0,7287	-1,2297	C	-1,6833
C	-3,0910	-0,6829	-0,7612	C	-2,4305	1,3978	-0,5595	C	-2,8564
C	-2,8937	-0,3164	0,7299	C	-2,1508	1,7076	0,9288	C	-2,5299
H	-1,2498	-0,4266	2,2130	H	-0,6990	1,0882	2,4509	H	-1,0629
H	-0,6724	-2,7260	1,9752	H	-0,8627	-1,3014	2,2485	H	-1,2276
H	-0,5731	-2,4881	-2,4212	H	-0,4865	-1,0437	-2,1798	H	-0,9092
H	-1,5369	-0,3183	-2,3171	H	-0,7138	1,3310	-1,9759	H	-1,1849
H	-2,1795	-4,2736	1,0602	H	-2,6714	-2,3534	1,1995	H	-3,0735
H	-3,2678	-2,9791	0,5948	H	-3,3348	-0,7952	0,7448	H	-3,7318
H	-1,1052	-4,3513	-1,0217	H	-1,5753	-2,6864	-0,8426	H	-1,9631
H	-2,7069	-3,8515	-1,5566	H	-2,9666	-1,7666	-1,4062	H	-3,3757
H	-3,6003	0,1449	-1,2674	H	-2,6654	2,3284	-1,0876	H	-3,0994
H	-3,7602	-1,5467	-0,8563	H	-3,3133	0,7564	-0,6570	H	-3,7475
H	-2,8215	0,7738	0,8279	H	-1,6953	2,7016	1,0087	H	-2,0549
H	-3,7679	-0,6116	1,3320	H	-3,0909	1,7465	1,5015	H	-3,4535
Cl	1,4156	-0,6696	-2,0077	C	2,9394	-2,1147	2,9154	C	7,7419
N	0,2455	1,1652	0,3003	C	2,1799	-1,6598	1,6855	C	6,6636
C	1,6669	1,6092	0,4351	N	1,7510	-0,2014	1,7301	N	5,6432
C	2,4790	0,9384	1,5587	C	2,9662	0,6903	1,7337	C	4,5411
C	2,7481	-0,5536	1,2433	H	1,2728	-0,0683	2,6267	H	5,2712
C	1,5517	-1,4765	1,3079	C	2,7416	2,1510	2,1877	C	3,5115
C	1,4246	-2,6095	0,4560	H	3,7040	0,2353	2,4072	H	4,0040
H	1,6726	2,6952	0,6033	H	3,3577	0,6676	0,7128	H	4,9873
C	3,8396	1,6674	1,5928	C	4,1842	2,7516	2,2779	C	2,4207
C	1,7919	1,1156	2,9263	C	1,9155	2,9412	1,1605	C	4,1945
H	3,5007	-0,9118	1,9653	C	2,0733	2,1959	3,5759	C	2,8934
H	3,2026	-0,6196	0,2478	C	4,2547	4,2062	2,6528	C	1,3004
H	2,1403	1,4052	-0,5299	H	4,7435	2,1659	3,0235	H	2,0012
H	1,1132	-1,5709	2,3044	H	4,6823	2,6056	1,3107	H	2,9072
H	0,9754	-3,5295	0,8203	C	4,7775	5,1652	1,8841	C	1,2605
H	2,1317	-2,7359	-0,3600	H	3,8650	4,4777	3,6347	H	0,7037
C	-0,4663	2,0122	-0,7203	H	4,8185	6,2007	2,2132	H	0,6848
H	-0,2150	1,3126	1,2004	H	5,1864	4,9470	0,8990	H	2,0276
H	1,6271	2,1779	3,1450	C	2,2694	-2,2868	4,1365	C	8,4805
H	0,8244	0,6015	2,9750	C	4,3303	-2,9598	5,2101	C	9,7499
H	2,4191	0,7004	3,7242	C	4,3138	-2,3838	2,8591	C	8,0205
H	4,3574	1,5739	0,6309	C	5,0058	-2,8042	3,9978	C	9,0190
H	3,7127	2,7344	1,8126	H	6,0713	-3,0099	3,9374	H	9,2225
H	4,4822	1,2338	2,3679	H	4,8437	-2,2662	1,9165	H	7,4512
H	0,0339	1,8249	-1,6736	C	2,9582	-2,7011	5,2773	C	9,4761
H	-1,4832	1,6227	-0,7948	H	1,1967	-2,1073	4,1955	H	8,2620
C	-0,4980	3,4954	-0,4013	H	4,8674	-3,2867	6,0966	H	10,5266
C	-1,2834	3,9793	0,6564	H	2,4239	-2,8326	6,2147	H	10,0428
C	-0,5760	6,2460	0,1923	H	2,6386	1,6093	4,3111	H	2,4259
C	0,2397	4,4127	-1,1613	H	1,0465	1,8125	3,5441	H	3,6544
C	0,2017	5,7785	-0,8690	H	2,0064	3,2259	3,9405	H	2,1299
H	0,7795	6,4763	-1,4696	H	0,9433	2,4605	0,9841	H	5,0304
H	0,8466	4,0529	-1,9895	H	2,4355	2,9860	0,1975	H	4,5879
C	-1,3206	5,3419	0,9556	H	1,7445	3,9656	1,5095	H	3,4903
H	-1,8799	3,2868	1,2489	H	1,2639	-2,2434	1,5639	H	7,1023
H	-0,6068	7,3080	0,4213	H	2,7777	-1,7731	0,7789	H	6,2308
H	-1,9367	5,7001	1,7764	Cl	1,9975	0,0346	-1,4710	Cl	1,4934

C	3,0670	5,4782	2,9783	O	-1,6397	-2,7093	-4,3030	O	-0,4578	-2,4928	-5,1533
H	2,5689	6,2881	1,1161	C	-0,2020	-2,6071	-4,4007	C	0,8706	-2,5299	-4,5919
H	3,0608	6,4373	3,4906	C	0,2031	-2,0443	-5,7550	C	1,8837	-1,9542	-5,5709
H	3,3062	4,6025	3,5793	O	-0,3968	-0,7481	-5,9711	O	1,5393	-0,5969	-5,9193
C	-0,3773	3,3231	-3,8607	C	-1,8288	-0,8467	-5,8588	C	0,2070	-0,5522	-6,4654
C	0,8516	4,9658	-5,1436	C	-2,2280	-1,4113	-4,5013	C	-0,8012	-1,1330	-5,4833
C	2,0251	3,1873	-3,9972	H	0,1865	-3,6211	-4,2711	H	1,0857	-3,5824	-4,3844
C	2,0456	4,3242	-4,8092	H	0,1774	-1,9656	-3,5926	H	0,8858	-1,9588	-3,6521
H	2,9924	4,7043	-5,1844	H	-0,1139	-2,7283	-6,5583	H	1,9154	-2,5685	-6,4851
H	2,9583	2,6839	-3,7523	H	1,2846	-1,8980	-5,8011	H	2,8792	-1,9176	-5,1205
C	-0,3623	4,4596	-4,6696	H	-2,2178	-1,4939	-6,6612	H	0,1790	-1,1175	-7,4110
H	-1,3297	2,9307	-3,5075	H	-2,2196	0,1667	-5,9932	H	-0,0064	0,5014	-6,6689
H	0,8641	5,8480	-5,7780	H	-1,8996	-0,7322	-3,6991	H	-0,8282	-0,5272	-4,5649
H	-1,2968	4,9453	-4,9388	H	-3,3117	-1,5496	-4,4397	H	-1,8012	-1,1679	-5,9260
H	1,7071	4,9718	-1,4971	O	1,0828	3,6727	-2,7988	O	2,4093	3,9241	-2,9917
H	0,0277	4,4899	-1,2182	C	0,6004	2,5251	-3,5349	C	2,0781	2,7096	-3,7004
H	0,7626	5,7098	-0,1829	C	1,2970	2,4193	-4,8840	C	3,2715	2,2114	-4,5030
H	-0,5675	3,1450	0,9574	O	2,7279	2,3317	-4,7132	O	4,4067	1,9842	-3,6378
H	0,7206	2,7394	2,0913	C	3,2047	3,4726	-3,9784	C	4,7335	3,1954	-2,9328
H	0,2146	4,4356	1,8904	C	2,5097	3,5727	-2,6267	C	3,5368	3,6920	-2,1313
H	0,0191	0,7544	-2,9608	H	-0,4750	2,6781	-3,6647	H	1,2426	2,9605	-4,3596
H	1,7547	0,9307	-2,7062	H	0,7693	1,6137	-2,9438	H	1,7556	1,9409	-2,9828
				H	1,0579	3,2999	-5,5016	H	3,5452	2,9523	-5,2705
				H	0,9896	1,5096	-5,4060	H	3,0435	1,2550	-4,9802
				H	3,0227	4,3908	-4,5599	H	5,0467	3,9683	-3,6524
				H	4,2829	3,3327	-3,8543	H	5,5733	2,9539	-2,2741
				H	2,7461	2,6878	-2,0154	H	3,2690	2,9492	-1,3626
				H	2,8204	4,4760	-2,0933	H	3,7606	4,6485	-1,6489

O	-3.6765	-1.8935	2.7803	O	4.6555	-2.8401	-4.0434
C	-3.7538	-0.5916	3.4091	C	4.7856	-3.0177	-2.6111
C	-4.0544	-0.7355	4.8947	C	6.1043	-2.4350	-2.1252
O	-3.0609	-1.5503	5.5532	O	6.2057	-1.0334	-2.4613
C	-2.9599	-2.8298	4.9046	C	6.0690	-0.8646	-3.8834
C	-2.6400	-2.6587	3.4256	C	4.7464	-1.4437	-4.3693
H	-4.5692	-0.0608	2.9078	H	4.7522	-4.0970	-2.4366
H	-2.8094	-0.0537	3.2444	H	3.9379	-2.5469	-2.0931
H	-5.0477	-1.1931	5.0345	H	6.9516	-2.9757	-2.5767
H	-4.0257	0.2402	5.3870	H	6.1776	-2.4908	-1.0357
H	-3.9079	-3.3812	5.0215	H	6.9061	-1.3642	-4.3973
H	-2.1623	-3.3735	5.4205	H	6.1195	0.2122	-4.0728
H	-1.6770	-2.1396	3.3065	H	3.9092	-0.8980	-3.9063
H	-2.6073	-3.6288	2.9187	H	4.6655	-1.3733	-5.4585
O	2.1515	-0.8867	5.6118	O	3.7885	0.9234	2.3499
C	0.7248	-0.9743	5.8312	C	4.2175	0.5755	1.0109
C	0.3251	-0.1149	7.0216	C	5.7345	0.4655	0.9544
O	0.6938	1.2637	6.8082	O	6.2134	-0.5232	1.8912
C	2.1024	1.3631	6.5281	C	5.7700	-0.1936	3.2194
C	2.4884	0.4894	5.3409	C	4.2513	-0.0817	3.2714
H	0.5082	-2.0290	6.0269	H	3.8696	1.3852	0.3619
H	0.1991	-0.6441	4.9251	H	3.7405	-0.3665	0.7045
H	0.8172	-0.4862	7.9359	H	6.1918	1.4398	1.1926
H	-0.7592	-0.1250	7.1608	H	6.0647	0.1406	-0.0359
H	2.6772	1.0571	7.4182	H	6.2254	0.7592	3.5354
H	2.2986	2.4194	6.3190	H	6.1264	-0.9968	3.8719
H	1.9646	0.8176	4.4312	H	3.7933	-1.0494	3.0200
H	3.5707	0.5172	5.1781	H	3.9181	0.2321	4.2657
O	1.9228	-1.1846	-3.5786	O	-1.4801	-0.1635	-1.9166
C	2.7320	-2.1732	-4.3009	C	-0.7680	-1.3959	-2.3457
C	3.8187	-1.4720	-5.1005	C	0.5187	-1.0222	-3.0567
O	3.2583	-0.5586	-6.0548	O	0.2632	-0.1702	-4.1952
C	2.4582	0.4098	-5.3609	C	-0.3700	1.0275	-3.7420
C	1.3504	-0.2662	-4.5688	C	-1.6975	0.7184	-3.0702
H	3.1746	-2.8280	-3.5538	H	-0.5277	-1.9513	-1.4379
H	2.0709	-2.7505	-4.9585	H	-1.4456	-1.9578	-2.9990
H	4.4999	-0.9352	-4.4230	H	1.2063	-0.5358	-2.3538
H	4.3872	-2.2123	-5.6697	H	0.9946	-1.9289	-3.4337
H	3.0935	1.0123	-4.6946	H	0.2909	1.5671	-3.0457
H	2.0191	1.0593	-6.1230	H	-0.5491	1.6517	-4.6223
H	0.6942	-0.8380	-5.2355	H	-2.3739	0.2156	-3.7719
H	0.7676	0.4613	-4.0065	H	-2.1620	1.6221	-2.6737

	M2c			TS[M2b–M4a]			M4a		
	E = -1478.081698 au			E = -1478.011876 au			E = -1478.079522 au		
Ir	-0,4443	-1,0237	0,2447	Ir	-1,4972	-0,3685	-0,6231	Ir	-1,3885
C	-1,7613	-1,8549	1,6438	C	-2,7164	-1,2640	0,8407	C	-2,7597
C	-1,9919	-0,4401	1,5570	C	-3,0652	0,1206	0,7179	C	-2,9634
C	-3,2174	0,1688	0,8697	C	-4,3458	0,5991	0,0288	C	-4,1528
C	-2,9259	0,5263	-0,6062	C	-4,0948	0,9315	-1,4607	C	-3,7896
C	-1,9014	-0,4023	-1,2353	C	-2,9865	0,0823	-2,0599	C	-2,7475
C	-1,9257	-1,8149	-1,1574	C	-2,8860	-1,3354	-1,9374	C	-2,7877
C	-3,0257	-2,5980	-0,4450	C	-3,9212	-2,1857	-1,2046	C	-3,9404
C	-2,6478	-2,9219	1,0215	C	-3,5281	-2,4177	0,2740	C	-3,6492
H	-1,2163	-2,2043	2,5247	H	-2,1208	-1,5434	1,7143	H	-2,2196
H	-1,5955	0,1592	2,3799	H	-2,6966	0,7876	1,5003	H	-2,5513
H	-1,3557	0,0290	-2,0754	H	-2,4923	0,5287	-2,9238	H	-2,1783
H	-1,3862	-2,3589	-1,9326	H	-2,3116	-1,8515	-2,7061	H	-2,2419
H	-3,5229	1,0733	1,4090	H	-4,7228	1,4906	0,5422	H	-4,4691
H	-4,0622	-0,5258	0,9362	H	-5,1259	-0,1645	0,1264	H	-5,0043
H	-2,5200	1,5448	-0,6515	H	-3,7864	1,9802	-1,5464	H	-3,3726
H	-3,8607	0,5398	-1,1899	H	-5,0240	0,8307	-2,0433	H	-4,6874
H	-3,2093	-3,5344	-0,9841	H	-4,0164	-3,1531	-1,7099	H	-4,0946
H	-3,9654	-2,0354	-0,4791	H	-4,9041	-1,7054	-1,2669	H	-4,8675
H	-2,0887	-3,8655	1,0457	H	-2,9090	-3,3200	0,3419	H	-3,1254
H	-3,5538	-3,0814	1,6286	H	-4,4237	-2,6059	0,8878	H	-4,5865
Cl	1,2713	-0,9625	-1,4953	Cl	0,1985	-0,2520	-2,3235	Cl	0,3519
N	2,2902	0,9669	0,7262	N	2,3177	0,8130	1,1670	N	2,5456
C	3,7281	1,3881	0,6064	C	2,8303	1,9014	2,0564	C	3,8984
C	4,5662	0,0864	0,7776	C	1,9293	3,1317	1,7793	C	3,6612
C	3,5330	-0,9519	1,3189	C	0,5727	2,4571	1,4592	C	2,3445
C	2,2991	-0,1689	1,7771	C	0,9171	1,2235	0,6239	C	1,8563
C	0,9791	-0,9322	1,8588	C	0,1337	-0,0410	0,9579	C	0,3349
H	3,9172	2,0985	1,4166	H	3,8904	2,0906	1,8619	H	4,4873
C	5,1527	-0,3717	-0,5700	C	1,8464	4,0515	3,0054	C	3,4391
C	5,7015	0,3360	1,7872	C	2,4443	3,9253	0,5623	C	4,8344
H	3,9413	-1,5387	2,1472	H	-0,1127	3,1228	0,9266	H	2,5088
H	3,2332	-1,6425	0,5243	H	0,0874	2,1507	2,3950	H	1,5921
H	3,8789	1,8912	-0,3501	H	2,7270	1,5772	3,0977	H	4,4301
H	2,5239	0,3639	2,7125	H	0,9826	1,4327	-0,4451	H	2,1692
H	0,4479	-0,6116	2,7678	H	-0,4620	-0,0433	1,8674	H	-0,1231
H	1,2383	-1,9917	2,0160	H	0,3486	-0,9890	0,4332	H	0,0388
H	1,9828	0,4897	-0,1587	H	1,4155	-0,1844	1,5450	H	-0,0423
C	1,3042	2,0652	1,0370	C	3,2525	0,3270	0,1133	C	2,5541
H	6,3546	1,1506	1,4504	H	3,4430	4,3321	0,7605	H	5,7639
H	5,3037	0,6041	2,7737	H	2,5041	3,3036	-0,3377	H	4,9912
H	6,3158	-0,5641	1,8994	H	1,7727	4,7631	0,3431	H	4,6456
H	4,3613	-0,5170	-1,3130	H	1,4786	3,5056	3,8822	H	2,6466
H	5,8667	0,3652	-0,9575	H	2,8301	4,4697	3,2505	H	4,3556
H	5,6810	-1,3242	-0,4482	H	1,1658	4,8887	2,8135	H	3,1481
H	1,5564	2,4380	2,0345	H	2,6562	-0,3054	-0,5558	H	1,5209
H	0,3332	1,5511	1,0661	H	3,6176	1,1772	-0,4763	H	3,1364
C	1,3204	3,1774	0,0171	C	4,4184	-0,4477	0,6882	C	3,0982
C	1,7762	4,4547	0,3707	C	5,7276	0,0315	0,5588	C	4,0368
C	1,3263	5,2608	-1,8652	C	6,5877	-1,9114	1,7159	C	4,0600
C	0,8605	2,9542	-1,2901	C	4,2084	-1,6723	1,3393	C	2,6478
C	0,8699	3,9892	-2,2259	C	5,2837	-2,3989	1,8500	C	3,1262
H	0,5126	3,8052	-3,2355	H	5,1066	-3,3499	2,3458	H	2,7697
H	0,5012	1,9670	-1,5727	H	3,1977	-2,0620	1,4404	H	1,9301
C	1,7765	5,4931	-0,5639	C	6,8078	-0,6945	1,0690	C	4,5149
H	2,1236	4,6404	1,3851	H	5,9049	0,9753	0,0470	H	4,3995
H	1,3281	6,0659	-2,5950	H	7,4255	-2,4801	2,1104	H	4,4325
H	2,1266	6,4808	-0,2756	H	7,8186	-0,3105	0,9576	H	5,2450

C	0,5528	1,0215	1,2707
H	-1,1421	2,1907	0,8831
H	0,2186	0,7365	2,2638
H	1,5436	0,7048	0,9554
C	3,7606	7,8113	-2,6222
C	4,1216	9,8680	-3,8524
C	2,7497	8,1089	-4,7917
C	3,3274	9,3781	-4,8912
H	3,1522	9,9842	-5,7766
H	2,1259	7,7343	-5,6013
C	4,3335	9,0809	-2,7158
H	3,9176	7,2000	-1,7377
H	4,5691	10,8560	-3,9249
H	4,9493	9,4568	-1,9022
H	-1,1277	4,8545	-0,8082
H	0,1419	5,8796	-0,0986
H	-0,5521	4,5636	0,8464
H	2,5237	4,9441	0,1805
H	2,8394	3,2272	-0,1356
H	1,8223	3,6955	1,2405
H	3,1519	5,1709	-3,7538
H	1,6275	5,7951	-4,3929

TS[M4b–M1c]			TS[M2c–M5a]			M5a			
E = -2079.230413 au			E = -2079.230633 au			E = -1478.061674 au			
Ir	-1.1197	-0.2095	-0.7377	Ir	-1.1676	-0.6106	0.0097	Ir	-1.1916
C	-2.3984	-1.0732	0.7212	C	-2.5415	-1.2950	1.4892	C	-2.4693
C	-2.6060	0.3387	0.6729	C	-2.5138	0.1595	1.4320	C	-2.8645
C	-3.8698	0.9359	0.0477	C	-3.6891	0.9679	0.8635	C	-4.1447
C	-3.6743	1.2555	-1.4540	C	-3.4878	1.2968	-0.6310	C	-3.9198
C	-2.5634	0.4248	-2.0707	C	-2.6471	0.2524	-1.3475	C	-2.7256
C	-2.5235	-1.0316	-2.0174	C	-2.8708	-1.1480	-1.2591	C	-2.5421
C	-3.6479	-1.8410	-1.3643	C	-4.0546	-1.7477	-0.4994	C	-3.5746
C	-3.3998	-2.0674	0.1470	C	-3.6807	-2.1423	0.9489	C	-3.2215
H	-1.7934	-1.4582	1.5420	H	-2.0252	-1.7495	2.3370	H	-1.9086
H	-2.1355	0.9395	1.4523	H	-1.9943	0.6588	2.2534	H	-2.5621
H	-2.0920	0.8834	-2.9412	H	-2.1628	0.6155	-2.2537	H	-2.2717
H	-2.0292	-1.5260	-2.8557	H	-2.4736	-1.7615	-2.0661	H	-1.9659
H	-4.1437	1.8495	0.5852	H	-3.7972	1.9011	1.4287	H	-4.5393
H	-4.7019	0.2339	0.1815	H	-4.6231	0.4123	1.0110	H	-4.9021
H	-3.4077	2.3099	-1.5733	H	-2.9696	2.2589	-0.7219	H	-3.7171
H	-4.6124	1.1060	-2.0109	H	-4.4591	1.4175	-1.1389	H	-4.8342
H	-3.7386	-2.8072	-1.8715	H	-4.4109	-2.6320	-1.0399	H	-3.6252
H	-4.5997	-1.3176	-1.5211	H	-4.8876	-1.0348	-0.4973	H	-4.5721
H	-3.0115	-3.0772	0.3071	H	-3.3469	-3.1864	0.9597	H	-2.5680
H	-4.3471	-2.0107	0.7037	H	-4.5689	-2.0918	1.6012	H	-4.1179
Cl	0.5160	0.0865	-2.4439	Cl	0.2046	-2.7031	-0.9996	Cl	0.4311
N	0.8926	-2.4943	0.2352	N	1.9744	-0.3002	-0.7423	N	1.7305
C	-0.1511	-3.5549	0.1674	C	2.1202	0.6420	-1.9140	C	1.6927
C	0.4679	-4.8637	-0.4400	C	1.7598	2.0714	-1.3986	C	1.0181
C	1.8457	-4.3711	-0.9575	C	1.1703	1.8275	0.0247	C	0.4442
C	1.7418	-2.8325	-0.9656	C	0.8804	0.3403	0.1212	C	0.4631
C	3.0842	-2.1177	-1.0549	C	0.4901	-0.3720	1.3181	C	0.1972
H	-0.9280	-3.1824	-0.5063	H	3.1348	0.5576	-2.3072	H	2.7074
C	0.6127	-5.9862	0.6021	C	0.7160	2.7092	-2.3341	C	-0.0999
C	-0.4142	-5.3616	-1.6010	C	3.0046	2.9752	-1.3279	C	2.0297
H	2.0787	-4.7622	-1.9543	H	0.2674	2.4128	0.2056	H	-0.5615
H	2.6519	-4.6910	-0.2846	H	1.9069	2.1021	0.7926	H	1.0738
H	-0.5979	-3.7077	1.1539	H	1.4173	0.2998	-2.6764	H	1.0822
H	1.1355	-2.5223	-1.8242	H	-0.1028	0.1437	-1.0770	H	-1.1960
H	3.5555	-2.3735	-2.0107	H	0.3044	0.2300	2.2075	H	-0.1657
H	3.7703	-2.4217	-0.2568	H	0.9713	-1.3292	1.5159	H	0.8612
H	2.9595	-1.0331	-1.0321	H	1.5566	-1.2372	-1.0377	H	1.6058
C	1.6817	-2.5536	1.4989	C	3.2772	-0.5735	-0.0047	C	3.0153
H	-1.4309	-5.5850	-1.2532	H	3.4320	3.1329	-2.3249	H	2.4509
H	-0.4872	-4.6047	-2.3914	H	3.7825	2.5424	-0.6874	H	2.8592
H	-0.0001	-6.2767	-2.0411	H	2.7389	3.9549	-0.9149	H	1.5386
H	1.2300	-5.6669	1.4491	H	-0.2021	2.1132	-2.3551	H	-0.8447
H	-0.3667	-6.2906	0.9918	H	1.1039	2.7849	-3.3571	H	0.3076
H	1.0859	-6.8698	0.1561	H	0.4652	3.7192	-1.9915	H	-0.5942
H	2.2047	-3.5174	1.6068	H	2.9973	-1.1472	0.8803	H	2.8323
H	2.4535	-1.7814	1.4247	H	3.6854	0.3881	0.3129	H	3.1310
C	0.8705	-2.3136	2.7569	C	4.2560	-1.3304	-0.8706	C	4.2210
C	0.7733	-3.3148	3.7322	C	5.4383	-0.7195	-1.3099	C	5.2357
C	-0.5281	-1.8616	5.1626	C	6.0715	-2.7384	-2.4815	C	6.4800
C	0.2557	-1.0780	3.0085	C	3.9937	-2.6591	-1.2402	C	4.3525
C	-0.4382	-0.8534	4.1985	C	4.8954	-3.3552	-2.0450	C	5.4726
H	-0.9064	0.1115	4.3768	H	4.6799	-4.3819	-2.3282	H	5.5628
H	0.3165	-0.2890	2.2626	H	3.0763	-3.1427	-0.9100	H	3.5776
C	0.0798	-3.0953	4.9256	C	6.3435	-1.4201	-2.1108	C	6.3613
H	1.2536	-4.2756	3.5588	H	5.6566	0.3067	-1.0204	H	5.1491
H	-1.0652	-1.6849	6.0909	H	6.7725	-3.2841	-3.1074	H	7.3542
H	0.0189	-3.8864	5.6688	H	7.2578	-0.9366	-2.4442	H	7.1430
C	3.5060	1.7891	0.4006						
C	2.1425	1.2423	0.8091						
N	0.9605	1.9507	0.2630						
C	0.9428	3.3677	0.6978						
H	1.0073	1.8978	-0.7569						
C	-0.0530	4.2787	-0.0543						
H	1.9485	3.8097	0.5915						
H	0.6991	3.3783	1.7693						
C	0.1629	5.7099	0.5321						
C	-1.4936	3.8148	0.1959						
C	0.2533	4.2724	-1.5654						
C	-0.7334	6.7790	-0.0280						
H	1.2107	5.9910	0.3453						
H	0.0294	5.6655	1.6215						

C	-1,6090	7,4927	0,6853
H	-0,6387	6,9852	-1,0949
H	-2,2237	8,2644	0,2282
H	-1,7384	7,3328	1,7548
C	3,8663	1,8647	-0,9535
C	6,0420	2,7495	-0,3611
C	4,4353	2,2025	1,3639
C	5,6955	2,6785	0,9895
H	6,4038	2,9950	1,7514
H	4,1709	2,1498	2,4189
C	5,1219	2,3420	-1,3322
H	3,1593	1,5427	-1,7161
H	7,0206	3,1191	-0,6565
H	5,3861	2,3897	-2,3858
H	1,2909	4,5715	-1,7588
H	0,0952	3,2794	-2,0024
H	-0,4068	4,9640	-2,0995
H	-1,6119	2,7789	-0,1353
H	-1,7376	3,8645	1,2645
H	-2,2080	4,4456	-0,3446
H	2,0539	0,2018	0,4817
H	2,0685	1,2542	1,9023

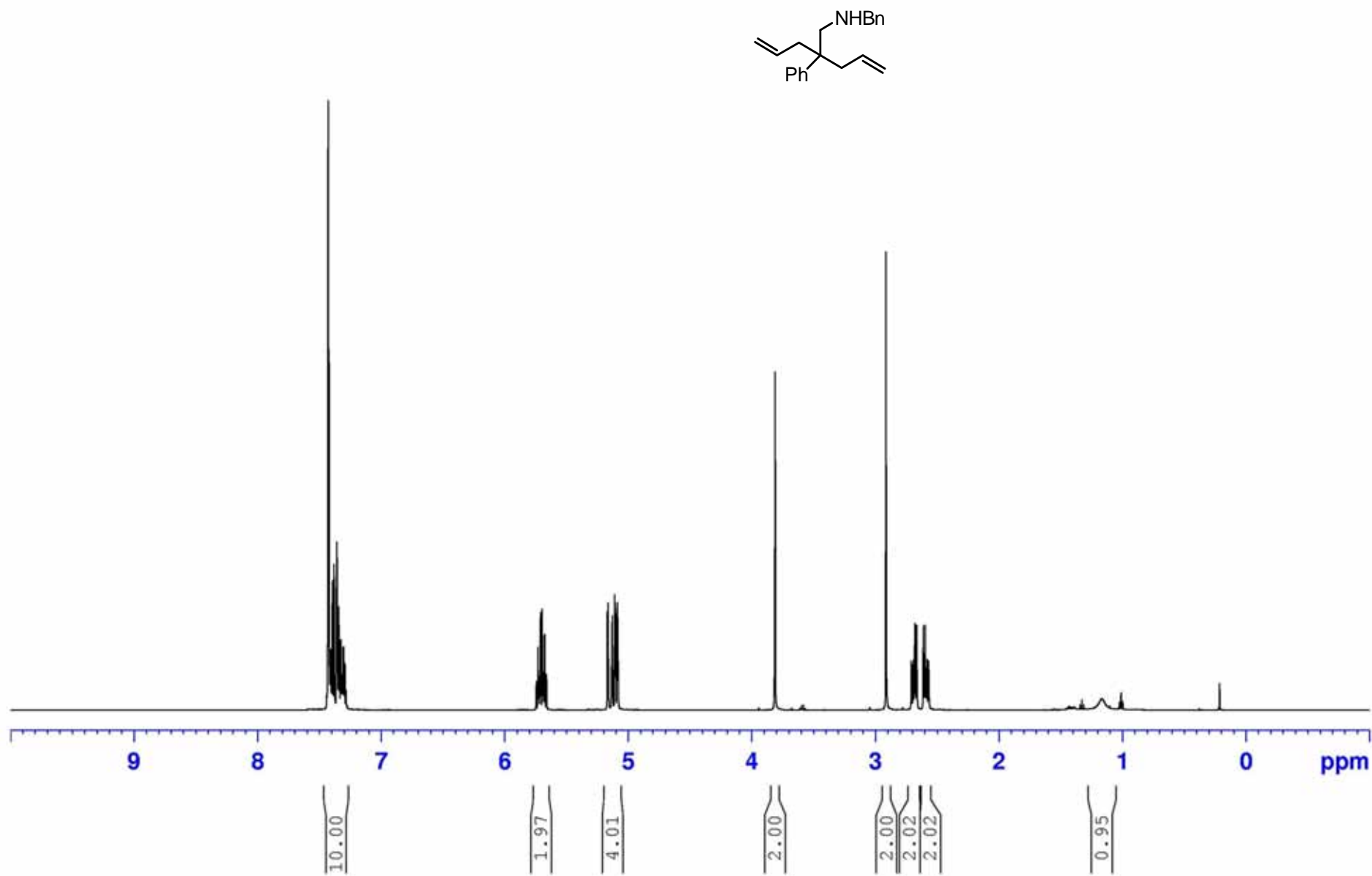
TS[M6'b–M7b]			TS[M6'c–M7c]			M7a					
E = -1478.024562 au			E = -1478.036032 au			E = -1478.067522 au					
Ir	-0,4938	1,0488	0,1058	Ir	-0,2739	0,1628	-0,8082	Ir	-0,8693	0,1954	-0,7943
C	-2,0418	1,6366	1,5093	C	-1,7881	0,7879	0,6794	C	-2,3359	0,7870	0,6807
C	-2,1063	0,2332	1,3043	C	-1,8348	-0,6125	0,5730	C	-2,3293	-0,6357	0,5684
C	-3,2051	-0,4450	0,4839	C	-2,9449	-1,3688	-0,1499	C	-3,4494	-1,4208	-0,1224
C	-2,8070	-0,6409	-0,9947	C	-2,6245	-1,6617	-1,6358	C	-3,1313	-1,7049	-1,6038
C	-1,8539	0,4257	-1,4947	C	-1,7184	-0,6250	-2,2717	C	-2,2532	-0,6304	-2,2180
C	-2,0145	1,8136	-1,2811	C	-1,9107	0,7663	-2,1562	C	-2,4988	0,7699	-2,1021
C	-3,2387	2,4163	-0,5955	C	-3,0997	1,3908	-1,4263	C	-3,7190	1,3472	-1,3851
C	-3,0090	2,6438	0,9118	C	-2,7954	1,7326	0,0509	C	-3,4226	1,6761	0,0923
H	-1,5772	1,9737	2,4342	H	-1,2101	1,1983	1,5045	H	-1,8527	1,2162	1,5548
H	-1,6825	-0,3794	2,0949	H	-1,2757	-1,1796	1,3106	H	-1,8331	-1,1894	1,3629
H	-1,2258	0,1364	-2,3341	H	-1,1473	-0,9841	-3,1260	H	-1,6769	-0,9461	-3,0855
H	-1,4791	2,4684	-1,9638	H	-1,4633	1,3887	-2,9284	H	-2,0733	1,3905	-2,8859
H	-3,4219	-1,4217	0,9292	H	-3,1068	-2,3189	0,3685	H	-3,5962	-2,3664	0,4102
H	-4,1274	0,1406	0,5650	H	-3,8799	-0,8040	-0,0616	H	-4,3888	-0,8657	-0,0257
H	-2,3071	-1,6073	-1,1020	H	-2,1144	-2,6250	-1,7046	H	-2,5975	-2,6574	-1,6800
H	-3,7010	-0,6729	-1,6364	H	-3,5558	-1,7408	-2,2176	H	-4,0568	-1,8161	-2,1905
H	-3,4760	3,3710	-1,0759	H	-3,3931	2,3054	-1,9527	H	-4,0332	2,2590	-1,9039
H	-4,1002	1,7612	-0,7602	H	-3,9525	0,7077	-1,4922	H	-4,5553	0,6439	-1,4654
H	-2,5876	3,6427	1,0658	H	-2,3873	2,7474	0,1078	H	-3,0781	2,7122	0,1665
H	-3,9607	2,6114	1,4631	H	-3,7246	1,7321	0,6401	H	-4,3350	1,5970	0,7046
Cl	1,2391	1,6358	-1,5021	Cl	0,4685	-2,2494	-0,8808	Cl	0,6017	0,5563	-2,7175
N	0,2661	-1,0759	-0,0296	N	1,2540	0,5317	0,6911	N	0,9082	0,0942	0,5693
C	-0,0689	-2,1419	0,9066	C	1,6858	1,8825	1,0205	C	2,1157	0,9331	0,2002
C	0,8200	-2,1857	2,1848	C	2,9410	2,3644	0,2335	C	3,2790	-0,0251	-0,1666
C	1,0268	-0,7391	2,6822	C	2,6567	2,0210	-1,2400	C	2,5245	-1,2912	-0,6370
C	1,4488	0,2475	1,6413	C	2,1499	0,6305	-1,4762	C	1,2155	-1,3704	0,1626
C	1,0699	1,5818	1,7018	C	1,1894	0,3791	-2,4708	C	-0,0060	-1,8077	-0,6518
H	0,0471	-3,1110	0,3995	H	1,9095	1,9509	2,0962	H	2,3655	1,5904	1,0376
C	0,1102	-3,0029	3,2789	C	3,1100	3,8832	0,4069	C	4,1252	0,5809	-1,3003
C	2,1873	-2,8235	1,8867	C	4,2266	1,6556	0,7011	C	4,1963	-0,3419	1,0291
H	1,8355	-0,7496	3,4327	H	3,5904	2,1117	-1,8178	H	3,1233	-2,1979	-0,4947
H	0,1353	-0,3650	3,2021	H	1,9432	2,7370	-1,6674	H	2,2817	-1,1965	-1,6978
H	-1,1237	-2,1044	1,2311	H	0,8722	2,5928	0,8204	H	1,8435	1,5393	-0,6641
H	2,2455	-0,0368	0,9645	H	2,7414	-0,2062	-1,1170	H	1,3652	-1,9440	1,0838
H	1,6680	2,3271	1,1878	H	1,1807	-0,6004	-2,9398	H	-0,6202	-2,5503	-0,1352
H	0,5000	1,9244	2,5622	H	0,8686	1,2158	-3,0897	H	0,2765	-2,1863	-1,6373
C	0,5850	-1,5705	-1,3769	C	1,8248	-0,5352	1,5140	C	0,5050	0,2864	2,0137
H	2,0632	-3,8606	1,5555	H	2,0909	-1,3899	0,8823	H	4,6456	0,5724	1,4330
H	2,7169	-2,2876	1,0947	H	2,7549	-0,1654	1,9678	H	3,6617	-0,8416	1,8418
H	2,8135	-2,8252	2,7883	C	0,9386	-1,0572	2,6474	H	5,0085	-1,0028	0,7023
H	-0,8630	-2,5642	3,5345	H	2,2146	4,4199	0,0693	H	3,4977	0,8158	-2,1661
H	-0,0624	-4,0315	2,9394	H	3,2798	4,1351	1,4609	H	4,6222	1,5009	-0,9675
H	0,7140	-3,0487	4,1933	H	3,9679	4,2549	-0,1666	H	4,9042	-0,1241	-1,6136
H	-0,2101	-2,2496	-1,7450	H	4,3903	1,8115	1,7742	H	0,1917	1,3308	2,0912
H	0,6269	-0,7124	-2,0509	H	4,1909	0,5772	0,5185	H	-0,3699	-0,3438	2,1768
C	1,9145	-2,3036	-1,5078	H	5,0960	2,0579	0,1656	C	1,5147	-0,0071	3,1053
C	3,1213	-1,5854	-1,4824	C	0,3767	-0,1937	3,6004	C	1,6311	-1,2948	3,6534
C	4,3886	-3,6310	-1,7635	C	-0,6234	-2,0640	4,7702	C	3,3170	-0,5229	5,2084
C	1,9697	-3,6922	-1,6812	C	0,7087	-2,4332	2,7821	C	2,2879	1,0244	3,6596
C	3,1959	-4,3551	-1,8028	C	-0,0676	-2,9349	3,8312	C	3,1856	0,7705	4,6980
H	3,2185	-5,4347	-1,9328	H	-0,2414	-4,0057	3,9109	H	3,7754	1,5832	5,1137
H	1,0421	-4,2610	-1,7260	H	1,1238	-3,1118	2,0405	H	2,1779	2,0390	3,2829
C	4,3463	-2,2404	-1,6093	C	-0,3965	-0,6891	4,6516	C	2,5310	-1,5544	4,6886
H	3,0841	-0,5034	-1,3751	H	0,5413	0,8781	3,5194	H	1,0030	-2,0995	3,2781
H	5,3434	-4,1421	-1,8608	H	-1,2283	-2,4504	5,5869	H	4,0142	-0,7226	6,0179
H	5,2706	-1,6669	-1,5965	H	-0,8207	-0,0031	5,3817	H	2,6089	-2,5583	5,0979
H	-0,5052	2,6432	0,1951	H	-0,3306	1,7436	-0,8414	H	-0,8523	1,8413	-0,7643

M8c			TS[M7b-M4b]			TS[M7c-M4b]					
	E = -1478.044893 au			E = -1478.044315 au			E = -1478.047093 au				
Ir	-0.1577	-0.1446	0.5827	Ir	-0.7302	1.1758	-0.2796	Ir	-0.3855	0.2208	-0.8863
C	-1.4196	0.7615	2.0958	C	-2.1318	1.6209	1.3037	C	-1.6666	1.1491	0.5311
C	-1.8546	-0.5806	1.9115	C	-2.1307	0.2200	1.0733	C	-2.0701	-0.2291	0.3622
C	-3.1603	-0.9641	1.2162	C	-3.2792	-0.5253	0.3879	C	-3.3365	-0.6433	-0.3922
C	-2.9295	-1.2996	-0.2685	C	-3.0254	-0.7096	-1.1228	C	-3.0371	-0.9354	-1.8786
C	-1.8339	-0.4568	-0.8791	C	-2.1383	0.3950	-1.6754	C	-1.8819	-0.1071	-2.4115
C	-1.6618	0.9315	-0.6921	C	-2.3857	1.8062	-1.4528	C	-1.7381	1.2898	-2.2120
C	-2.6170	1.8148	0.1091	C	-3.5854	2.3272	-0.6581	C	-2.7810	2.1537	-1.5031
C	-2.1512	1.9859	1.5676	C	-3.2135	2.5725	0.8185	C	-2.4380	2.3418	-0.0136
H	-0.8171	0.9707	2.9784	H	-1.5887	1.9744	2.1807	H	-1.1429	1.3681	1.4626
H	-1.5116	-1.3071	2.6407	H	-1.5735	-0.3761	1.7909	H	-1.7916	-0.8959	1.1752
H	-1.3708	-0.8905	-1.7640	H	-1.6450	0.1520	-2.6175	H	-1.3728	-0.5424	-3.2693
H	-1.1423	1.4455	-1.4947	H	-2.0298	2.4752	-2.2340	H	-1.1227	1.8171	-2.9386
H	-3.5843	-1.8387	1.7213	H	-3.3988	-1.5028	0.8688	H	-3.7509	-1.5441	0.0728
H	-3.8963	-0.1609	1.3273	H	-4.2152	0.0169	0.5612	H	-4.1065	0.1316	-0.2916
H	-2.6220	-2.3463	-0.3568	H	-2.5140	-1.6657	-1.2869	H	-2.7489	-1.9856	-1.9847
H	-3.8570	-1.1880	-0.8525	H	-3.9784	-0.7705	-1.6717	H	-3.9304	-0.7800	-2.5041
H	-2.6694	2.7971	-0.3731	H	-3.9340	3.2647	-1.1038	H	-2.8322	3.1273	-2.0028
H	-3.6280	1.3987	0.0690	H	-4.4194	1.6203	-0.7360	H	-3.7672	1.6922	-1.6174
H	-1.4664	2.8404	1.6274	H	-2.8301	3.5931	0.9289	H	-1.8075	3.2317	0.1015
H	-3.0007	2.2227	2.2282	H	-4.0972	2.4969	1.4716	H	-3.3493	2.5228	0.5785
Cl	0.1672	-2.5553	0.4449	Cl	0.6258	1.7879	-2.1876	Cl	0.1880	-2.2029	-1.5695
N	1.3577	0.3173	-0.6150	N	1.0285	-0.4671	0.4668	N	1.4338	0.1938	0.4741
C	2.6193	-0.4350	-0.5857	C	0.6706	-1.6967	1.2550	C	1.5282	1.2925	1.5079
C	3.4336	-0.2046	0.7110	C	0.9850	-1.4117	2.7483	C	2.8755	2.0257	1.3163
C	2.6703	-0.8348	1.8846	C	0.9370	0.1317	2.7931	C	3.0031	1.9639	-0.2199
C	1.2816	-0.3008	2.2406	C	1.5000	0.5917	1.4456	C	2.4165	0.6106	-0.6567
C	0.8118	-1.0461	3.4939	C	1.0008	1.9673	0.9824	C	1.5868	0.6954	-1.9341
H	3.2297	-0.1612	-1.4558	H	1.2397	-2.5572	0.8915	H	1.3788	0.8760	2.5060
C	4.7766	-0.9424	0.5401	C	-0.0495	-2.0592	3.6817	C	2.7646	3.4718	1.8305
C	3.6976	1.2933	0.9373	C	2.3924	-1.9162	3.1240	C	4.0721	1.3445	2.0101
H	3.2979	-0.7069	2.7848	H	1.5168	0.5419	3.6270	H	4.0353	2.0819	-0.5665
H	2.5967	-1.9165	1.7122	H	-0.0969	0.4782	2.9061	H	2.4073	2.7729	-0.6641
H	2.3886	-1.5060	-0.6480	H	-0.3918	-1.9152	1.1103	H	0.7237	2.0011	1.3070
H	1.3450	0.7769	2.4611	H	2.5992	0.5798	1.5049	H	3.1921	-0.1595	-0.7148
H	1.5999	-1.0063	4.2611	H	1.7104	2.4528	0.3094	H	1.6021	-0.2043	-2.5509
H	0.6266	-2.1017	3.2674	H	0.8383	2.6134	1.8524	H	1.8657	1.5564	-2.5515
C	1.3436	1.2514	-1.7482	C	1.9754	-0.7555	-0.6663	C	1.8832	-1.1478	1.0414
H	0.5846	2.0180	-1.5798	H	2.4514	-3.0064	3.0241	H	1.8387	-1.8417	0.1997
H	2.3131	1.7714	-1.7437	H	3.1655	-1.4813	2.4826	H	2.9261	-1.0321	1.3554
C	1.1506	0.6302	-3.1313	H	2.6213	-1.6555	4.1644	C	1.0799	-1.6998	2.1975
H	4.6153	-2.0102	0.3499	H	-1.0659	-1.7145	3.4554	H	1.9250	3.9942	1.3576
H	5.3502	-0.5266	-0.2974	H	-0.0322	-3.1517	3.5874	H	2.6126	3.4913	2.9165
H	5.3836	-0.8467	1.4479	H	0.1659	-1.8107	4.7277	H	3.6826	4.0294	1.6123
H	4.2788	1.7181	0.1086	H	1.4327	-1.4126	-1.3529	H	3.8864	1.2219	3.0836
H	2.7617	1.8558	1.0213	H	2.1302	0.1902	-1.1879	H	4.3022	0.3610	1.5889
H	4.2714	1.4422	1.8600	C	3.3103	-1.3777	-0.3088	H	4.9675	1.9664	1.8934
C	0.8801	-0.7294	-3.3165	C	4.4135	-0.5729	0.0228	C	1.4679	-1.4610	3.5259
C	0.7805	-0.4110	-5.7178	C	5.8077	-2.5294	0.3226	C	-0.3299	-2.8567	4.3447
C	1.2375	1.4637	-4.2572	C	3.4972	-2.7688	-0.3545	C	-0.0078	-2.5546	1.9618
C	1.0514	0.9495	-5.5402	C	4.7307	-3.3420	-0.0390	C	-0.7080	-3.1251	3.0268
H	1.1206	1.6090	-6.4017	H	4.8540	-4.4212	-0.0859	H	-1.5449	-3.7894	2.8256
H	1.4518	2.5234	-4.1280	H	2.6729	-3.4096	-0.6616	H	-0.2850	-2.7749	0.9336
C	0.6970	-1.2464	-4.6035	C	5.6478	-1.1415	0.3443	C	0.7662	-2.0271	4.5927
H	0.8106	-1.3888	-2.4546	H	4.3119	0.5097	0.0042	H	2.3416	-0.8455	3.7306
H	0.6373	-0.8138	-6.7170	H	6.7699	-2.9726	0.5657	H	-0.8740	-3.3044	5.1725
H	0.4881	-2.3056	-4.7306	H	6.4889	-0.5004	0.5958	H	1.0834	-1.8317	5.6139
H	-0.0897	-0.6232	3.9452	H	-0.2644	2.6214	0.2860	H	0.4675	1.5319	-1.3805

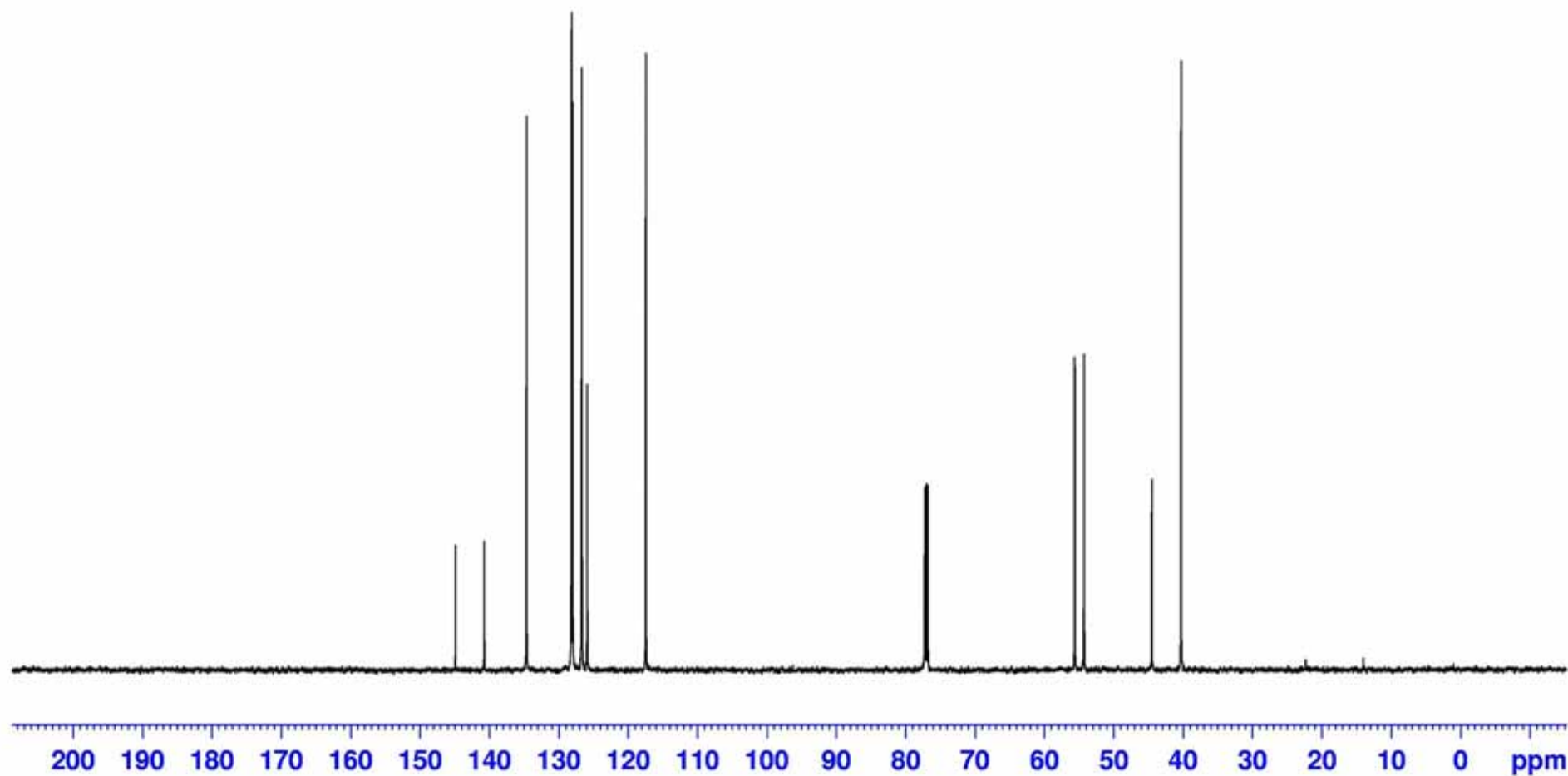
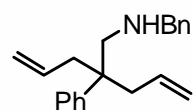
	TS[M8a–M4b]			TS[M8b–M4b]			
	E = -1478.044620 au			E = -1477.998595 au			
Ir	-0.7386	0,0058	-1,0901	Ir	-0,8544	0,7875	-0,2676
C	-2,1599	0,7757	-2,4919	C	-2,1592	1,4525	1,3047
C	-2,3540	-0,6316	-2,3276	C	-2,3157	0,0489	1,1529
C	-3,5428	-1,2252	-1,5731	C	-3,5418	-0,5944	0,5049
C	-3,1528	-1,5513	-0,1177	C	-3,3172	-0,8507	-1,0002
C	-2,1059	-0,5880	0,4172	C	-2,3286	0,1383	-1,5900
C	-2,1590	0,8338	0,2876	C	-2,4203	1,5869	-1,4321
C	-3,3241	1,5764	-0,3731	C	-3,5629	2,2487	-0,6548
C	-3,0913	1,8124	-1,8842	C	-3,1542	2,4933	0,8113
H	-1,6411	1,0956	-3,3960	H	-1,5519	1,7817	2,1505
H	-1,9298	-1,2675	-3,1033	H	-1,8116	-0,5696	1,8884
H	-1,5507	-0,9873	1,2667	H	-1,8556	-0,2023	-2,5124
H	-1,6596	1,4038	1,0698	H	-2,0327	2,1665	-2,2695
H	-3,8738	-2,1391	-2,0781	H	-3,7535	-1,5411	1,0136
H	-4,3908	-0,5322	-1,6015	H	-4,4164	0,0455	0,6638
H	-2,7261	-2,5601	-0,0740	H	-2,9052	-1,8569	-1,1384
H	-4,0351	-1,5552	0,5417	H	-4,2694	-0,8229	-1,5515
H	-3,4598	2,5401	0,1307	H	-3,8168	3,2044	-1,1255
H	-4,2507	1,0144	-0,2094	H	-4,4668	1,6311	-0,7097
H	-2,6459	2,8029	-2,0302	H	-2,6770	3,4769	0,8914
H	-4,0514	1,8299	-2,4226	H	-4,0302	2,5157	1,4788
Cl	0,7056	-0,4555	-2,9852	Cl	0,6039	1,1841	-2,1708
N	0,8501	-0,1074	0,2101	N	0,3903	-1,0398	0,3158
C	0,8022	0,2902	1,6175	C	0,4553	-1,7509	1,5792
C	1,3374	1,7317	1,8909	C	1,4341	-1,1215	2,6076
C	0,8169	2,5939	0,7301	C	1,2574	0,3911	2,4300
C	0,9750	1,9665	-0,6258	C	1,2497	0,8406	0,9923
C	0,4386	2,8003	-1,7741	C	0,8845	2,3019	0,8110
H	1,3786	-0,4333	2,2091	H	0,7747	-2,7811	1,3760
C	0,7669	2,2190	3,2357	C	1,0525	-1,5485	4,0346
C	2,8779	1,7994	1,9647	C	2,8940	-1,5207	2,3319
H	1,3807	3,5419	0,7119	H	2,0873	0,9168	2,9295
H	-0,2325	2,8718	0,8867	H	0,3359	0,7330	2,9218
H	-0,2323	0,2500	1,9695	H	-0,5353	-1,8229	2,0605
H	1,9796	1,6108	-0,8480	H	2,1070	0,5520	0,3973
H	0,4718	2,2690	-2,7258	H	1,6608	2,8188	0,2425
H	-0,5731	3,1663	-1,5876	H	0,6863	2,7740	1,7773
C	2,1293	-0,7701	-0,1390	C	0,7774	-1,8271	-0,8724
H	2,2297	-0,7466	-1,2257	H	3,0237	-2,6042	2,4312
H	2,9756	-0,2355	0,3069	H	3,2076	-1,2424	1,3225
C	2,1549	-2,2110	0,3497	H	3,5627	-1,0299	3,0507
H	-0,3293	2,2044	3,2284	H	0,0193	-1,2644	4,2707
H	1,1106	1,5809	4,0587	H	1,1398	-2,6360	4,1496
H	1,0949	3,2434	3,4477	H	1,7136	-1,0812	4,7745
H	3,2689	1,0524	2,6650	H	0,0644	-2,6695	-0,9441
H	3,3550	1,6385	0,9930	H	0,6233	-1,2009	-1,7506
H	3,1881	2,7892	2,3211	C	2,1847	-2,4003	-0,9315
C	3,1041	-2,6259	1,2924	C	3,2694	-1,6081	-1,3416
C	2,2308	-4,8814	1,2295	C	4,7816	-3,4848	-1,0918
C	1,2419	-3,1511	-0,1489	C	2,4227	-3,7475	-0,6260
C	1,2813	-4,4760	0,2847	C	3,7093	-4,2884	-0,7000
H	0,5735	-5,1972	-0,1168	H	3,8717	-5,3371	-0,4615
H	0,5026	-2,8324	-0,8809	H	1,5865	-4,3848	-0,3412
C	3,1437	-3,9532	1,7321	C	4,5561	-2,1433	-1,4182
H	3,8243	-1,9074	1,6803	H	3,0922	-0,5708	-1,6193
H	2,2582	-5,9139	1,5683	H	5,7832	-3,9026	-1,1557
H	3,8868	-4,2586	2,4647	H	5,3837	-1,5183	-1,7454
H	1,1062	3,6779	-1,8563	H	-0,0535	2,5359	0,1960

4. NMR Spectra for Isolated Compounds

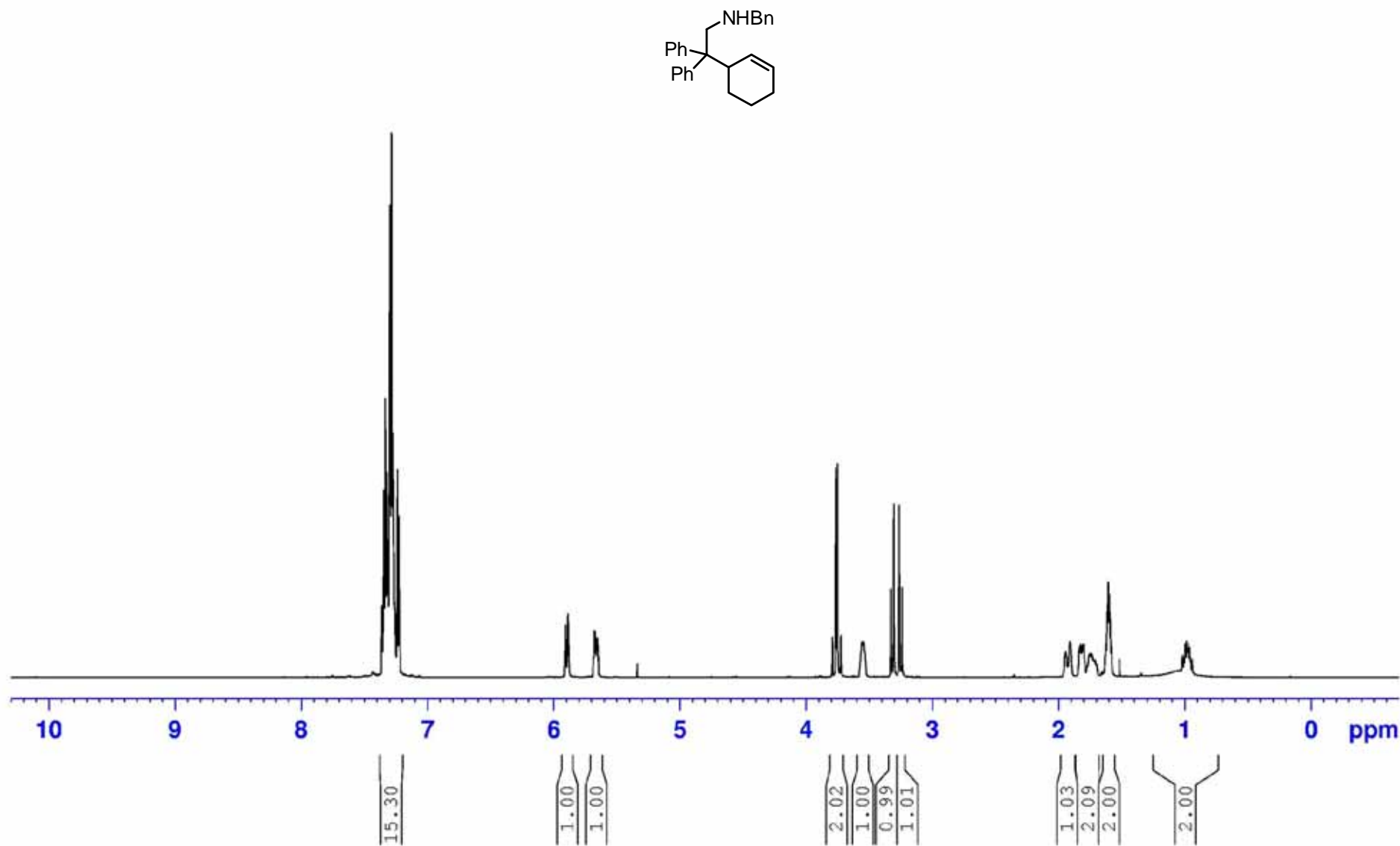
^1H NMR of *N*-Benzyl-2-Phenyl-2-(2-propenyl)-1-amino-4-pentene. (CDCl_3 , 500 MHz, 300 K)



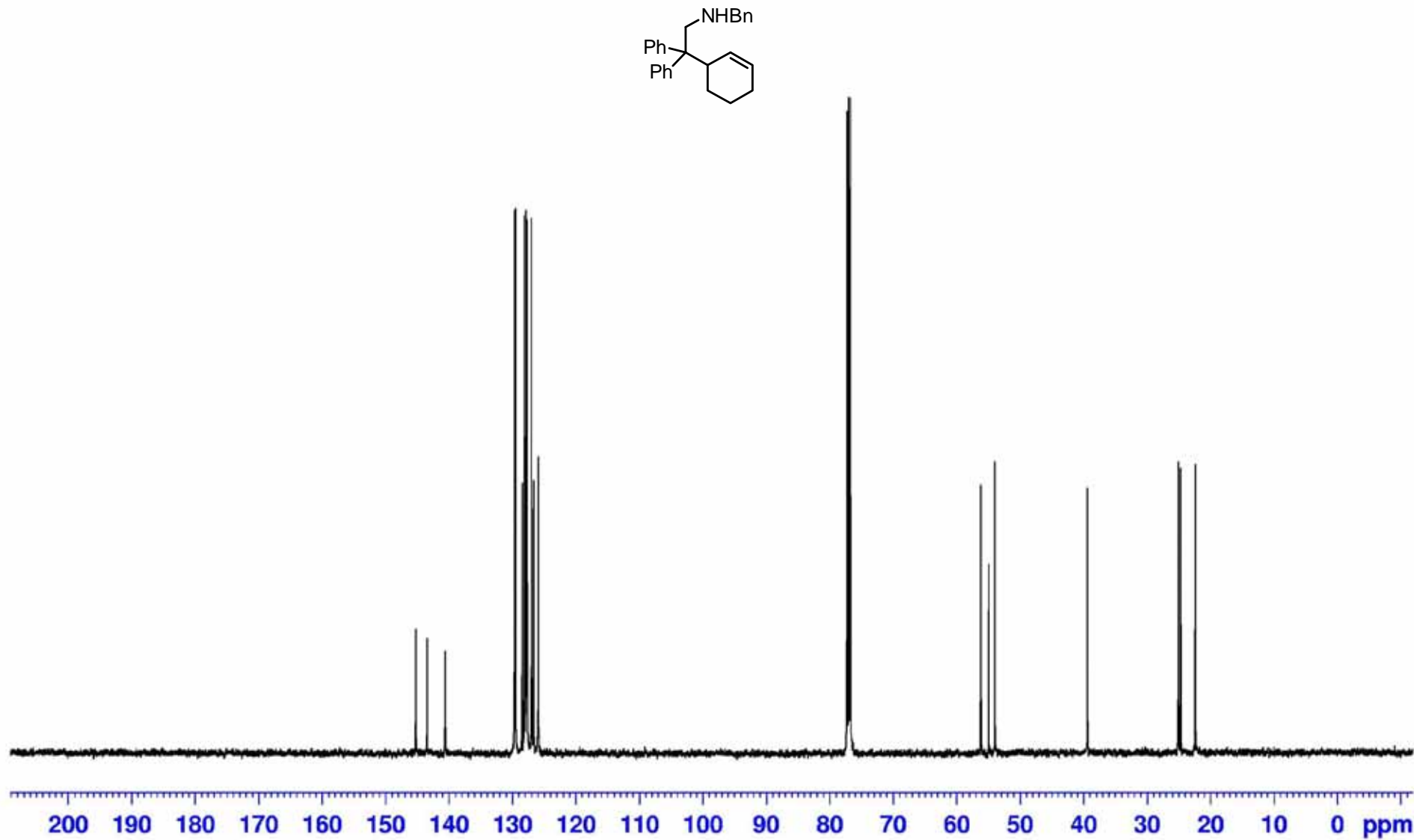
$^{13}\text{C}\{^1\text{H}\}$ NMR of *N*-Benzyl-2-Phenyl-2-(2-propenyl)-1-amino-4-pentene. (CDCl_3 , 126 MHz, 300 K)



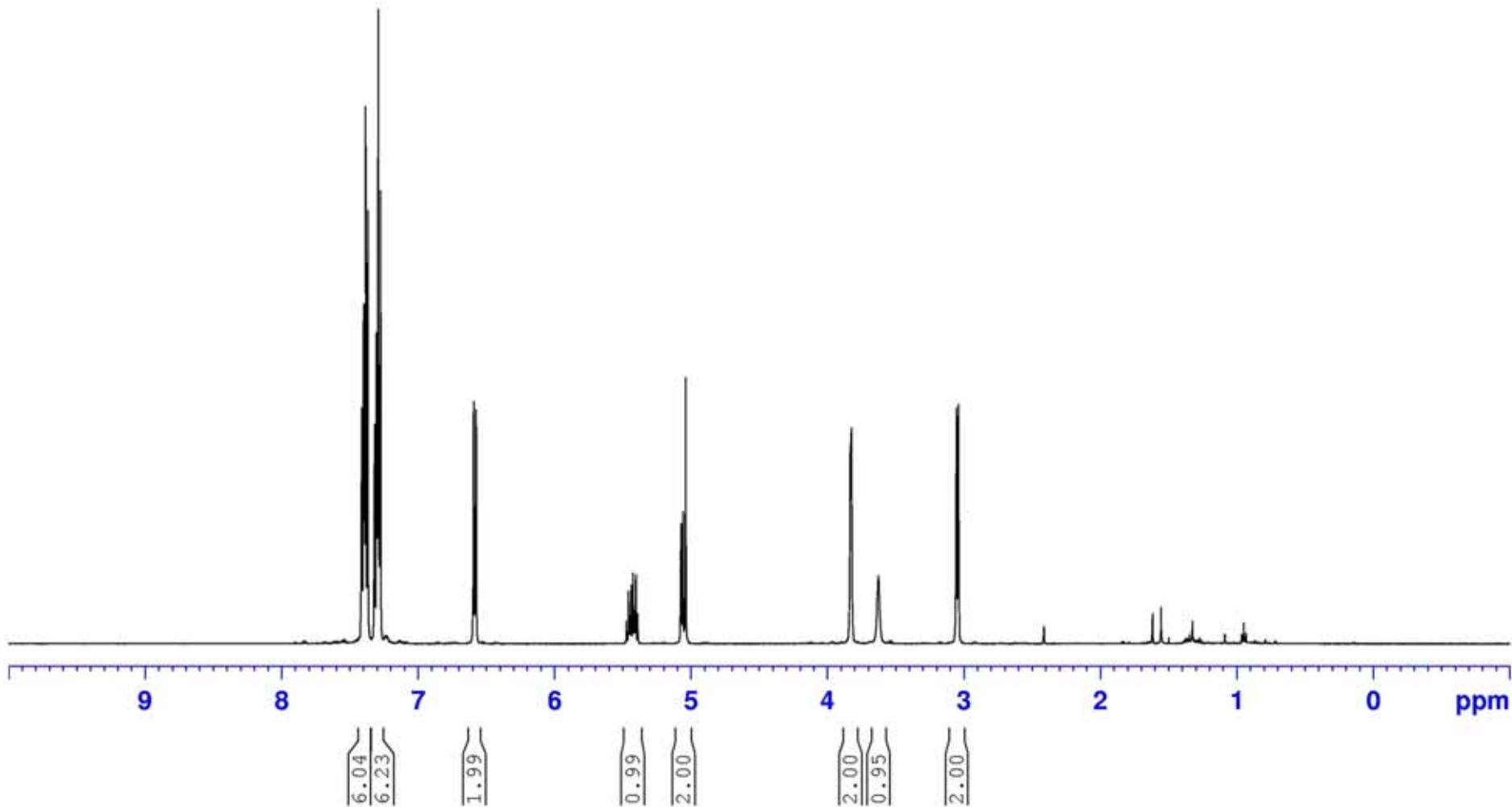
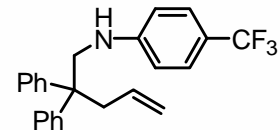
¹H NMR of *N*-Benzyl-2,2-diphenyl-2-cyclohex-3-en-1-amine (CDCl_3 , 500MHz, 300 K):



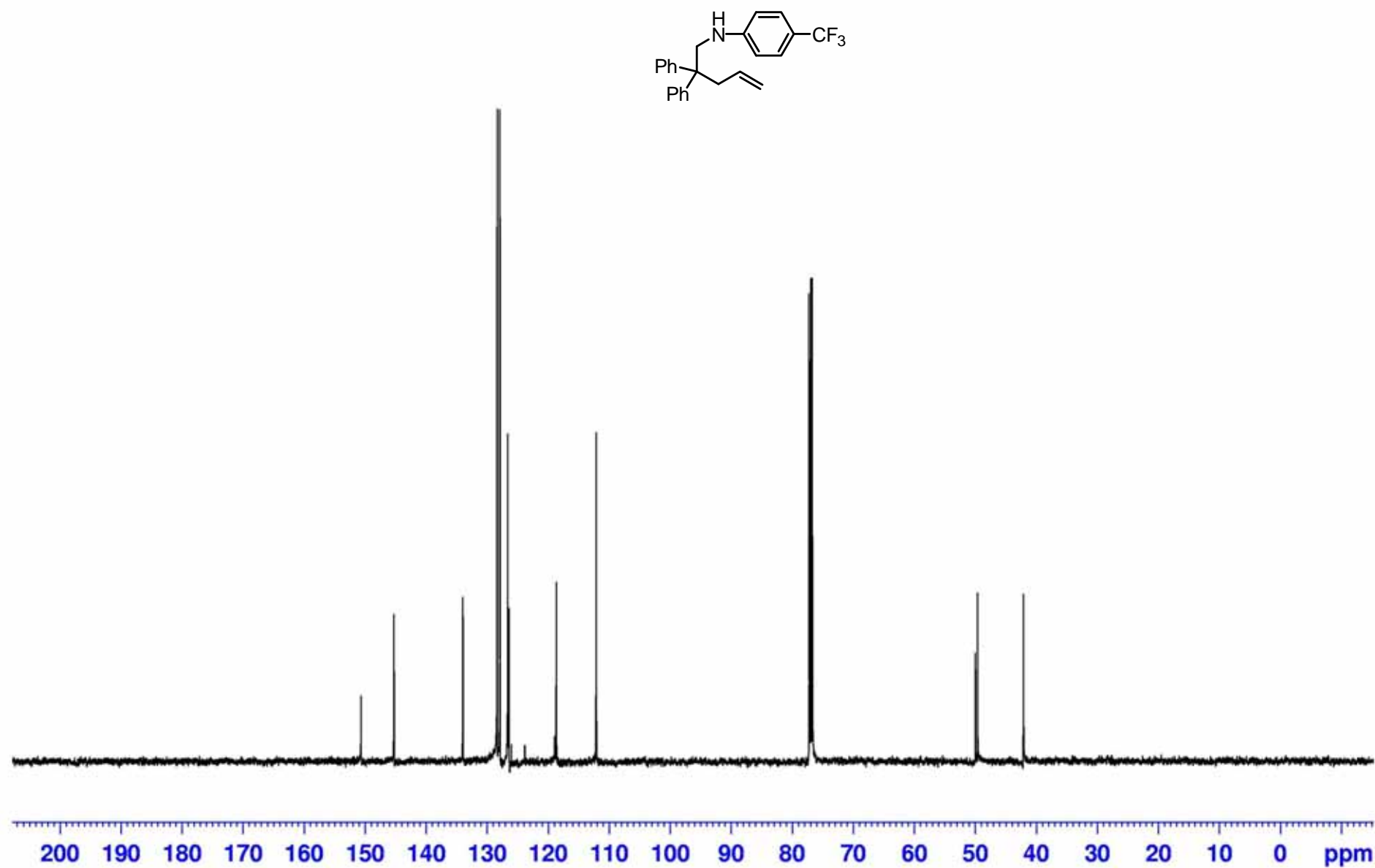
$^{13}\text{C}\{^1\text{H}\}$ NMR of *N*-Benzyl-2,2-diphenyl-2-cyclohex-3-en-1-amine (CDCl_3 , 125MHz, 300 K):



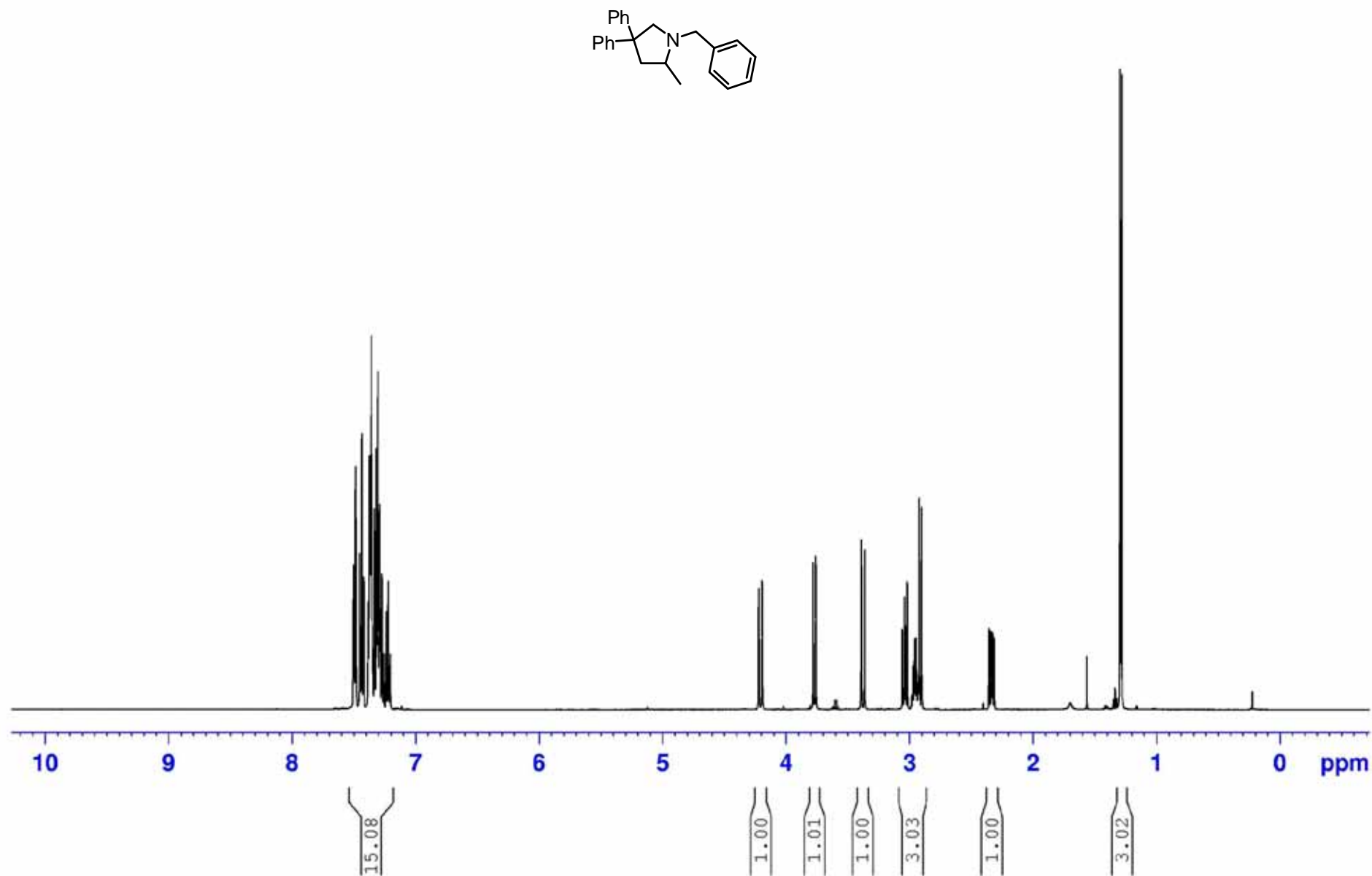
¹H NMR of *N*-(4-trifluoromethylphenyl)-2,2-diphenylpent-4-en-1-amine (CDCl_3 , 500 MHz, 300 K)



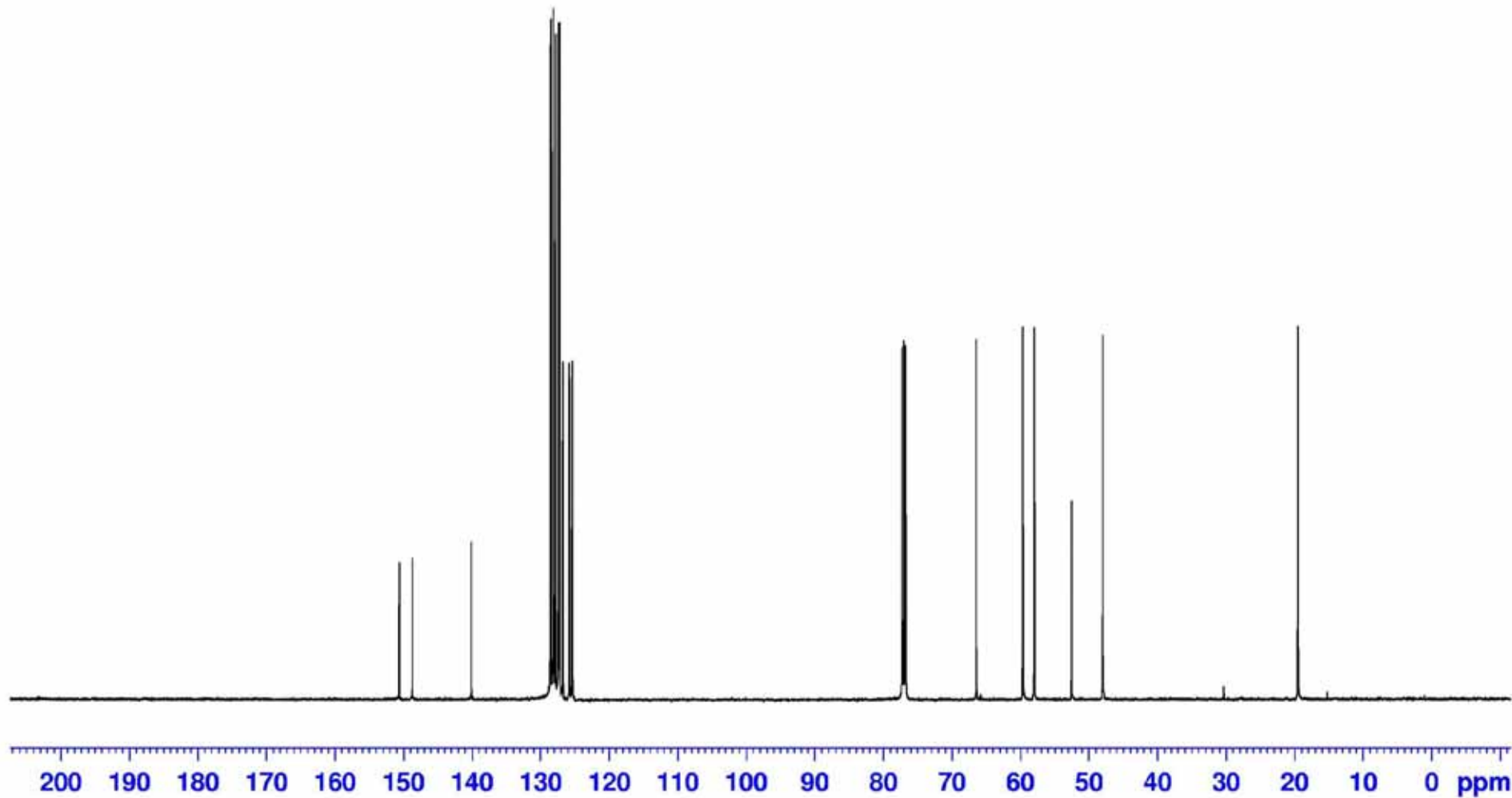
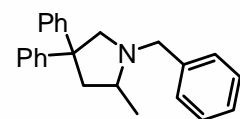
$^{13}\text{C}\{\text{H}\}$ NMR of *N*-(4-trifluoromethylphenyl)-2,2-diphenylpent-4-en-1-amine (CDCl_3 , 126 MHz, 300 K)



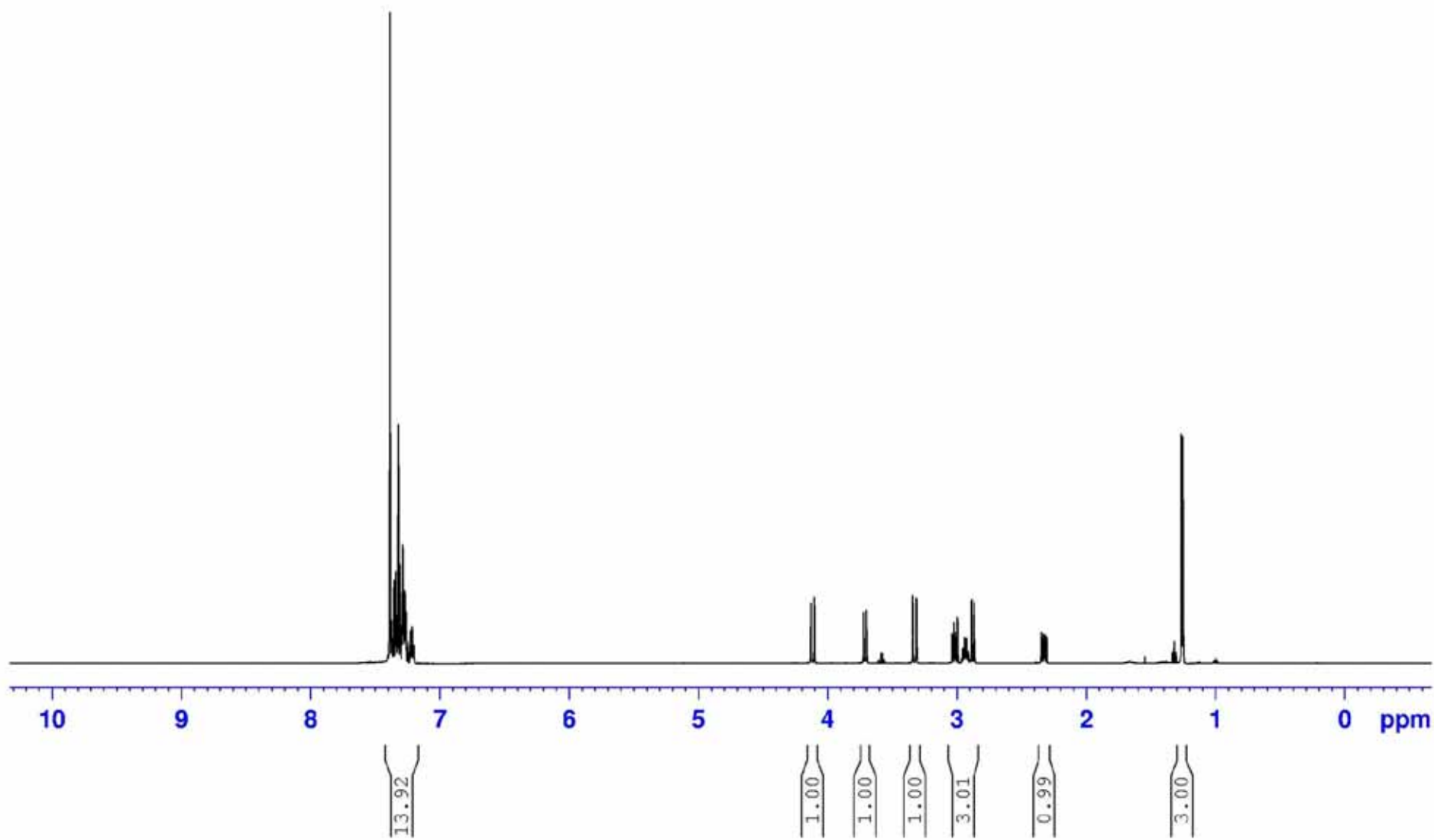
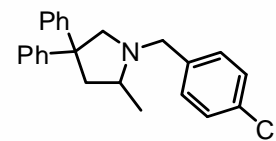
¹H NMR of 1-Benzyl-2-methyl-4,4-diphenylpyrrolidine. (CDCl₃, 500 MHz, 300 K)



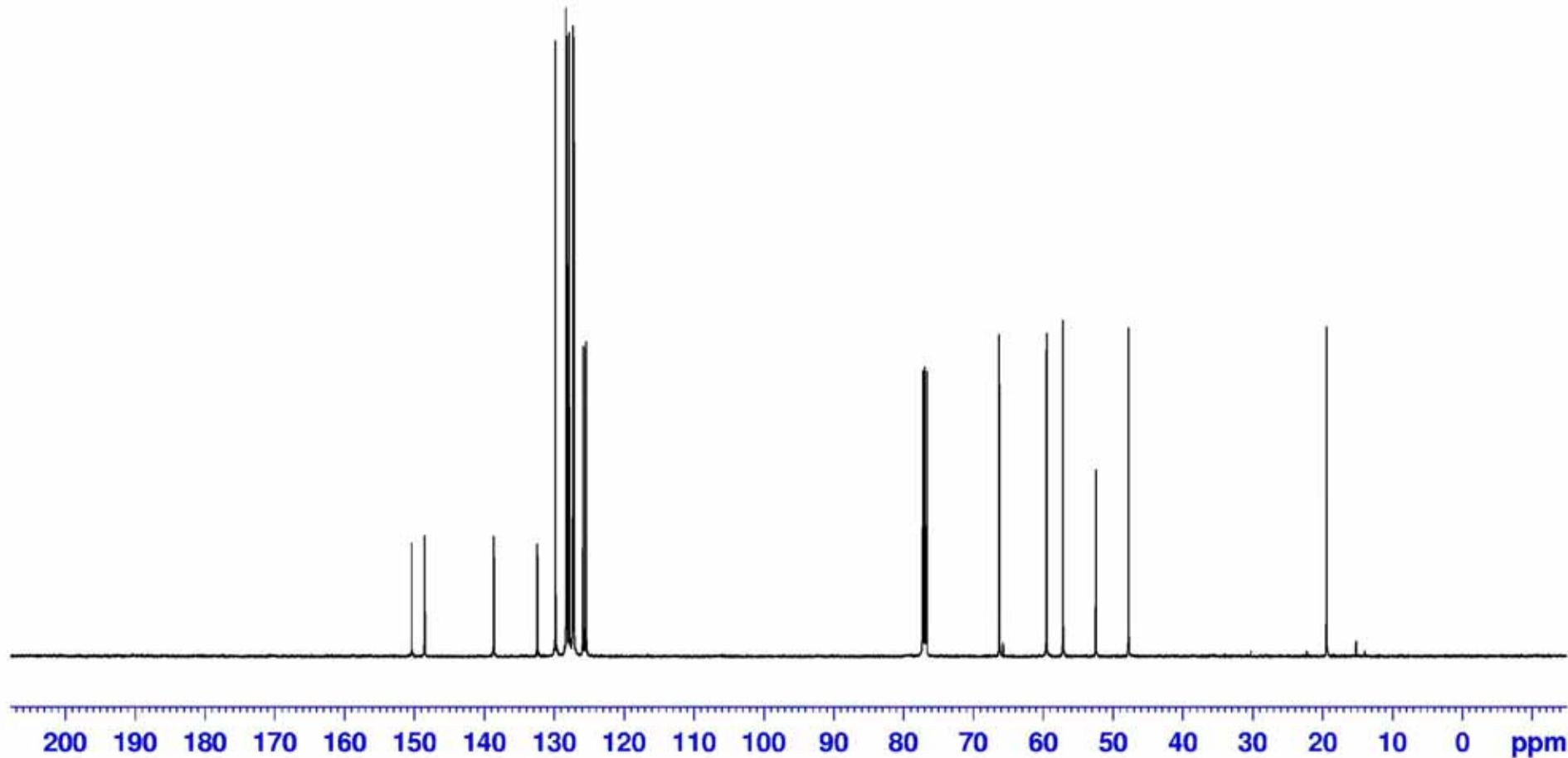
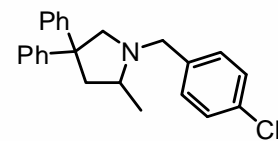
$^{13}\text{C}\{^1\text{H}\}$ NMR of 1-Benzyl-2-methyl-4,4-diphenylpyrrolidine. (CDCl_3 , 126 MHz, 300 K)



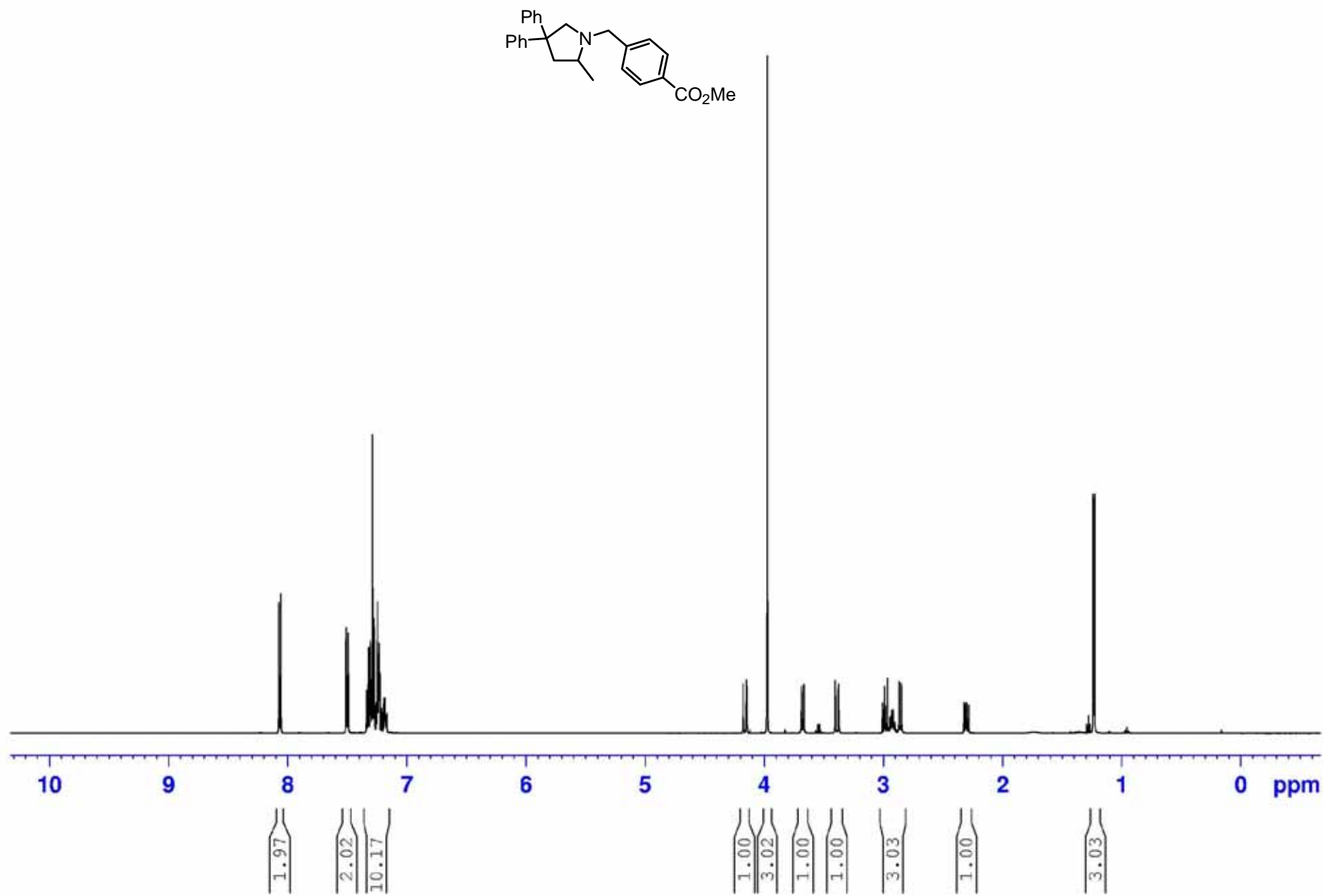
¹H NMR of 1-(4-Chlorobenzyl)-2-methyl-4,4-diphenylpyrrolidine (CDCl₃, 500 MHz, 300 K)



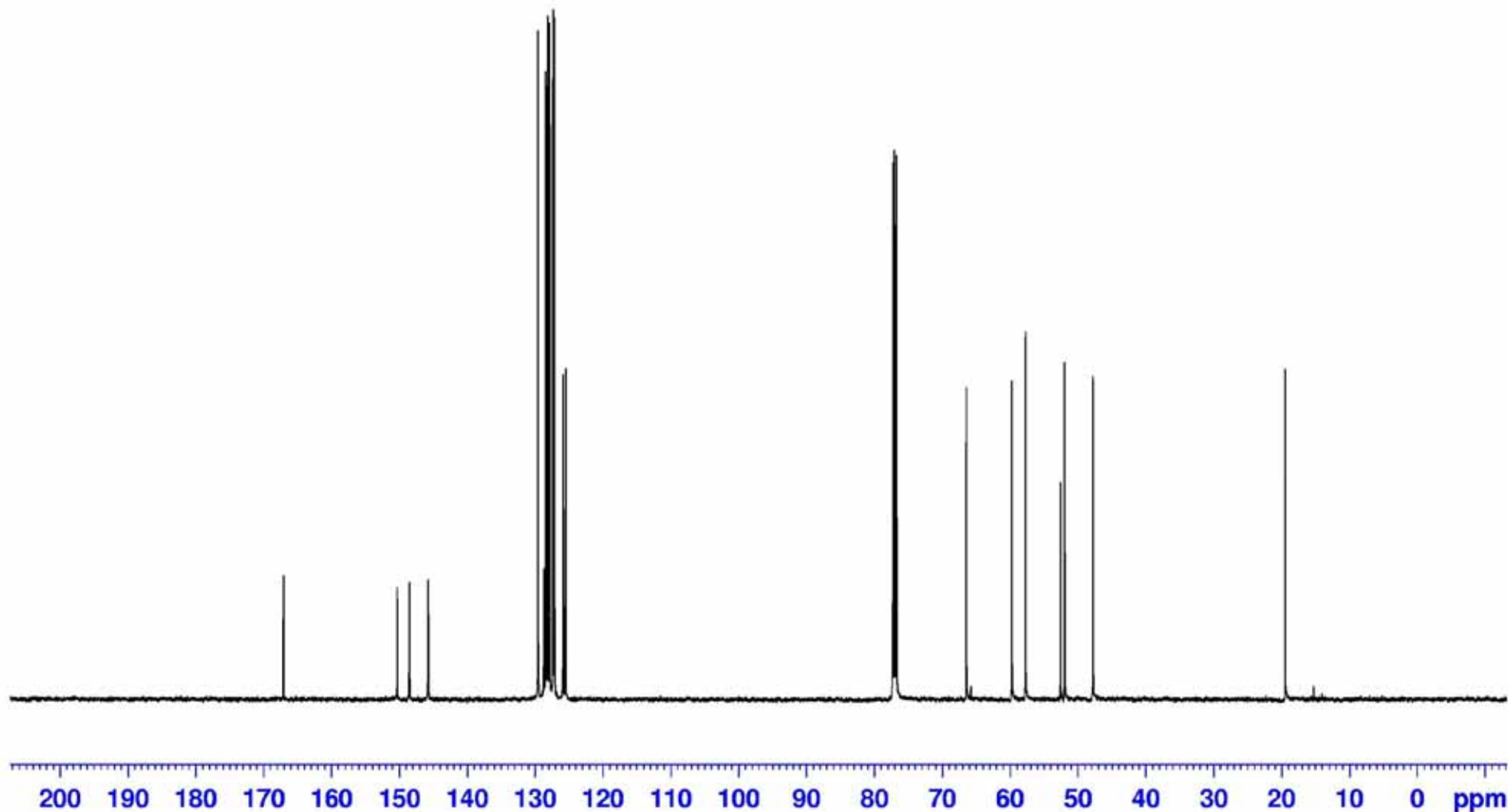
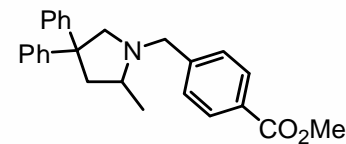
$^{13}\text{C}\{^1\text{H}\}$ NMR of 1-(4-Chlorobenzyl)-2-methyl-4,4-diphenylpyrrolidine (CDCl_3 , 126 MHz, 300 K)



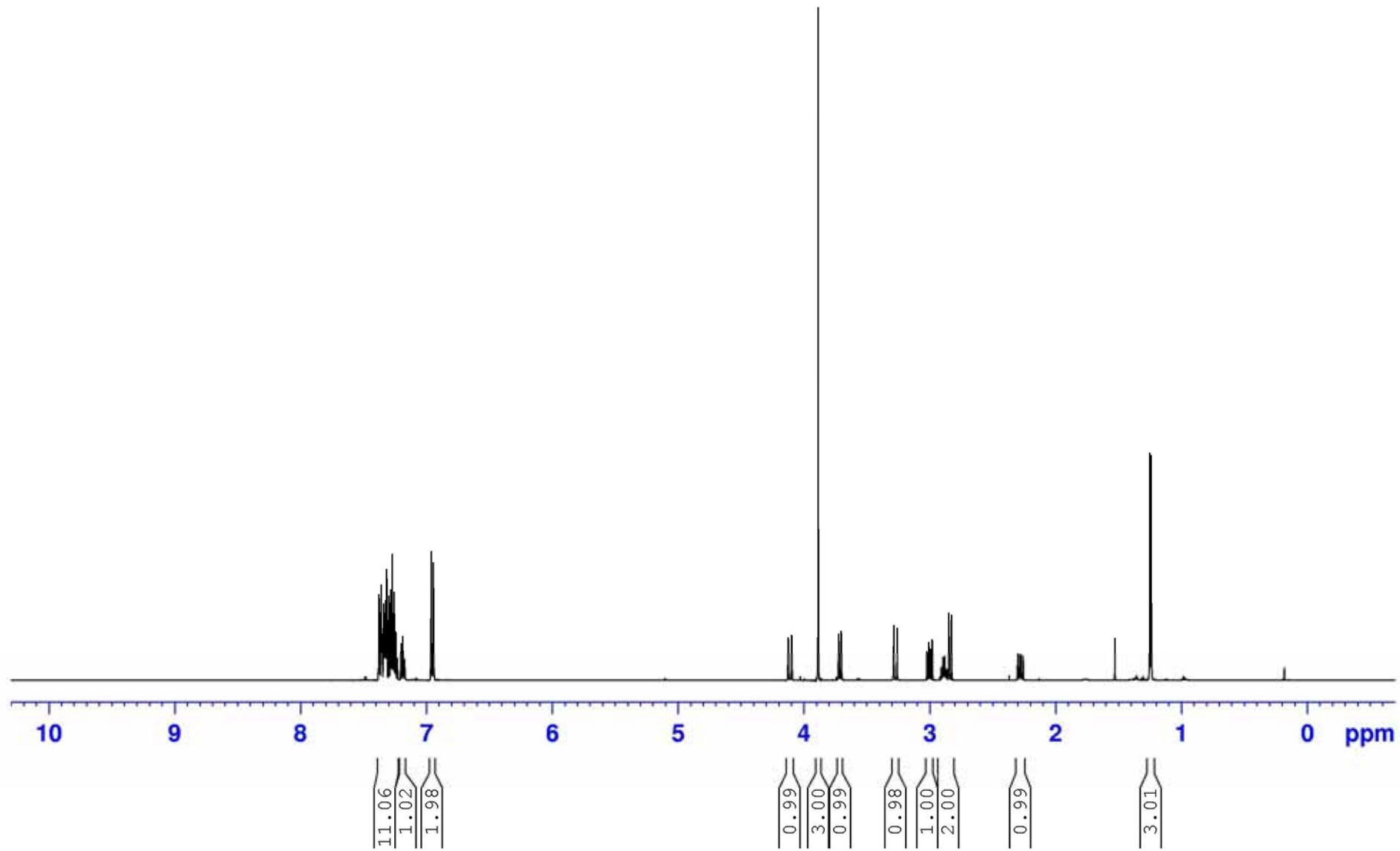
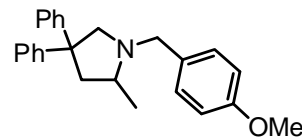
¹H NMR of Methyl 4-(2-methyl-4,4-diphenylpyrrolidin-1-ylmethyl)-benzoate. (CDCl₃, 500 MHz, 300 K)



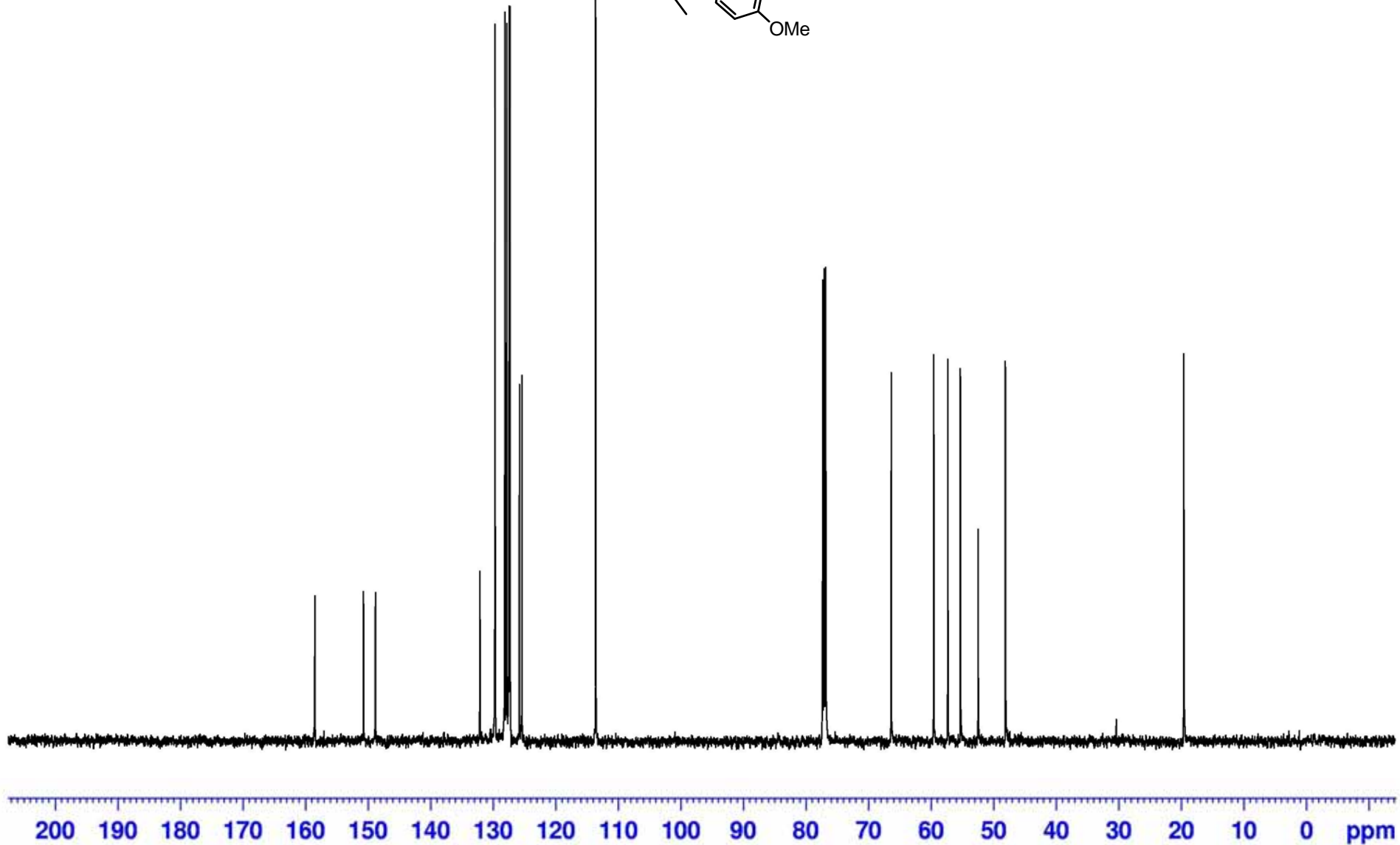
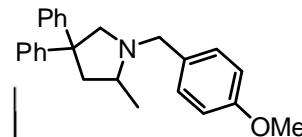
$^{13}\text{C}\{^1\text{H}\}$ NMR of Methyl 4-(2-methyl-4,4-diphenylpyrrolidin-1-ylmethyl)-benzoate. (CDCl_3 , 126 MHz, 300 K)



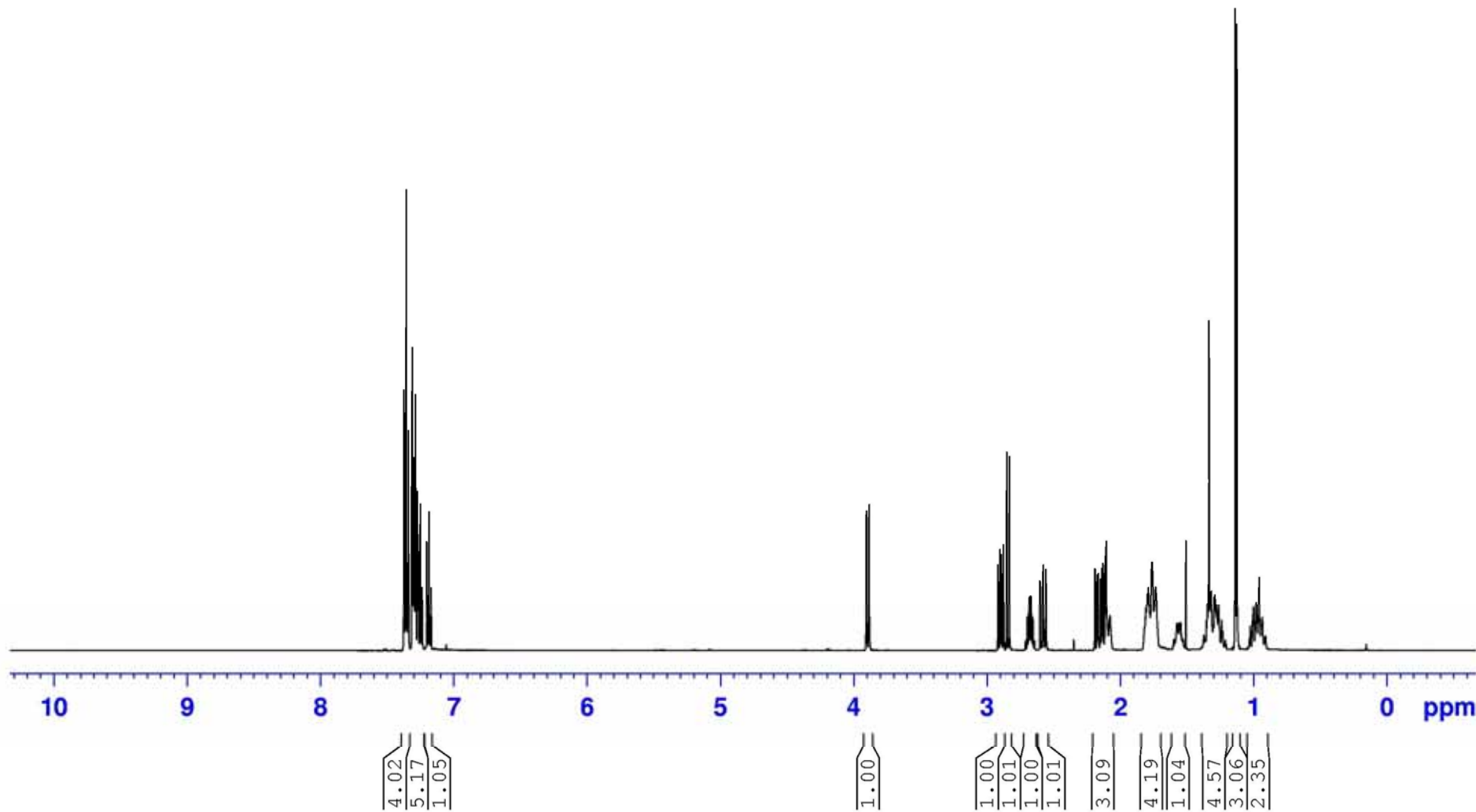
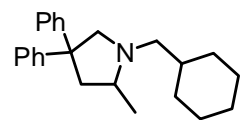
¹H NMR of 1-(4-Methoxybenzyl)-2-methyl-4,4-diphenylpyrrolidine. (CDCl₃, 500 MHz, 300 K)



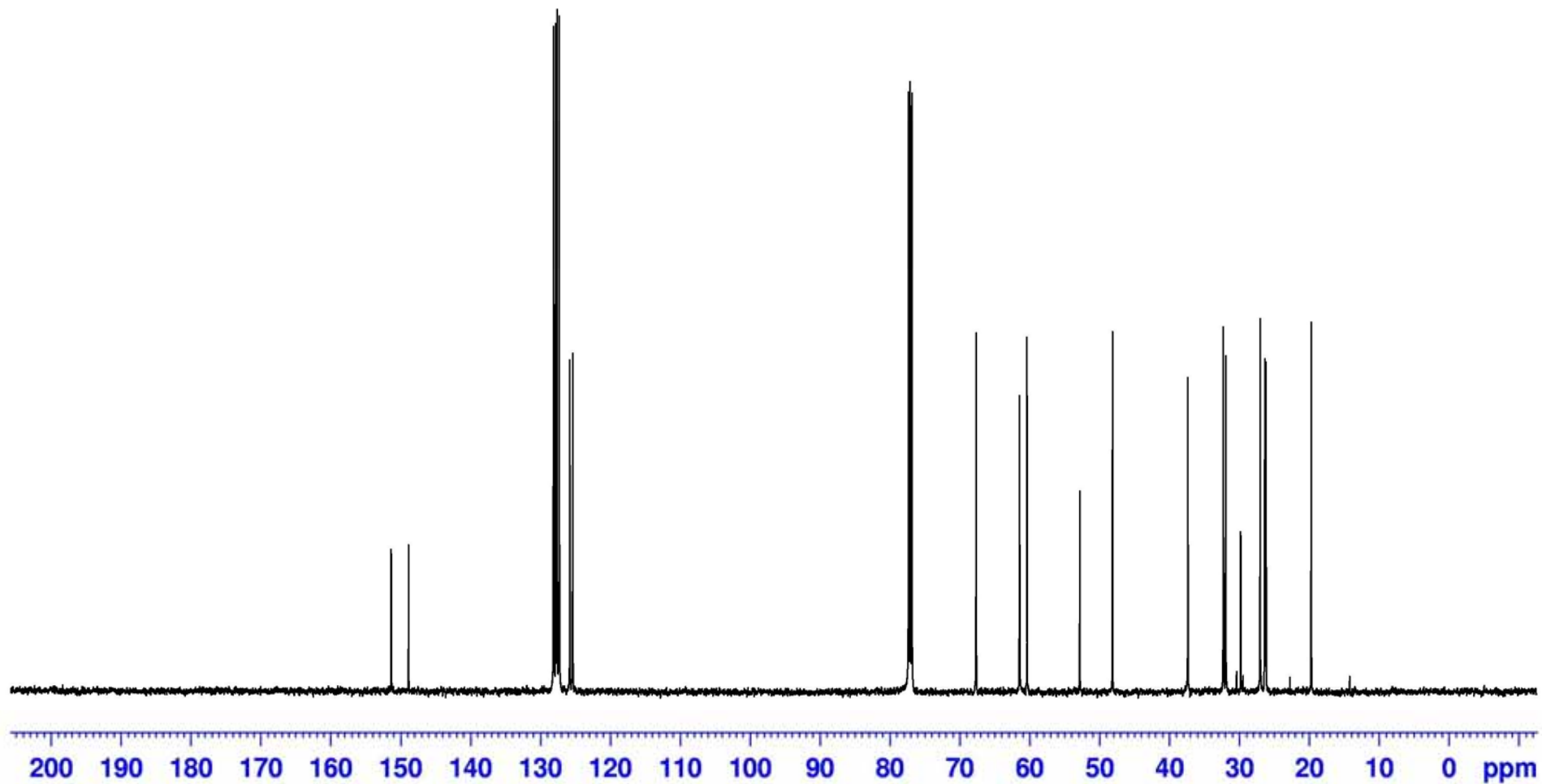
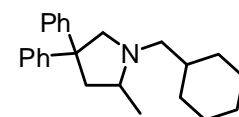
$^{13}\text{C}\{\text{H}\}$ NMR of 1-(4-Methoxybenzyl)-2-methyl-4,4-diphenylpyrrolidine. (CDCl_3 , 126 MHz, 300 K)



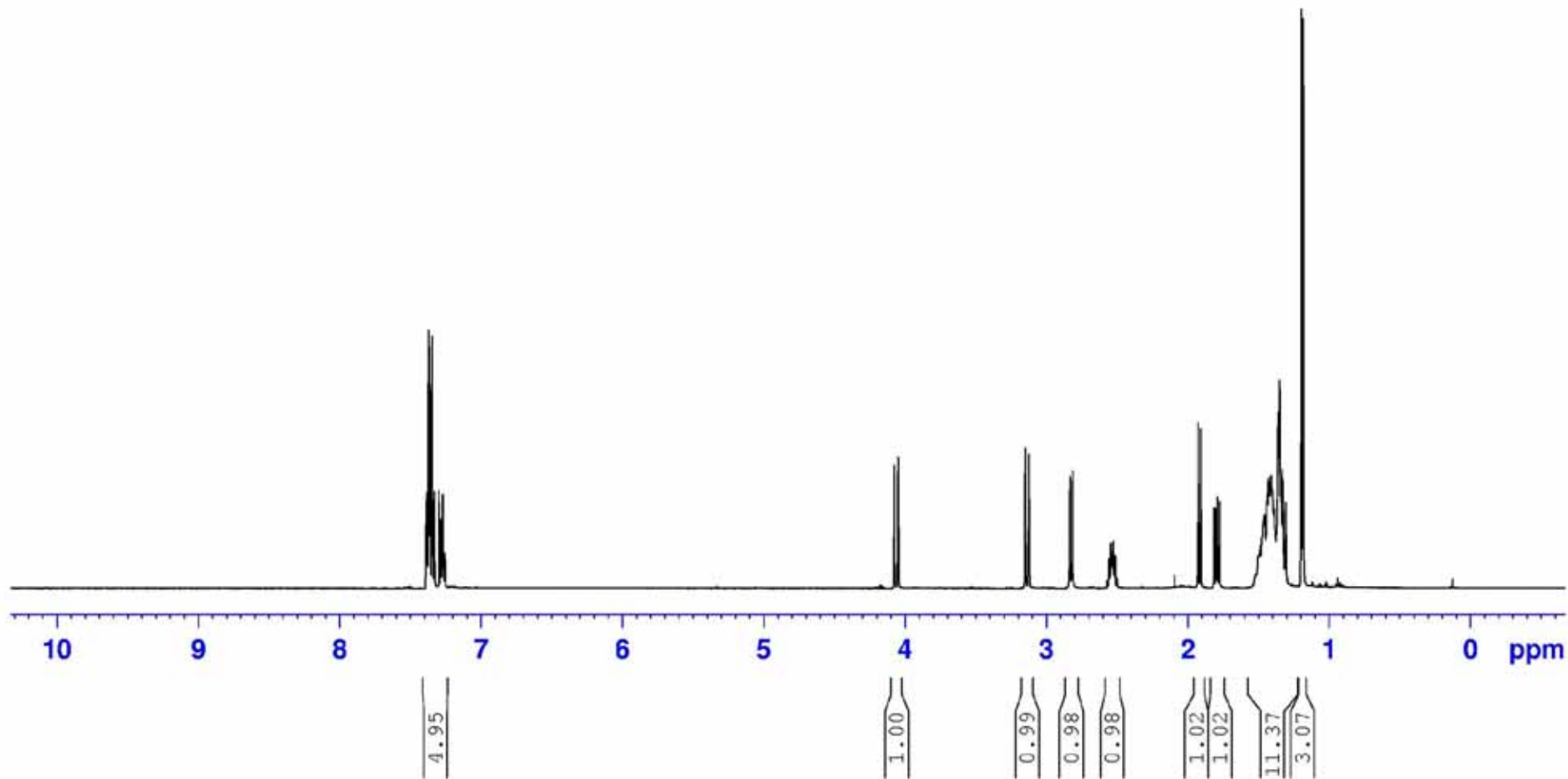
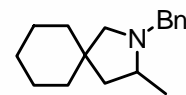
¹H NMR of 1-Cyclohexylmethyl-2-methyl-4,4-diphenylpyrrolidine. (CDCl₃, 500 MHz, 300 K)



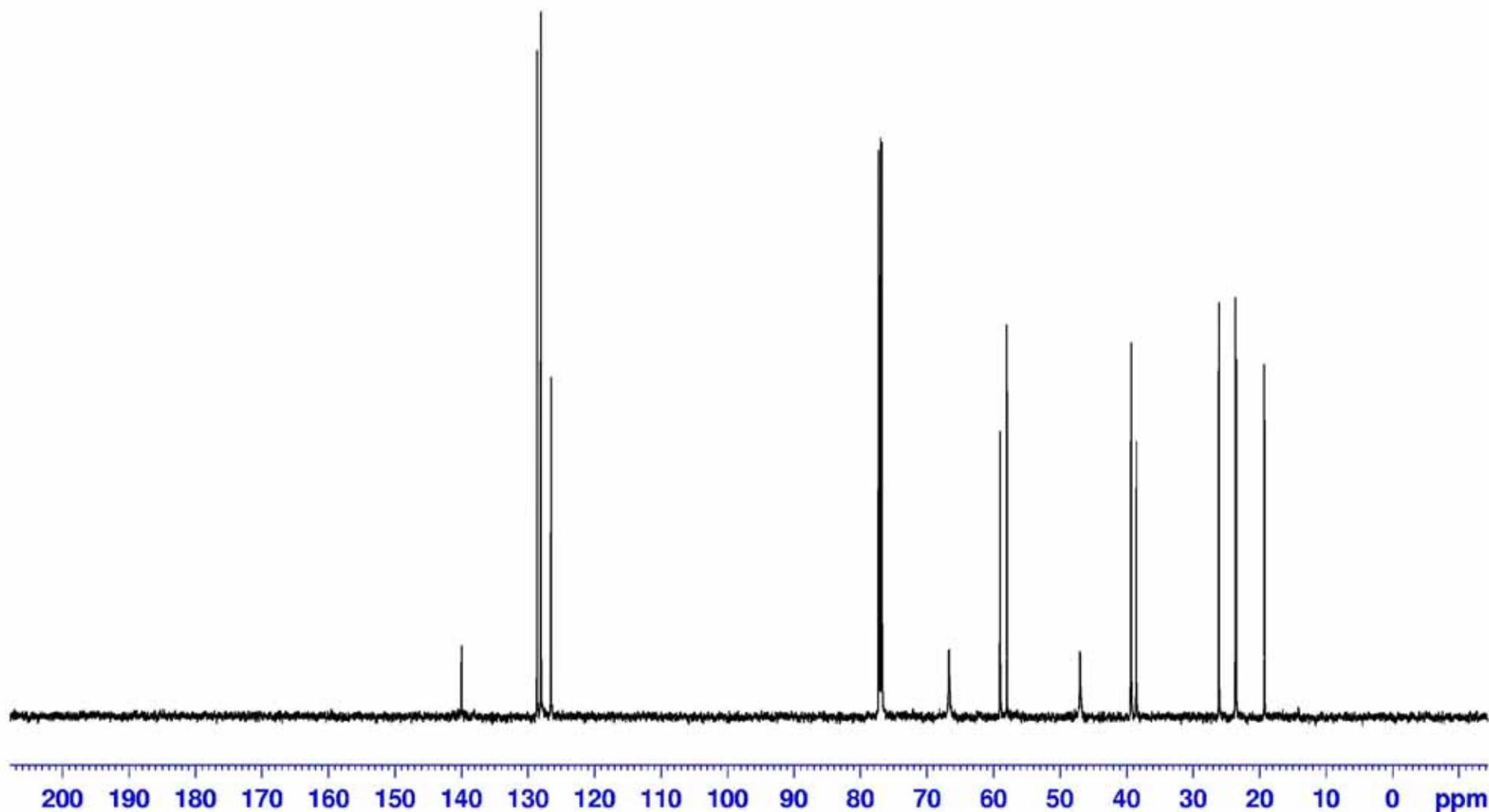
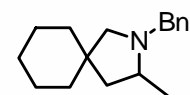
$^{13}\text{C}\{^1\text{H}\}$ NMR of 1-Cyclohexylmethyl-2-methyl-4,4-diphenylpyrrolidine. (CDCl_3 , 126 MHz, 300 K)



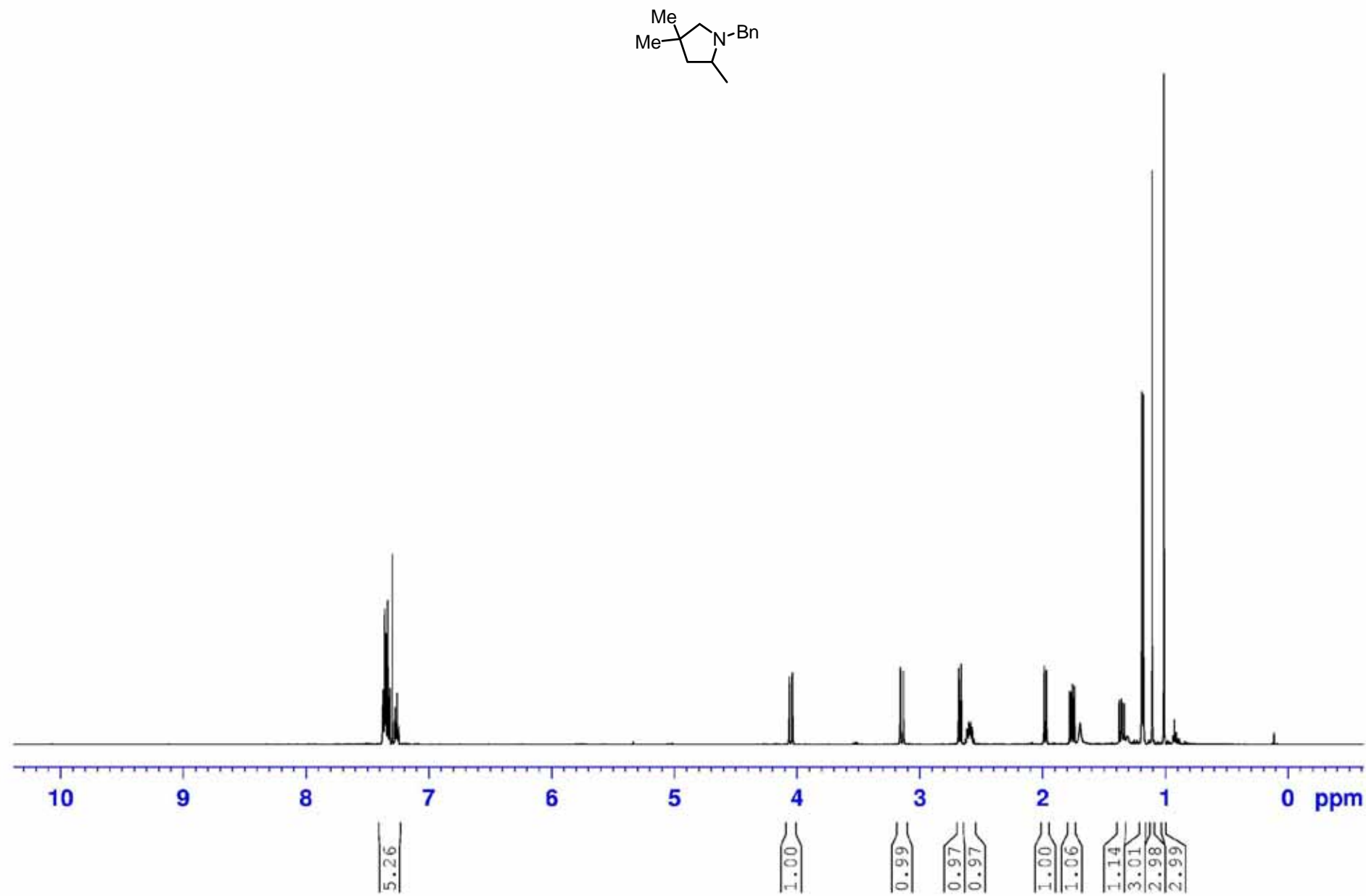
¹H NMR of 2-Benzyl-3-methyl-2-aza-spiro[4,5]decane. (CDCl₃, 500 MHz, 300 K)



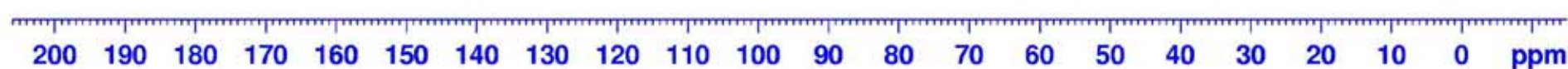
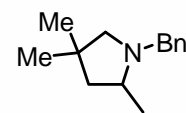
$^{13}\text{C}\{1\text{H}\}$ NMR of 2-Benzyl-3-methyl-2-aza-spiro[4,5]decane. (CDCl_3 , 126 MHz, 300 K)



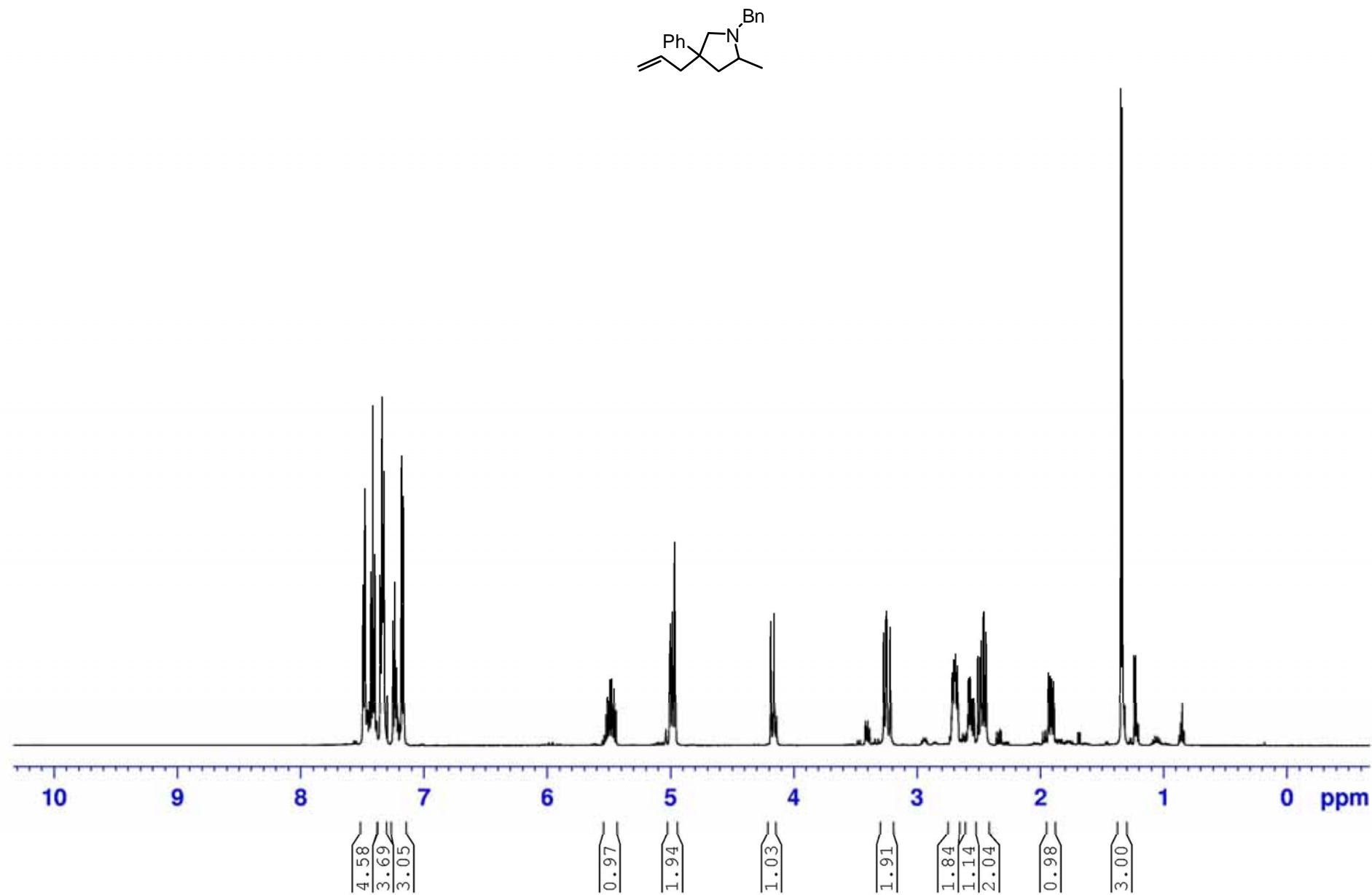
¹H NMR of 1-Benzyl-2,4,4-trimethylpyrrolidine. (CDCl₃, 500 MHz, 300 K)



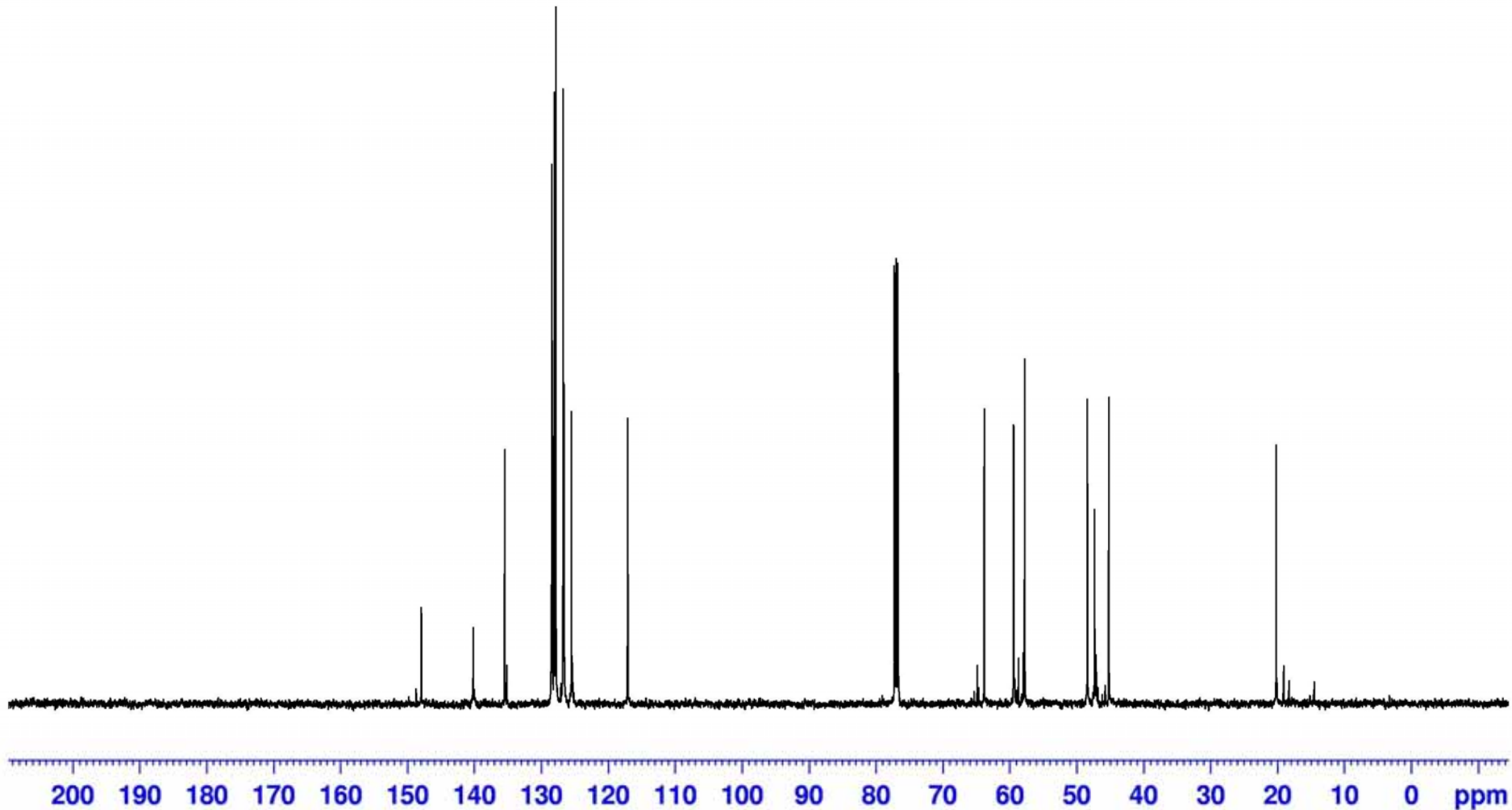
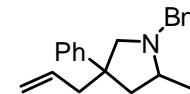
$^{13}\text{C}\{^1\text{H}\}$ NMR of 1-Benzyl-2,4,4-trimethylpyrrolidine. (CDCl_3 , 126 MHz, 300 K)



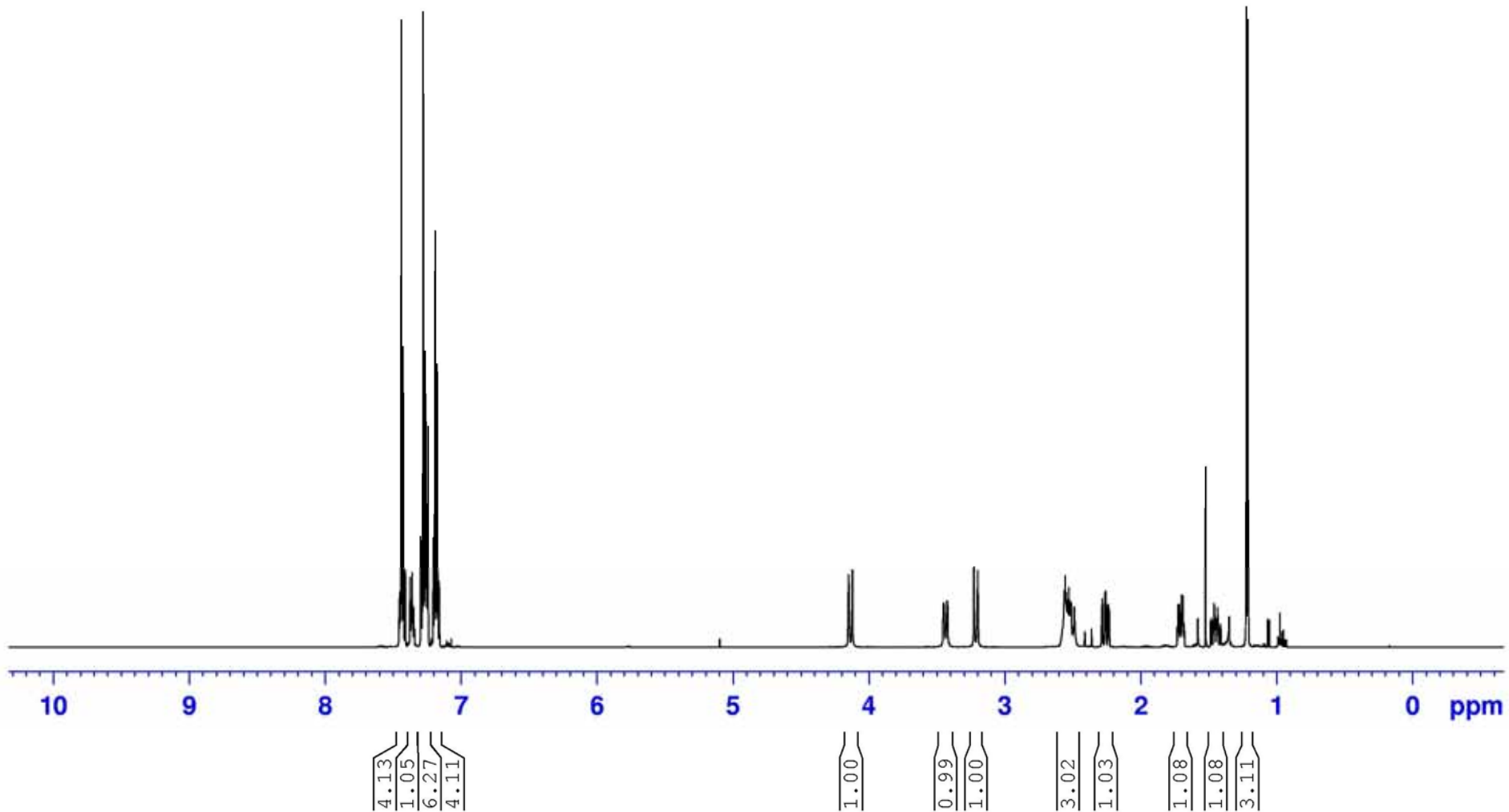
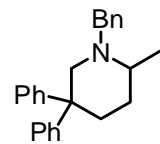
¹H NMR of 1-Benzyl-4-Allyl-2-methyl-4-phenyl-pyrrolidine. (CDCl₃, 500 MHz, 300 K)



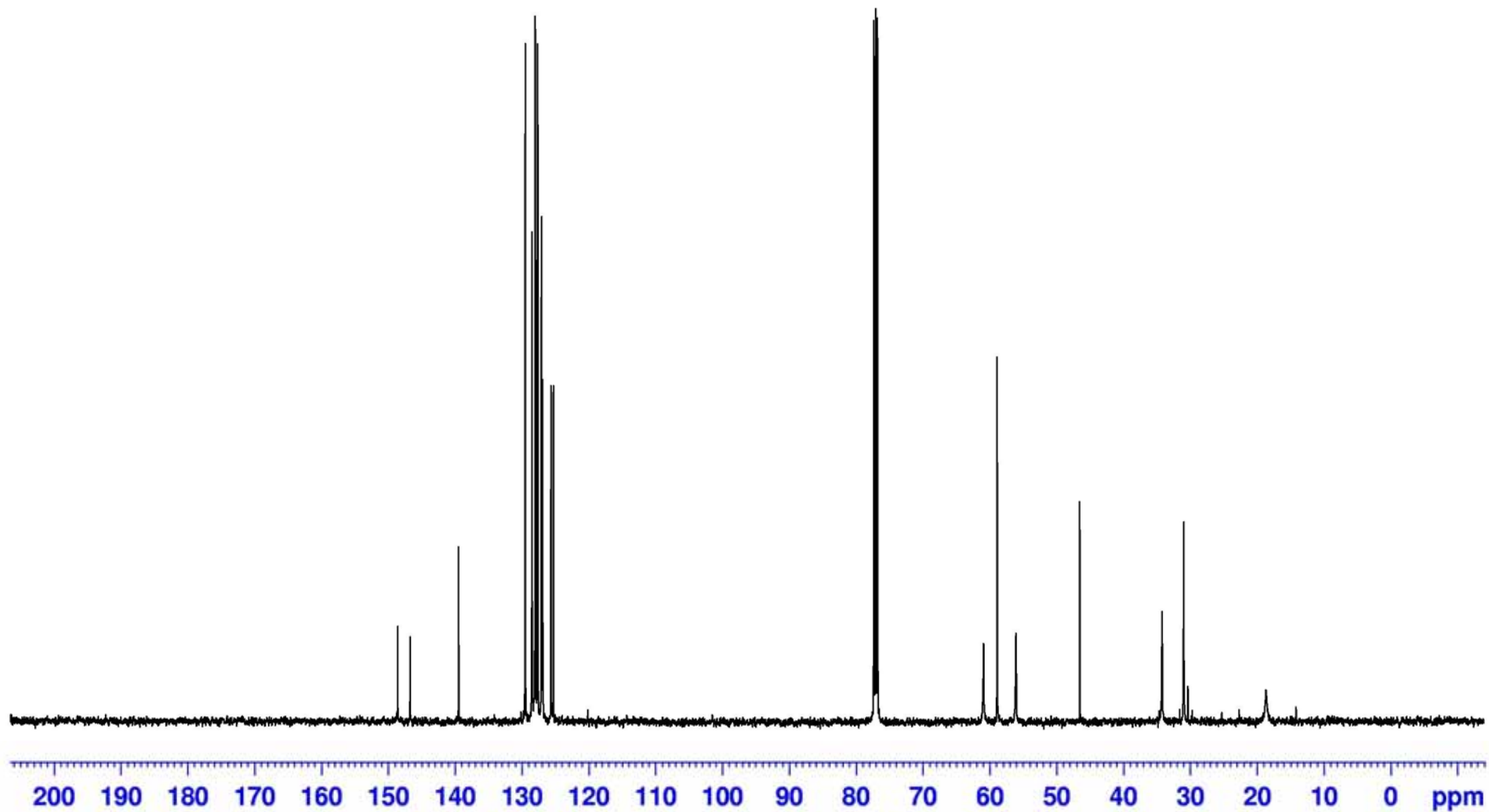
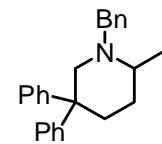
$^{13}\text{C}\{^1\text{H}\}$ NMR of 1-Benzyl-4-Allyl-2-methyl-4-phenyl-pyrrolidine. (CDCl_3 , 126 MHz, 300 K)



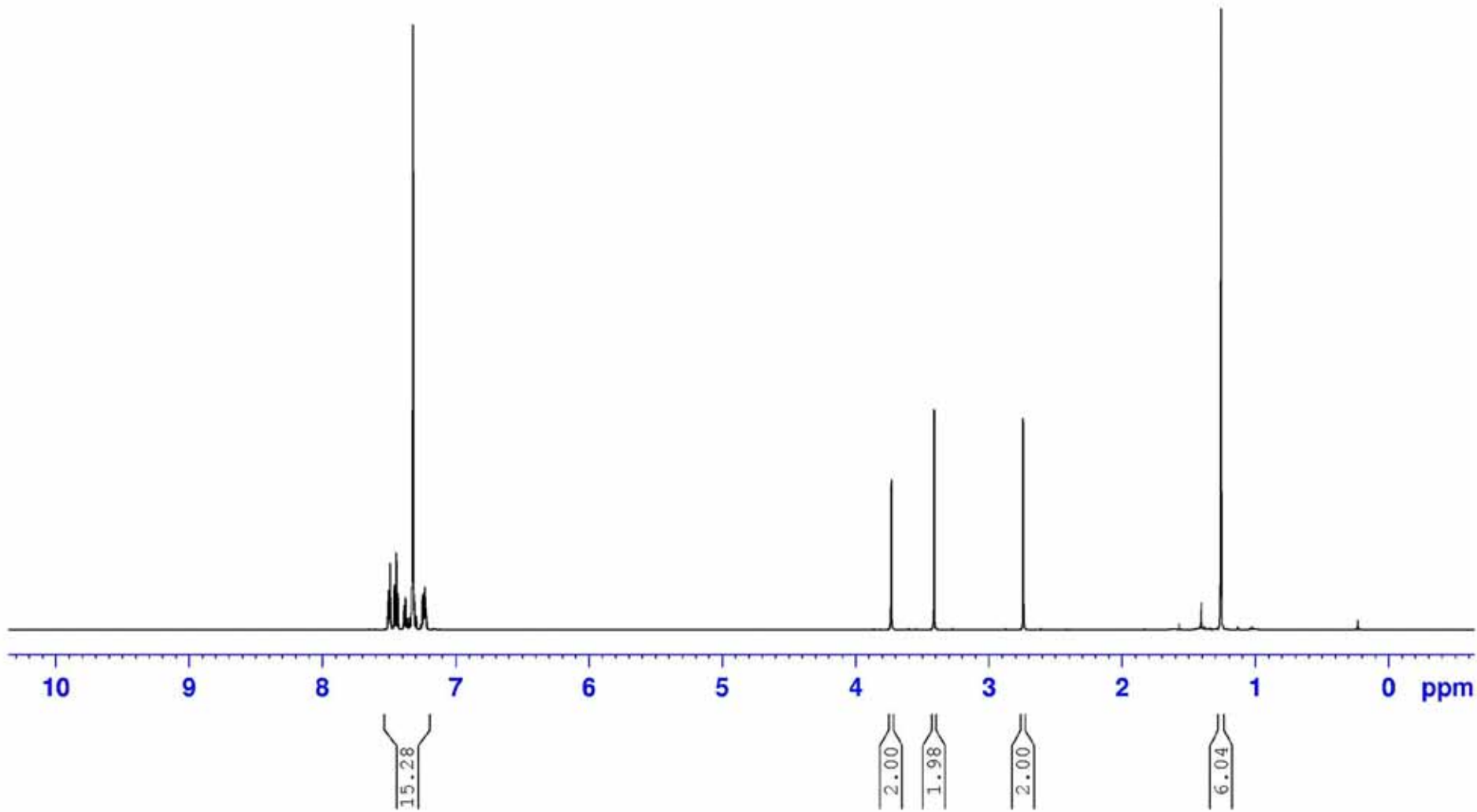
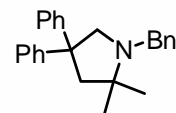
¹H NMR of 1-Benzyl-2-methyl-5,5-diphenylpiperidine. (CDCl₃, 500 MHz, 300 K)



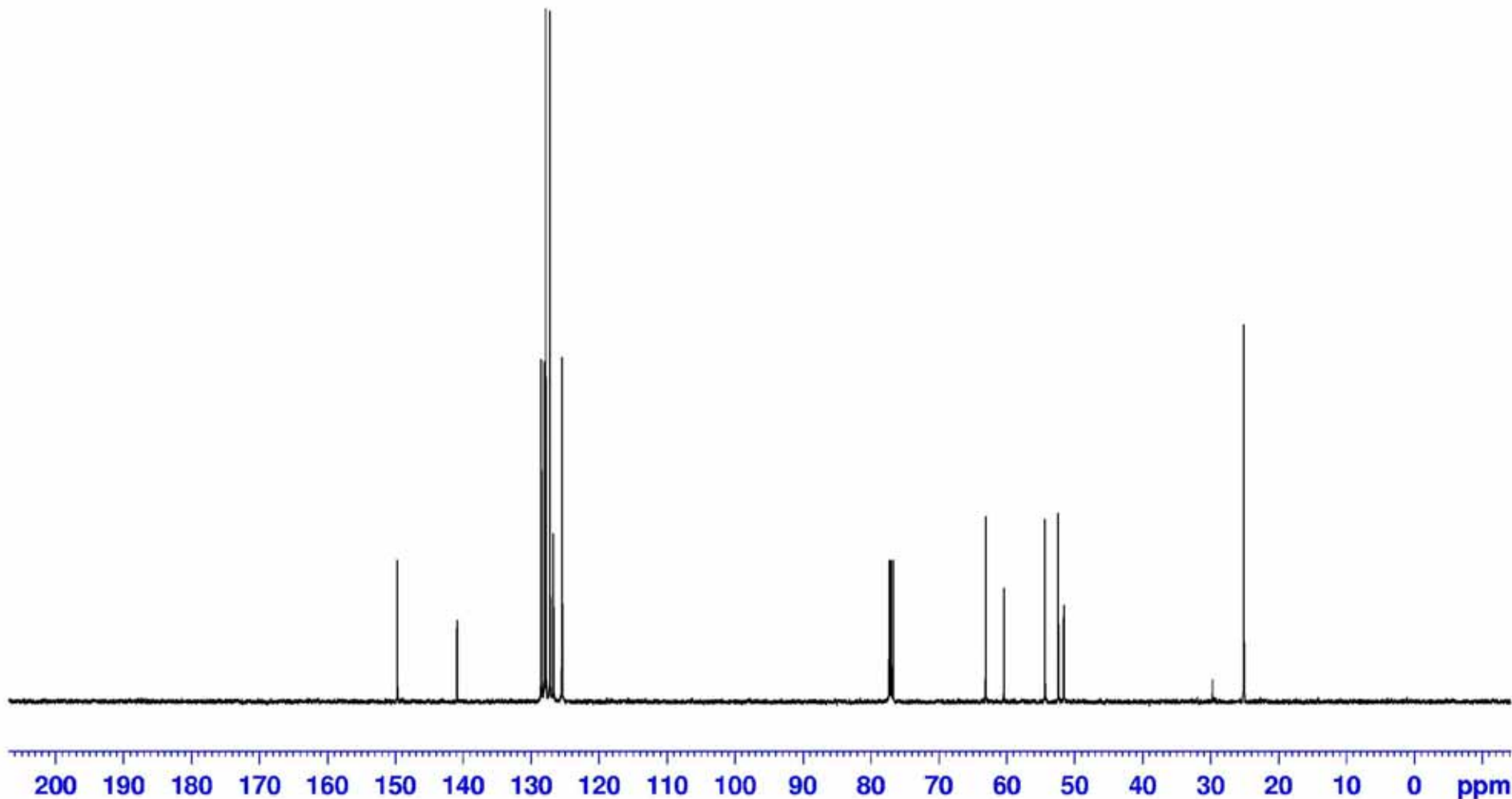
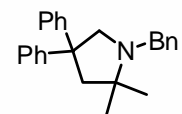
$^{13}\text{C}\{^1\text{H}\}$ NMR of 1-Benzyl-2-methyl-5,5-diphenylpiperidine. (CDCl_3 , 126 MHz, 300 K)



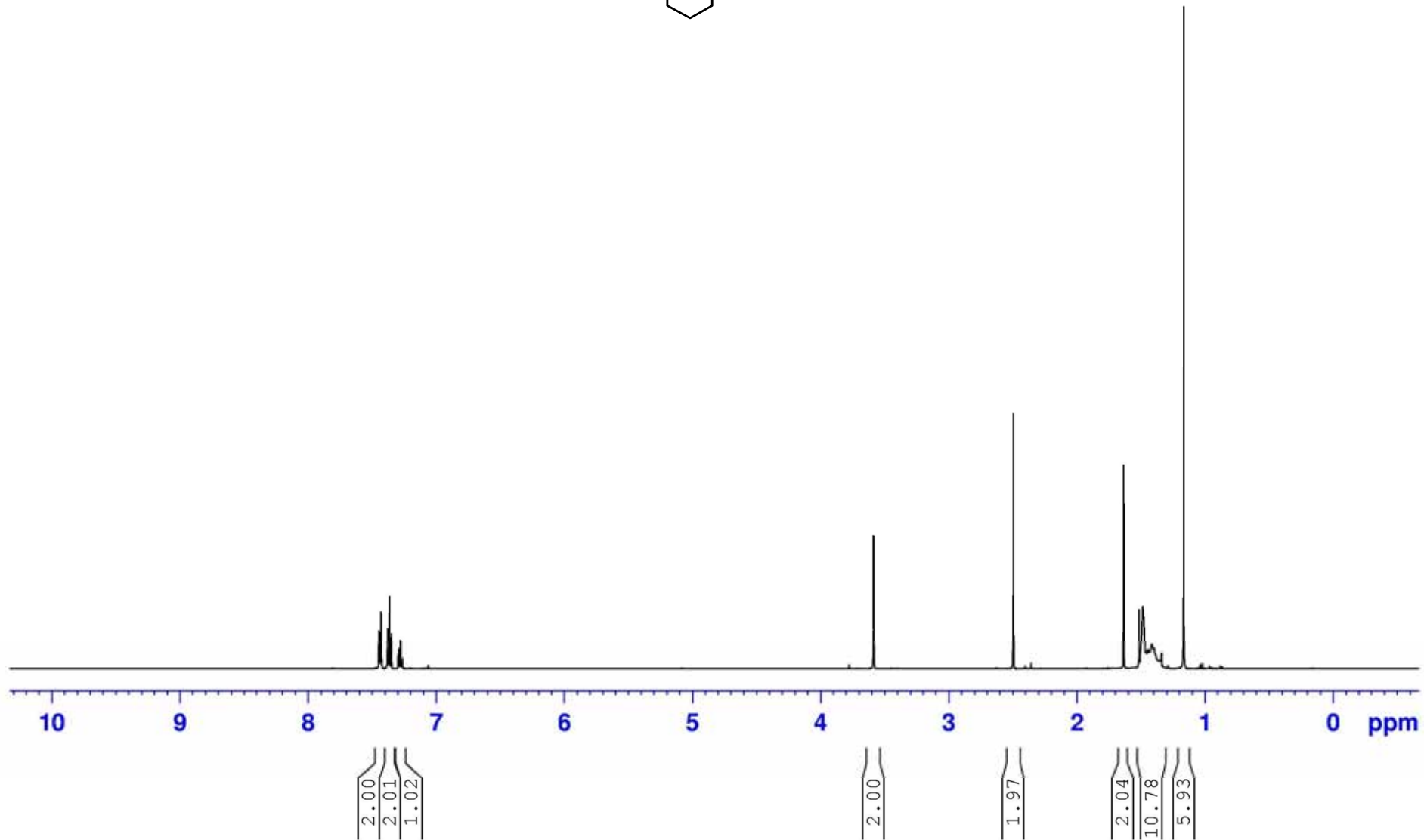
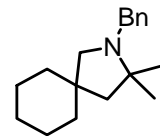
¹H NMR of 1-Benzyl-2,2-dimethyl-4,4-diphenylpyrrolidine. (CDCl₃, 500 MHz, 300 K)



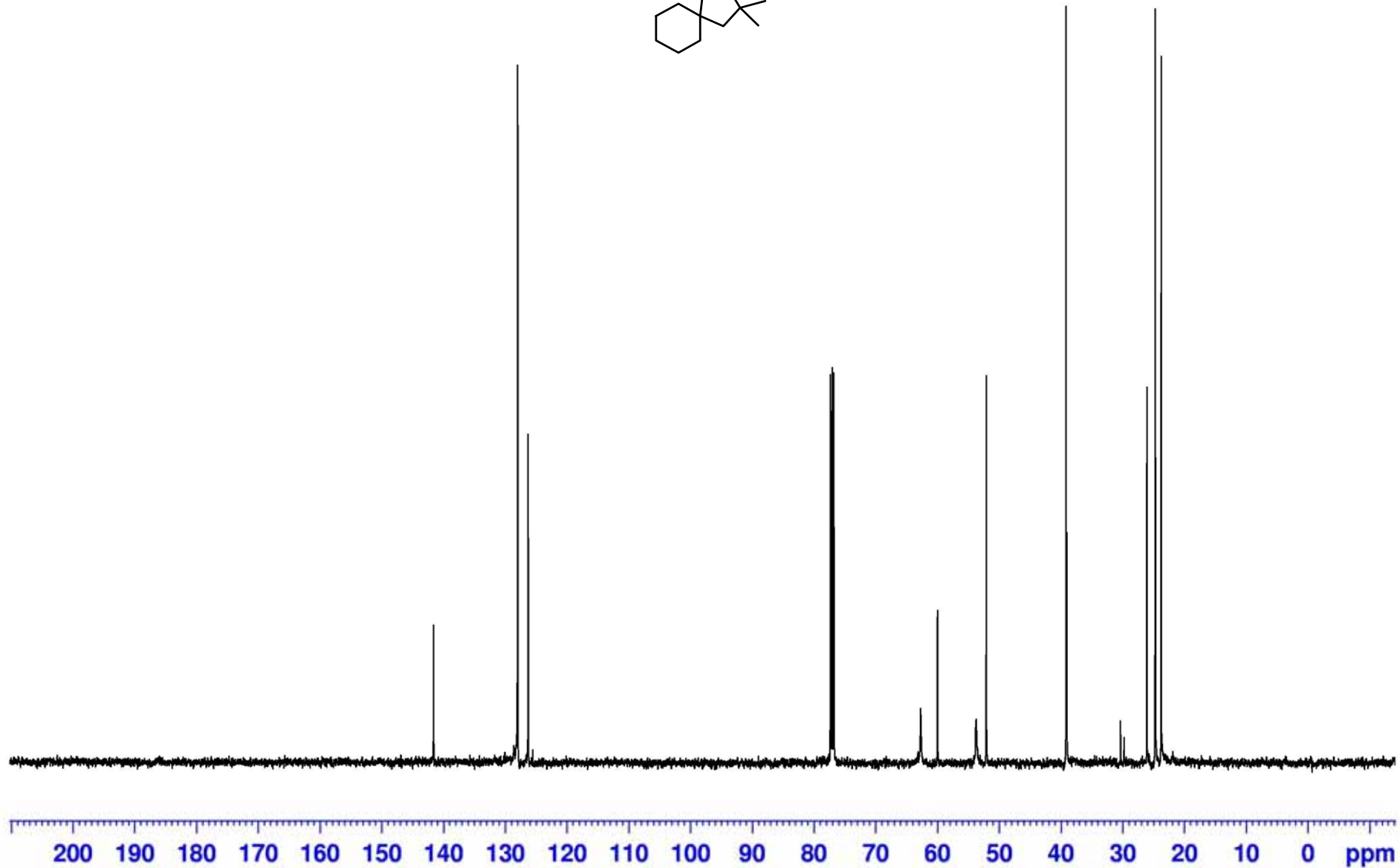
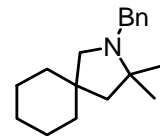
$^{13}\text{C}\{^1\text{H}\}$ NMR of 1-Benzyl-2,2-dimethyl-4,4-diphenylpyrrolidine. (CDCl_3 , 126 MHz, 300 K)



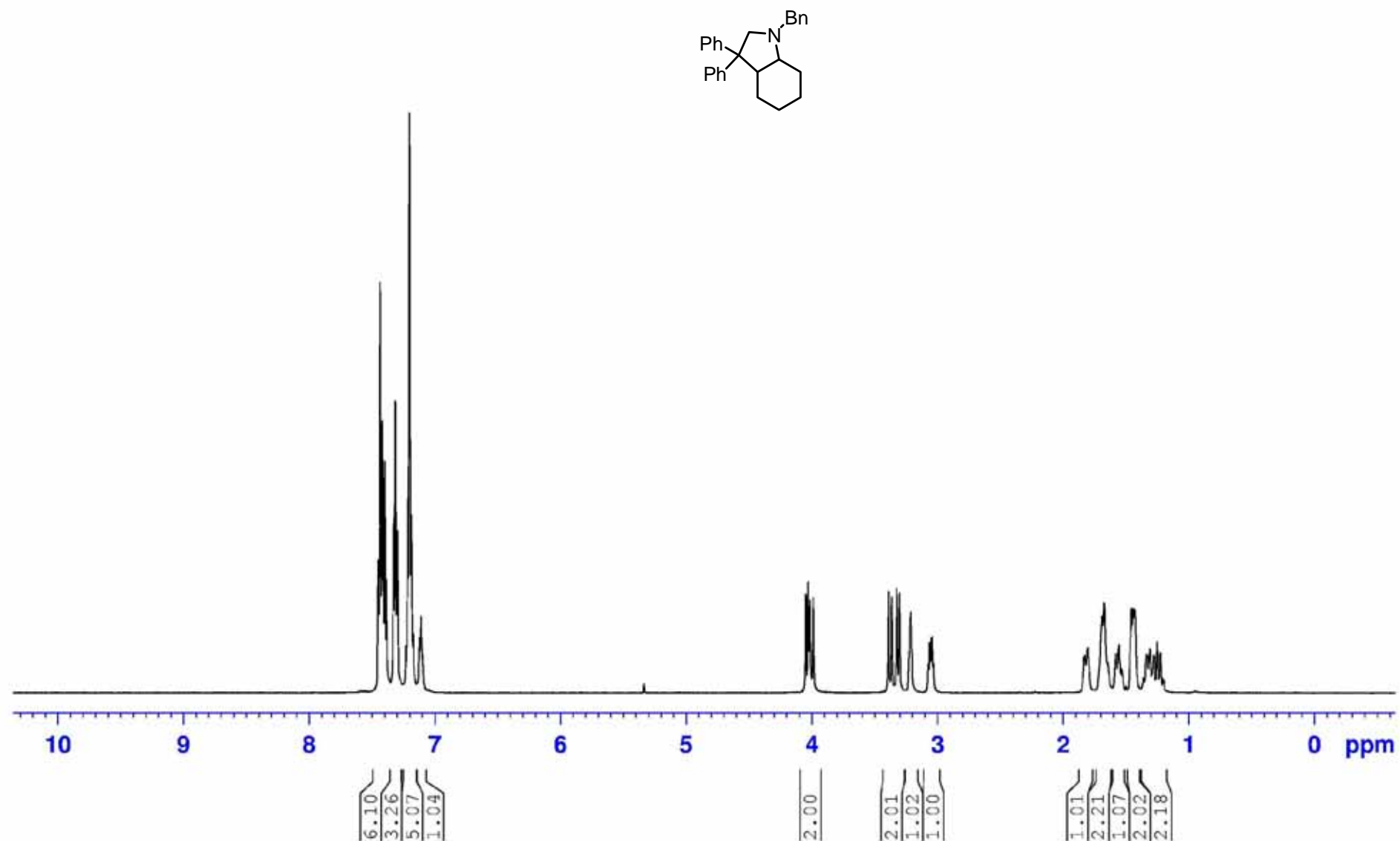
¹H NMR of 2-benzyl-3,3-dimethyl-2-azaspiro[4.5]decane. (CDCl₃, 500 MHz, 300 K)



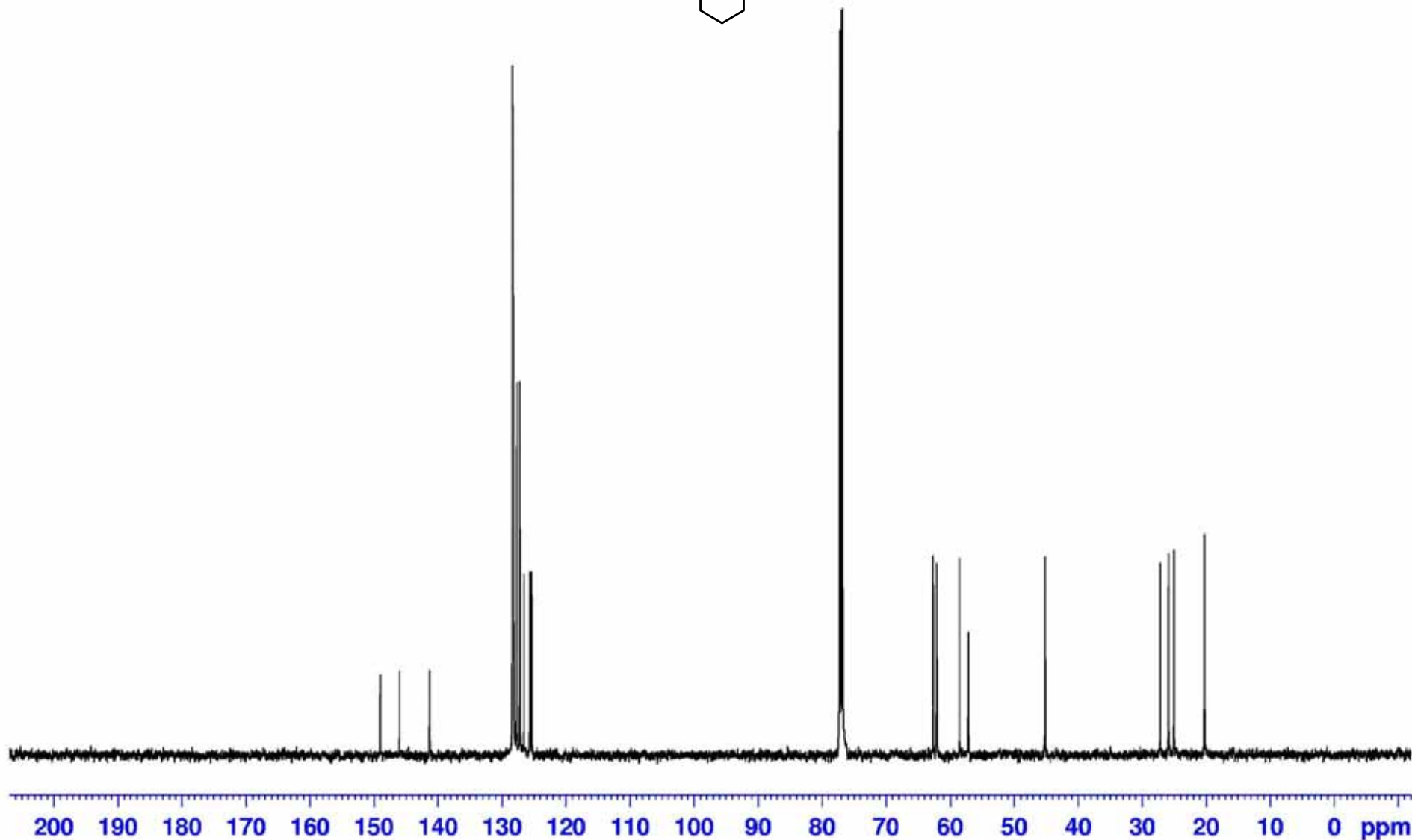
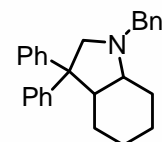
$^{13}\text{C}\{^1\text{H}\}$ NMR of 2-benzyl-3,3-dimethyl-2-azaspiro[4.5]decane. (CDCl_3 , 126 MHz, 300 K)



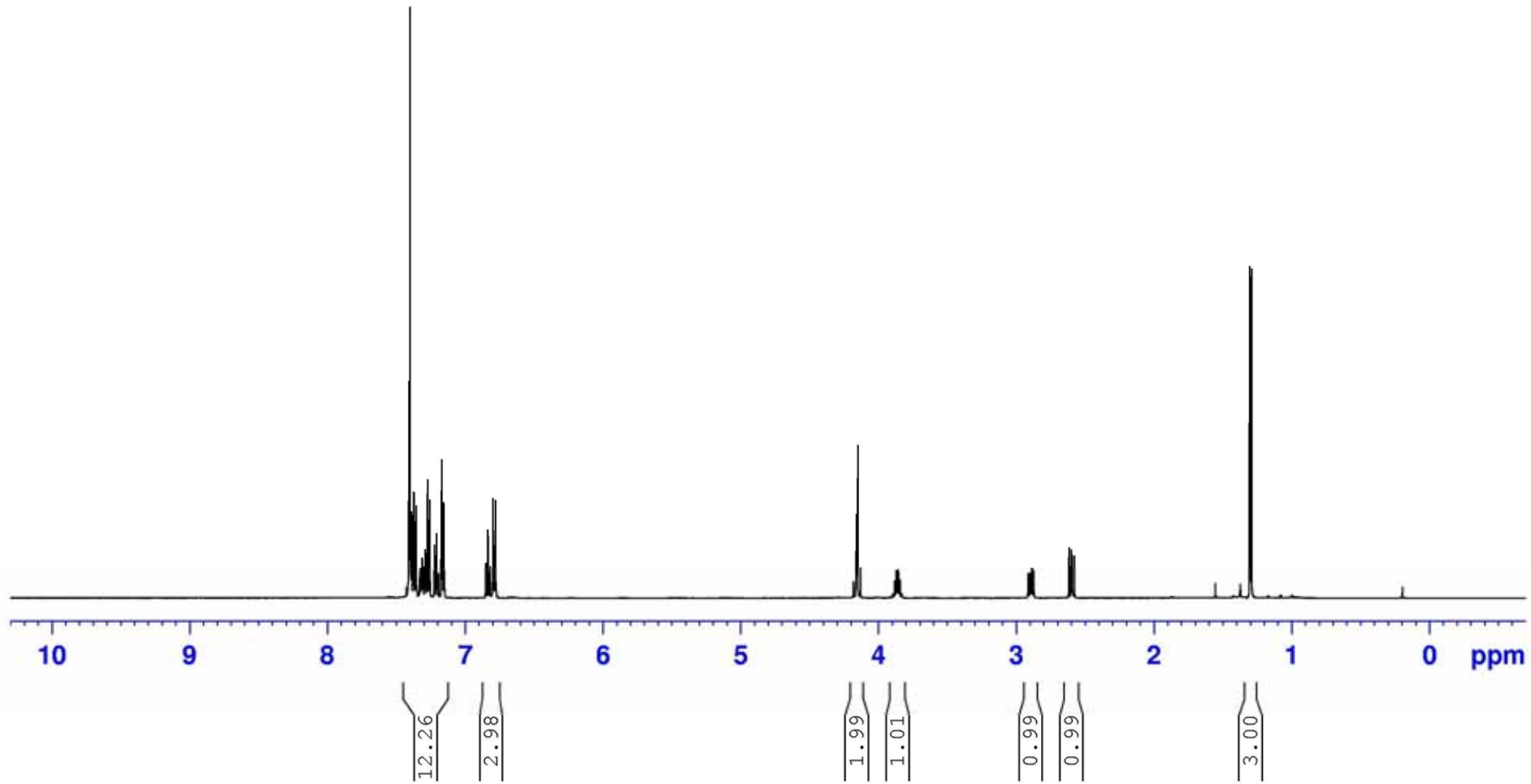
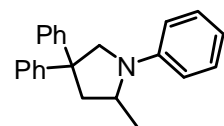
¹H NMR of 3,3-Diphenyl-1-benzyl-octahydro-indole (CDCl₃, 500MHz, 300 K):



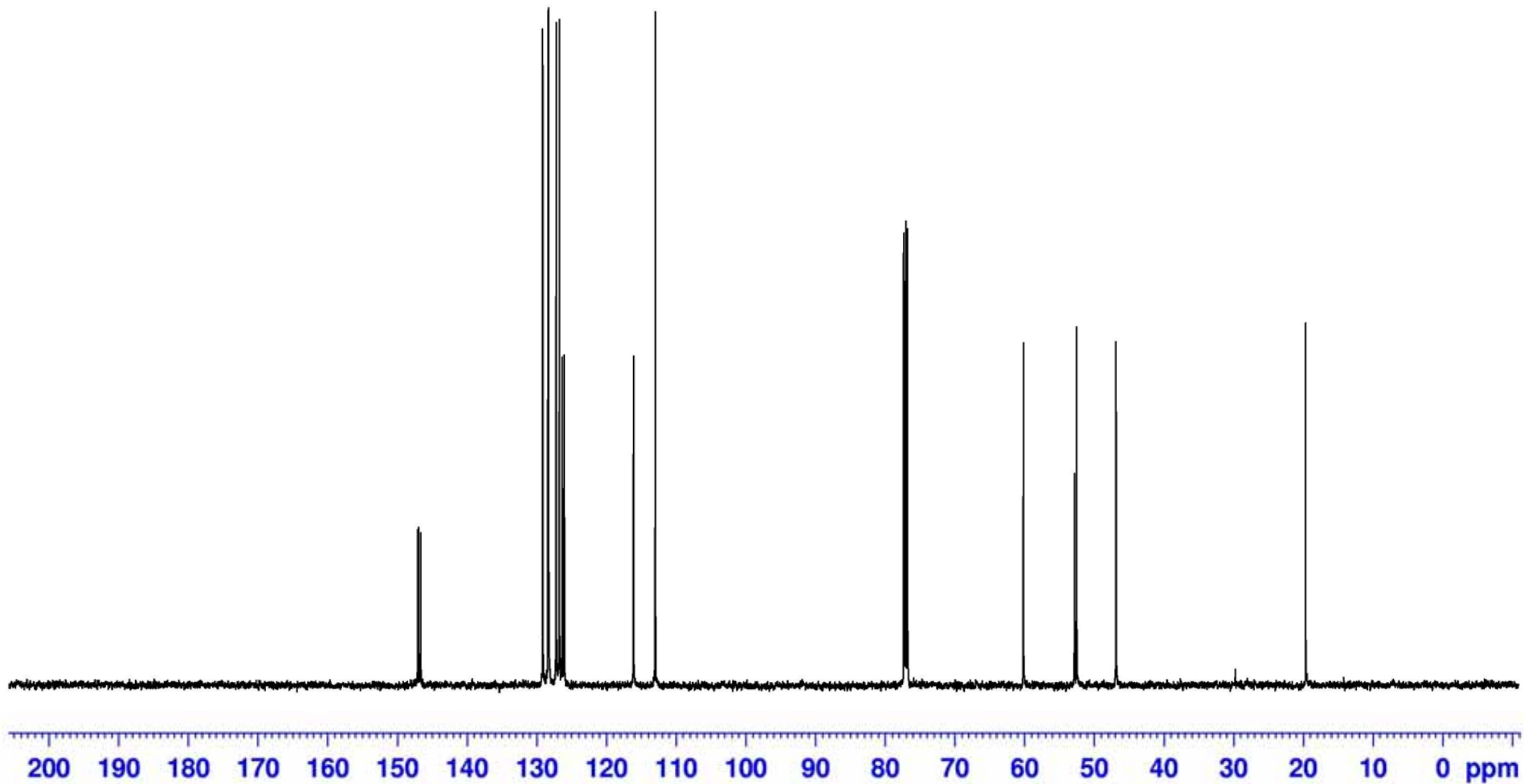
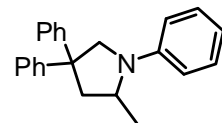
$^{13}\text{C}\{\text{H}\}$ NMR of 3,3-Diphenyl-1-benzyl-octahydro-indole (CDCl_3 , 125MHz, 300 K):



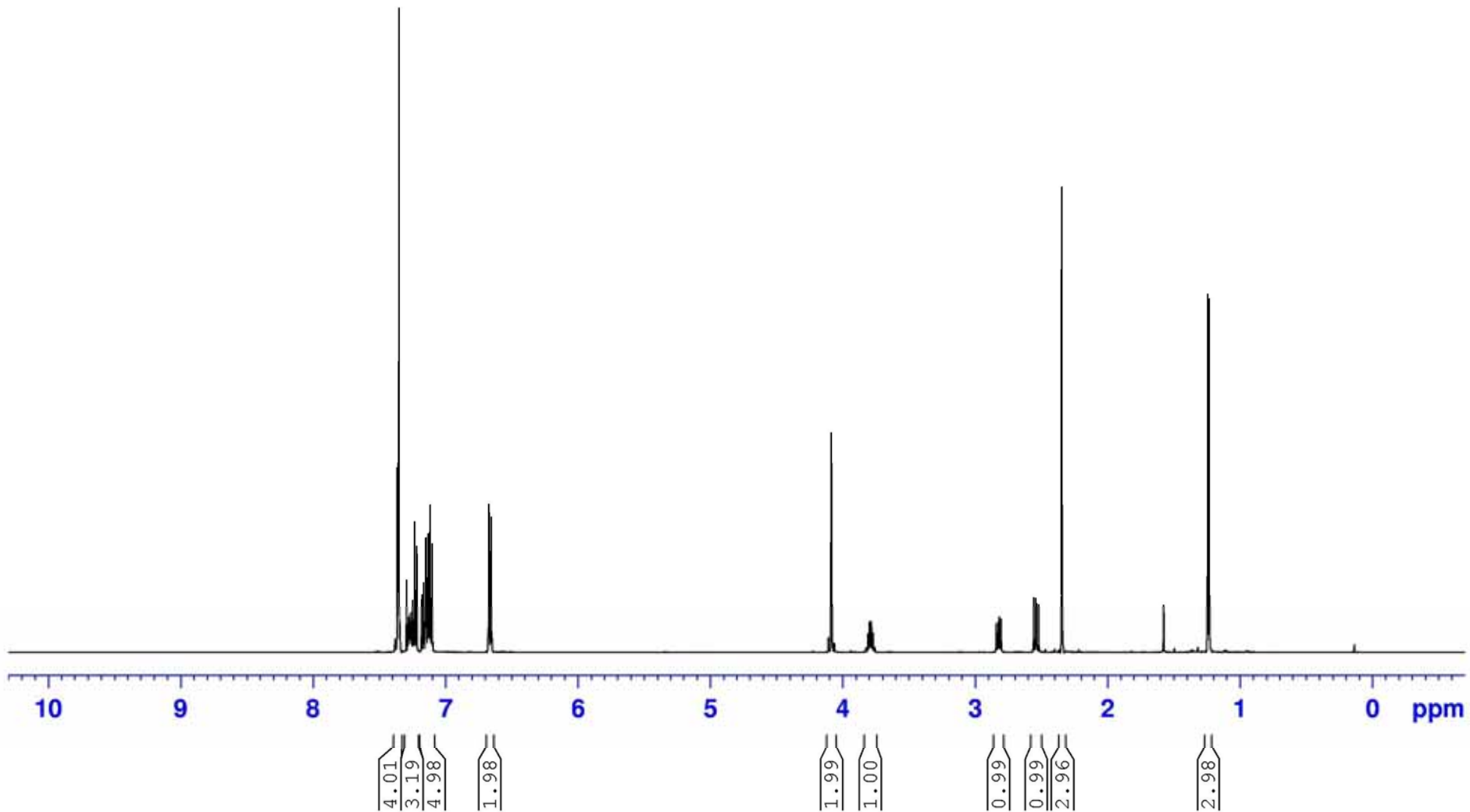
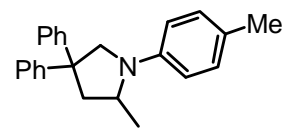
¹H NMR of 1-Phenyl-2-methyl-4,4-diphenylpyrrolidine. (CDCl₃, 500 MHz, 300 K)



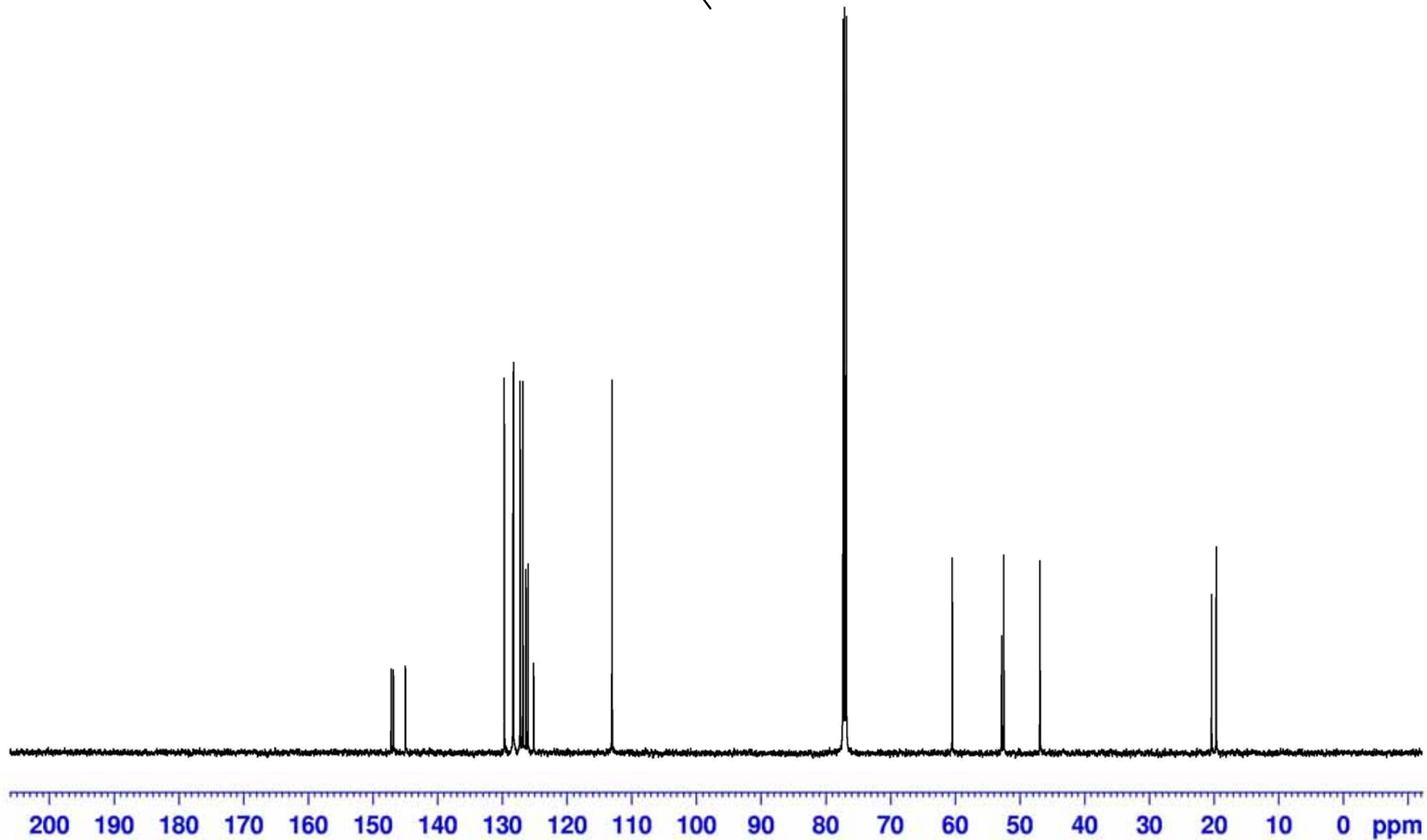
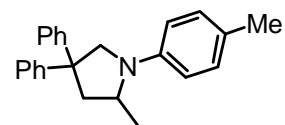
$^{13}\text{C}\{^1\text{H}\}$ NMR of 1-Phenyl-2-methyl-4,4-diphenylpyrrolidine. (CDCl_3 , 126 MHz, 300 K)



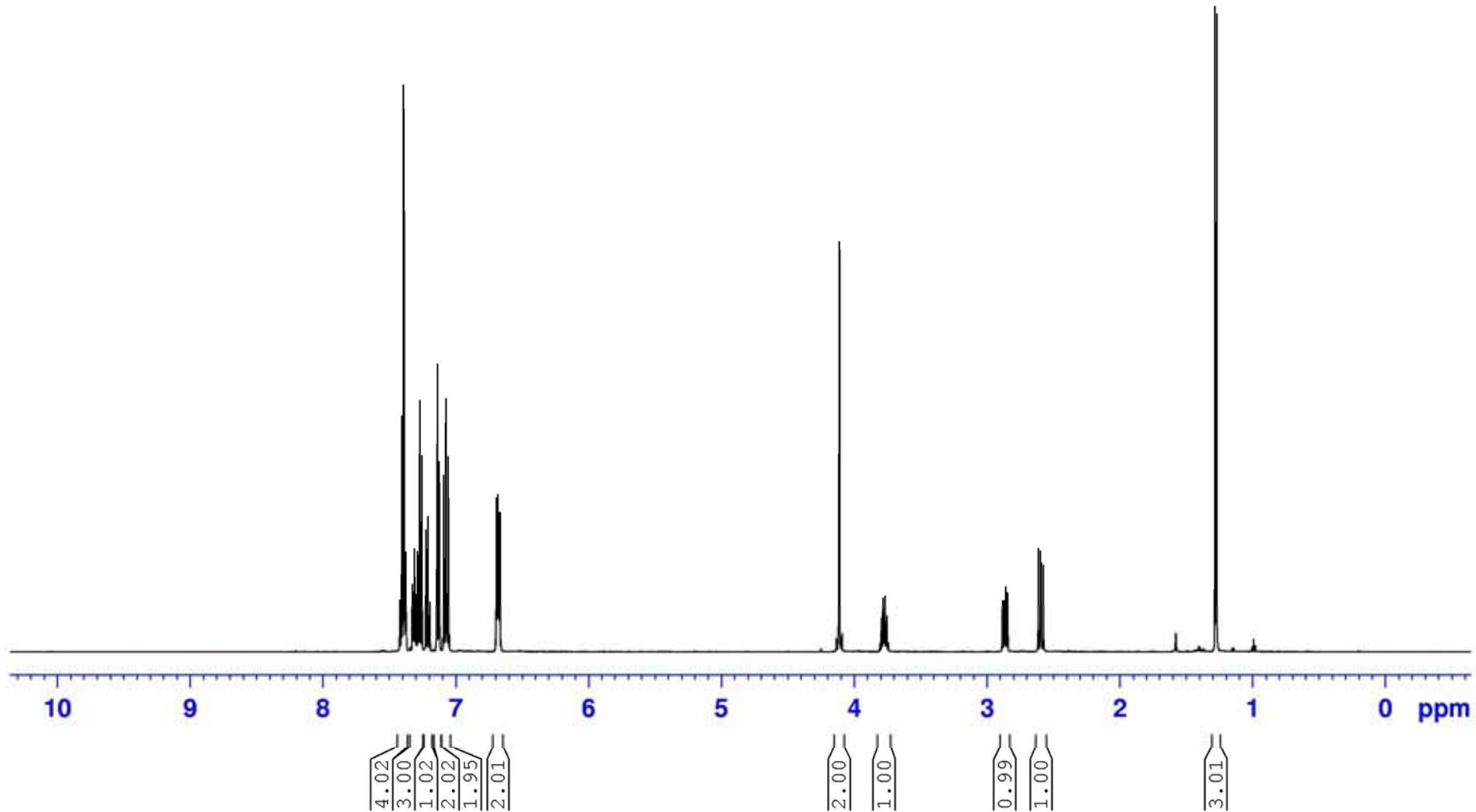
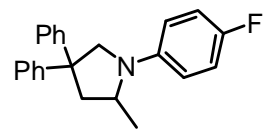
¹H NMR of 1-(4-Methylphenyl)-2-methyl-4,4-diphenylpyrrolidine. (CDCl₃, 500 MHz, 300 K)



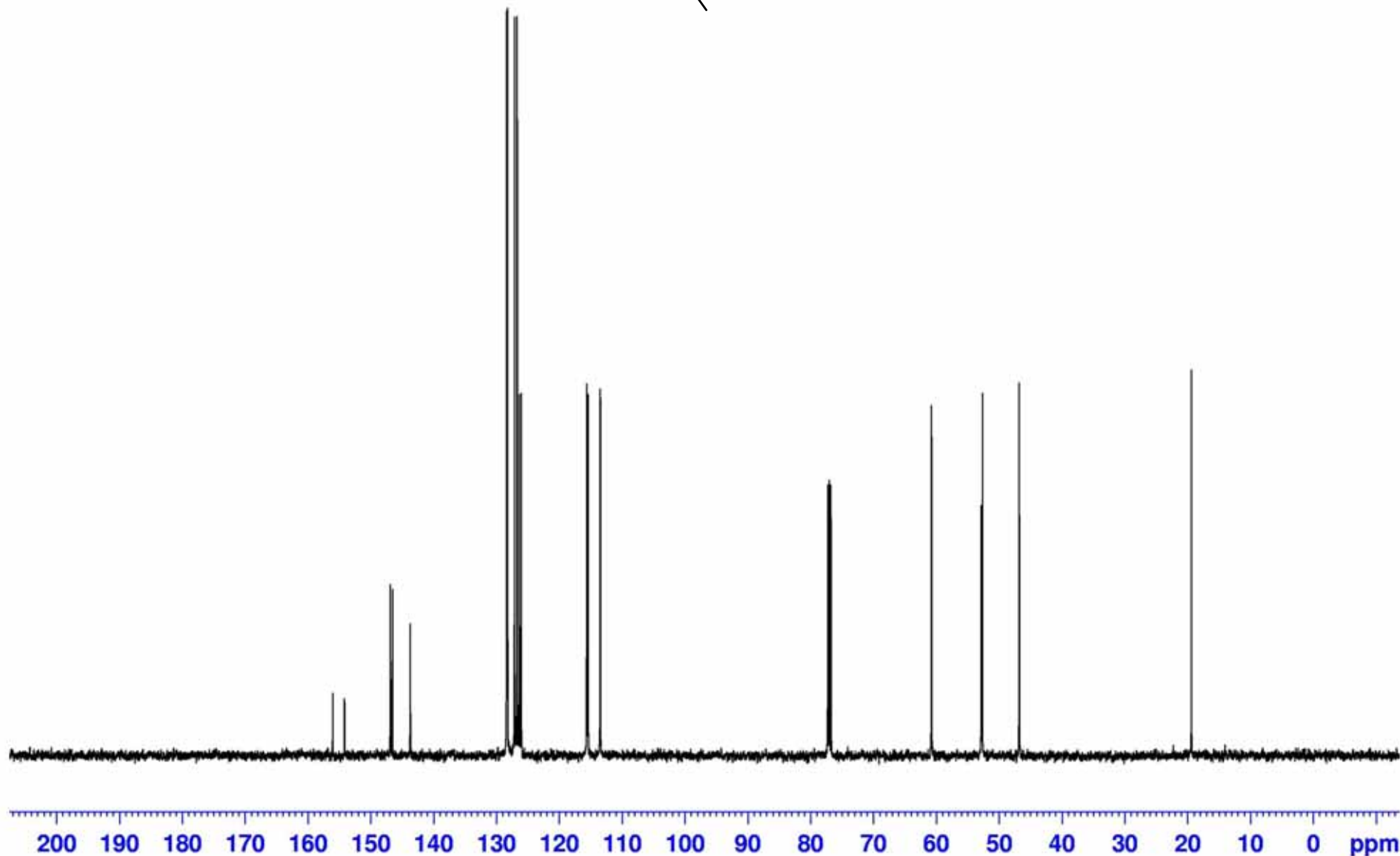
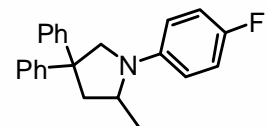
$^{13}\text{C}\{^1\text{H}\}$ NMR of 1-(4-Methylphenyl)-2-methyl-4,4-diphenylpyrrolidine. (CDCl_3 , 126 MHz, 300 K)



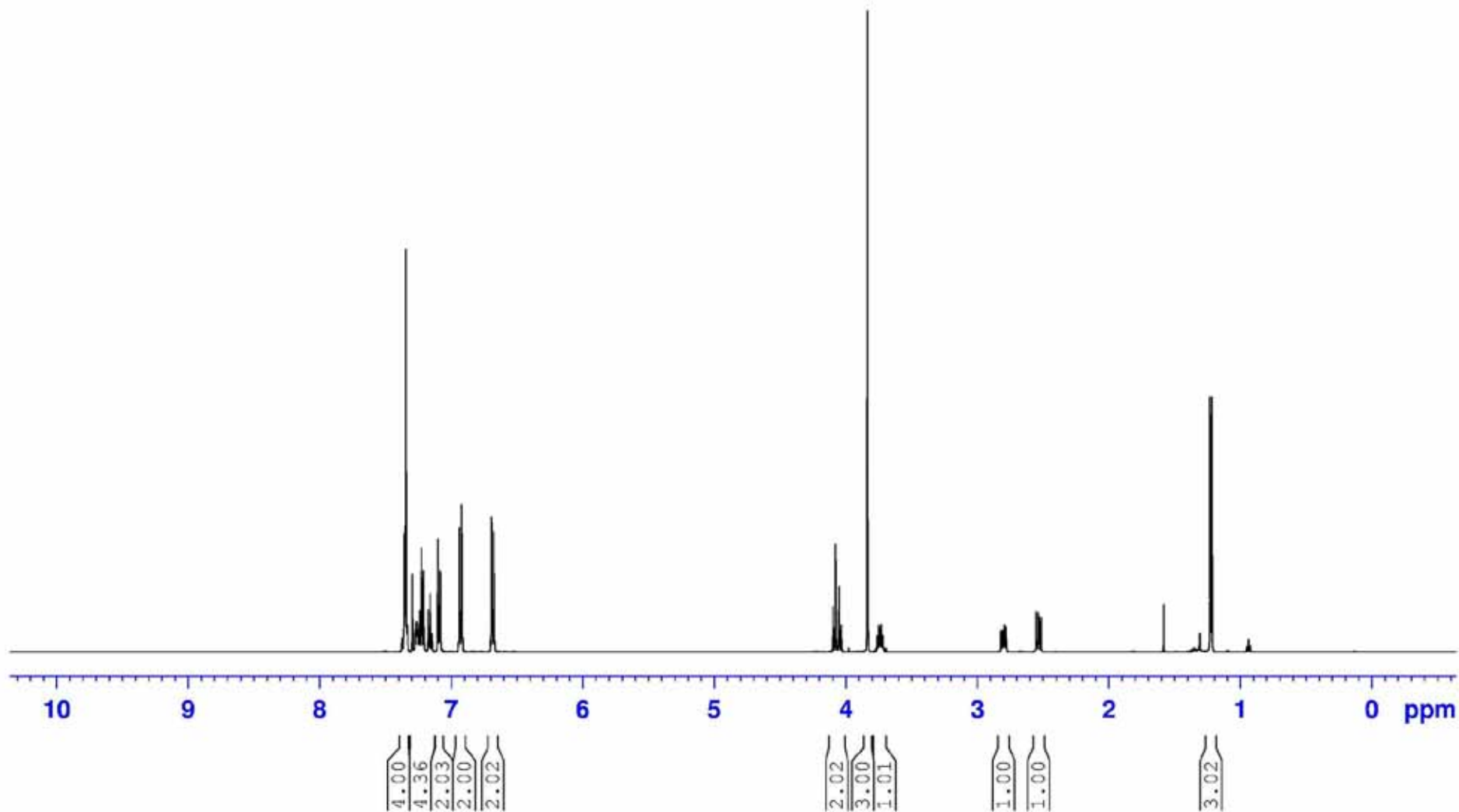
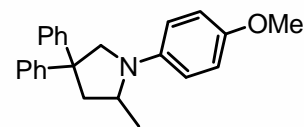
¹H NMR of 1-(4-Fluorophenyl)-2-methyl-4,4-diphenylpyrrolidine. (CDCl₃, 500 MHz, 300 K)



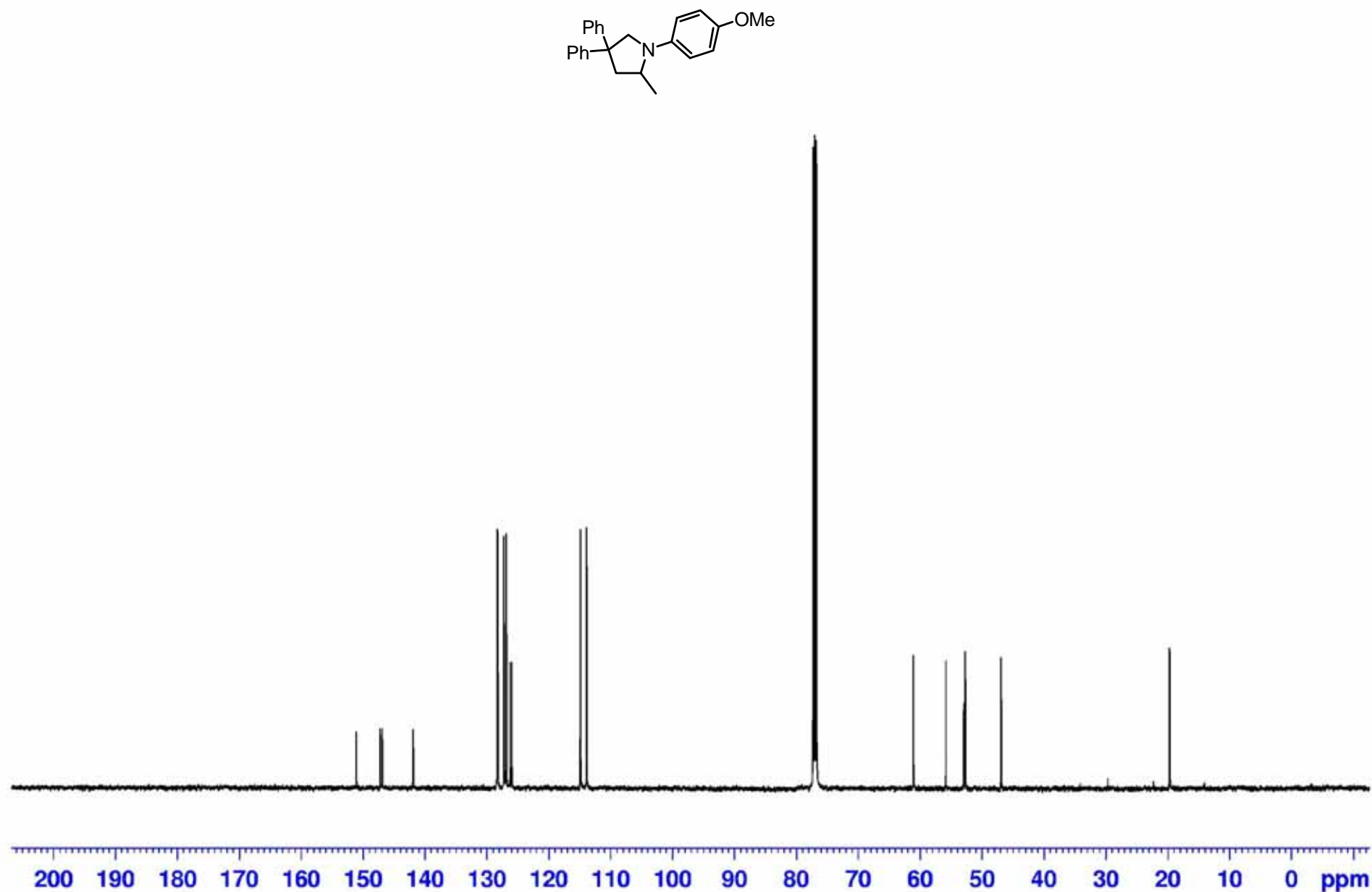
$^{13}\text{C}\{^1\text{H}\}$ NMR of 1-(4-Fluorophenyl)-2-methyl-4,4-diphenylpyrrolidine. (CDCl_3 , 126 MHz, 300 K)



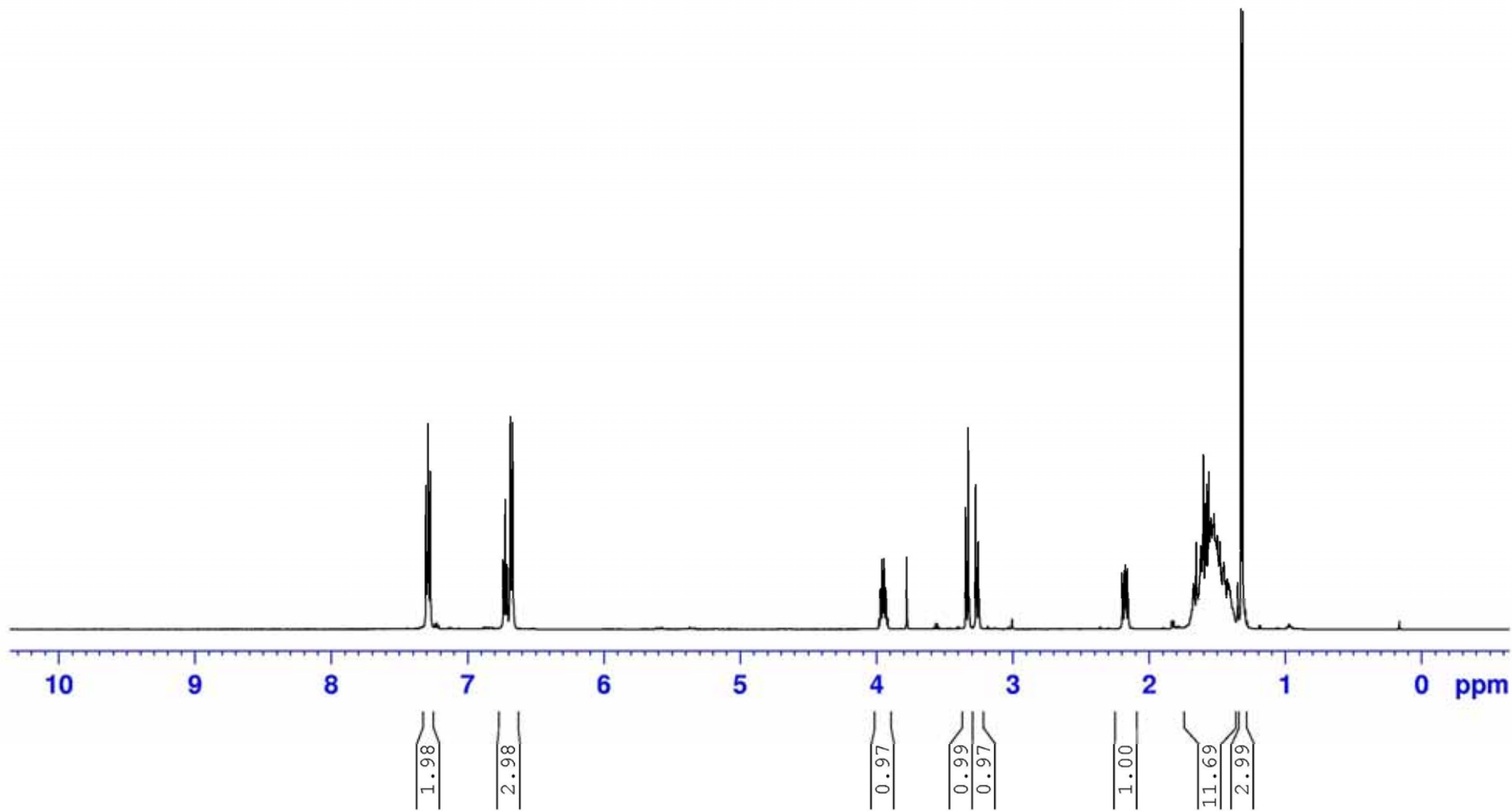
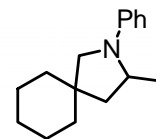
¹H NMR of 1-(4-Methoxyphenyl)-2-methyl-4,4-diphenylpyrrolidine. (CDCl₃, 500 MHz, 300 K)



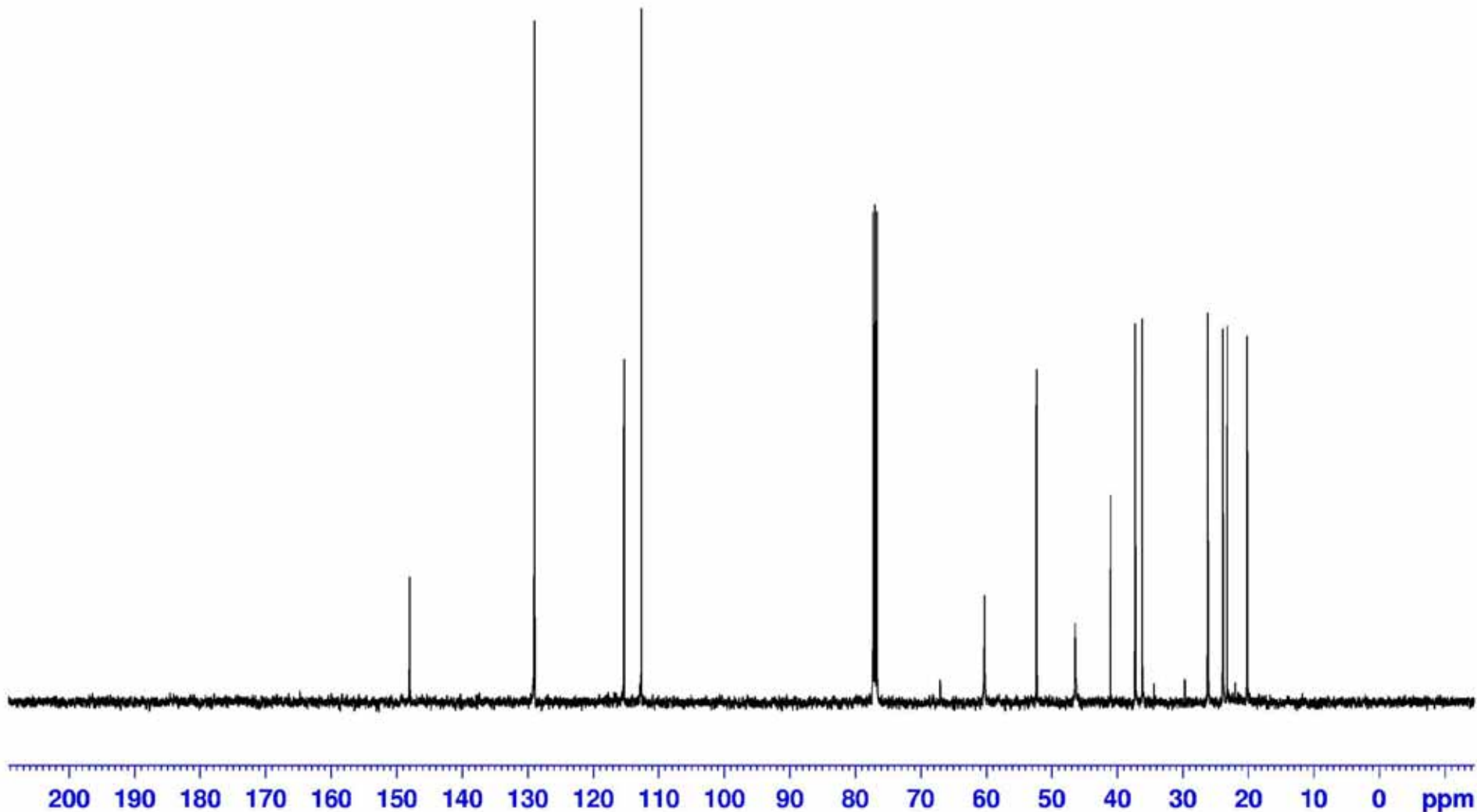
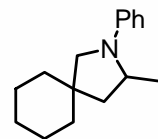
$^{13}\text{C}\{^1\text{H}\}$ NMR of 1-(4-Methoxyphenyl)-2-methyl-4,4-diphenylpyrrolidine. (CDCl_3 , 126 MHz, 300 K)



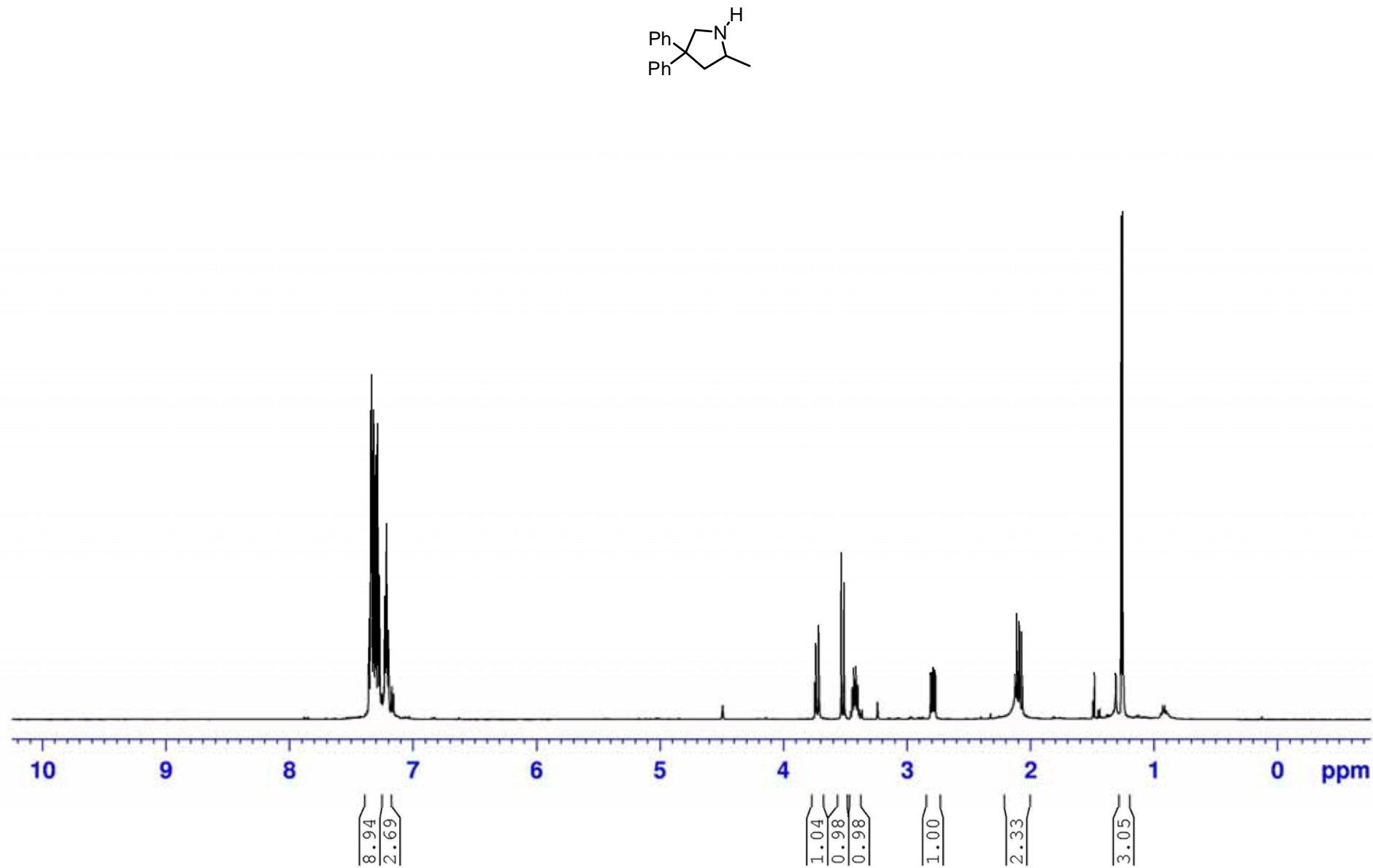
¹H NMR of 2-Phenyl-3-methyl-2-aza-spiro[4,5]decane. (CDCl₃, 500 MHz, 300 K)



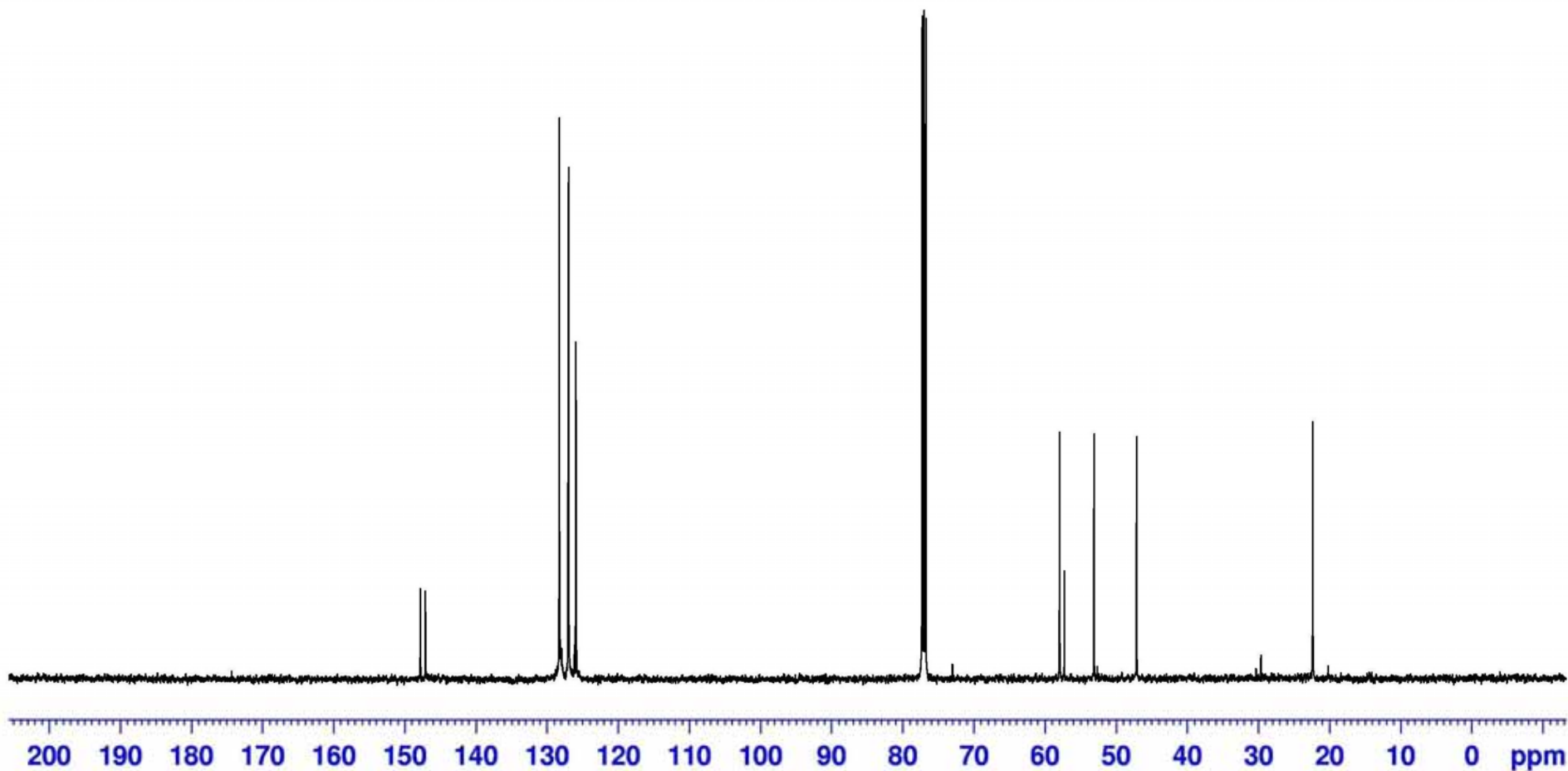
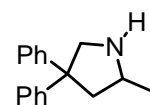
$^{13}\text{C}\{^1\text{H}\}$ NMR of 2-Phenyl-3-methyl-2-aza-spiro[4,5]decane. (CDCl_3 , 126 MHz, 300 K)



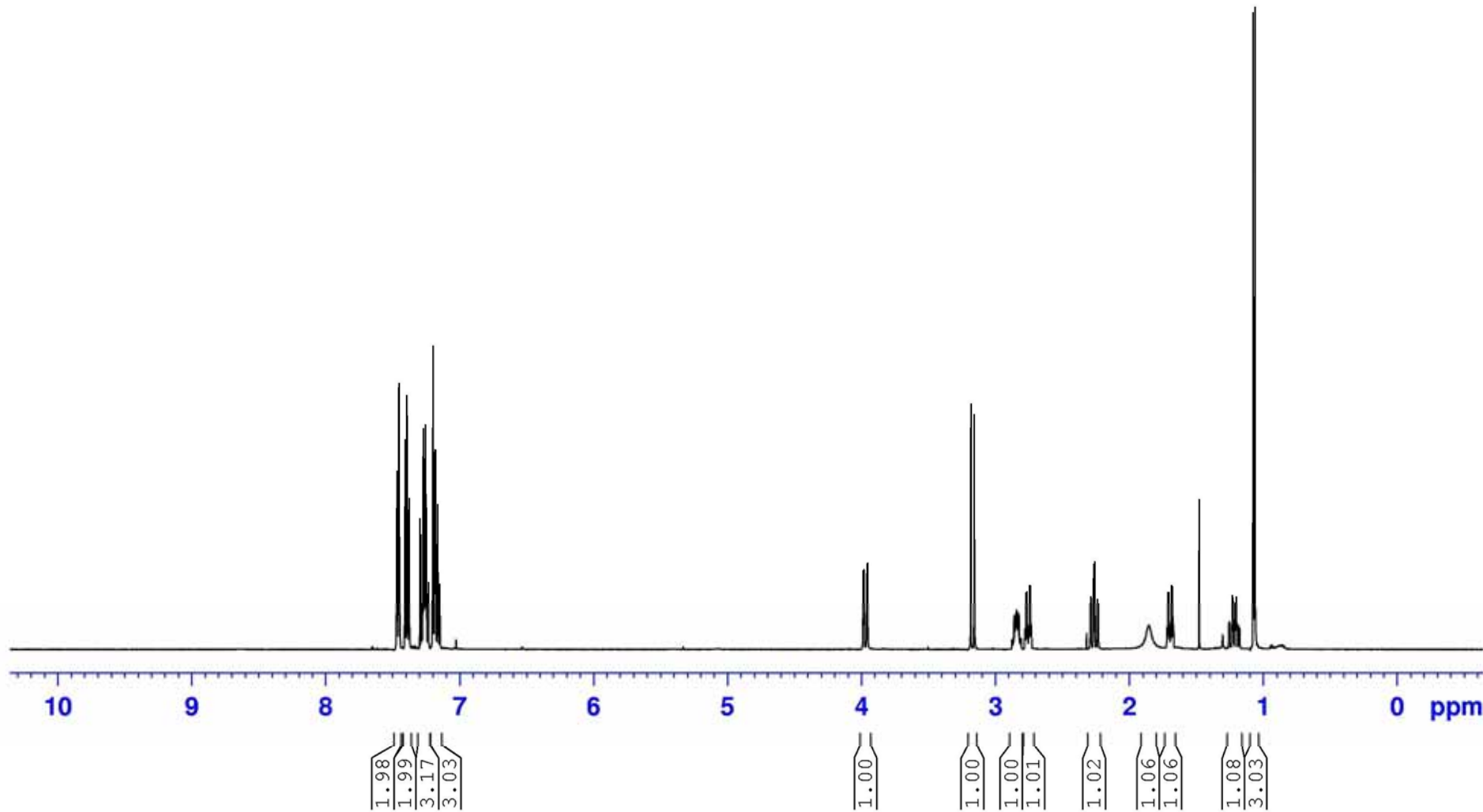
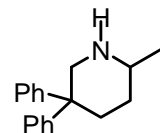
¹H NMR of 2-Methyl-4,4-diphenylpyrrolidine. (CDCl₃, 500 MHz, 300 K)



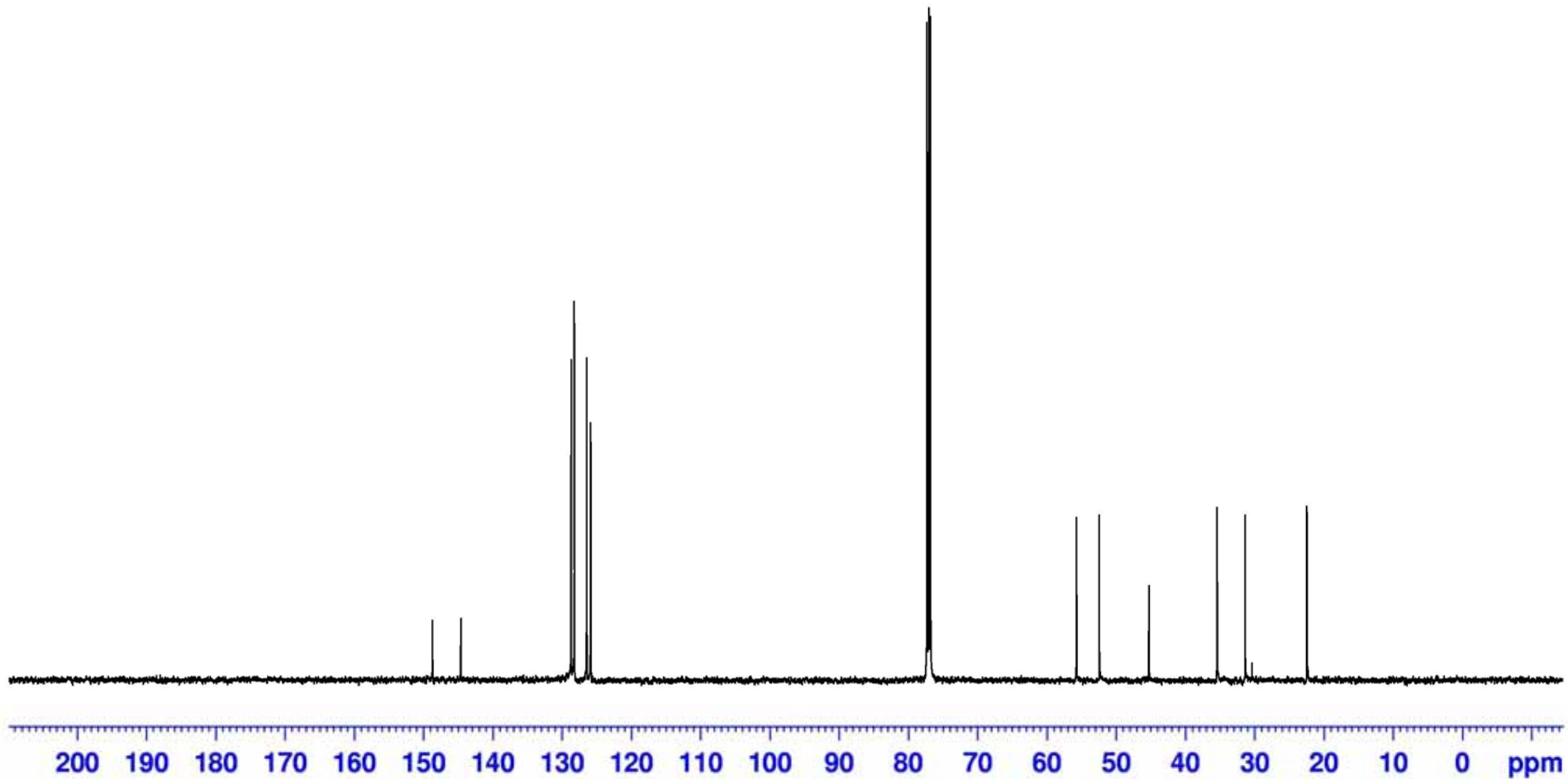
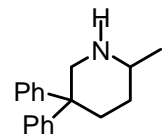
$^{13}\text{C}\{^1\text{H}\}$ NMR of 2-Methyl-4,4-diphenylpyrrolidine. (CDCl_3 , 126 MHz, 300 K)



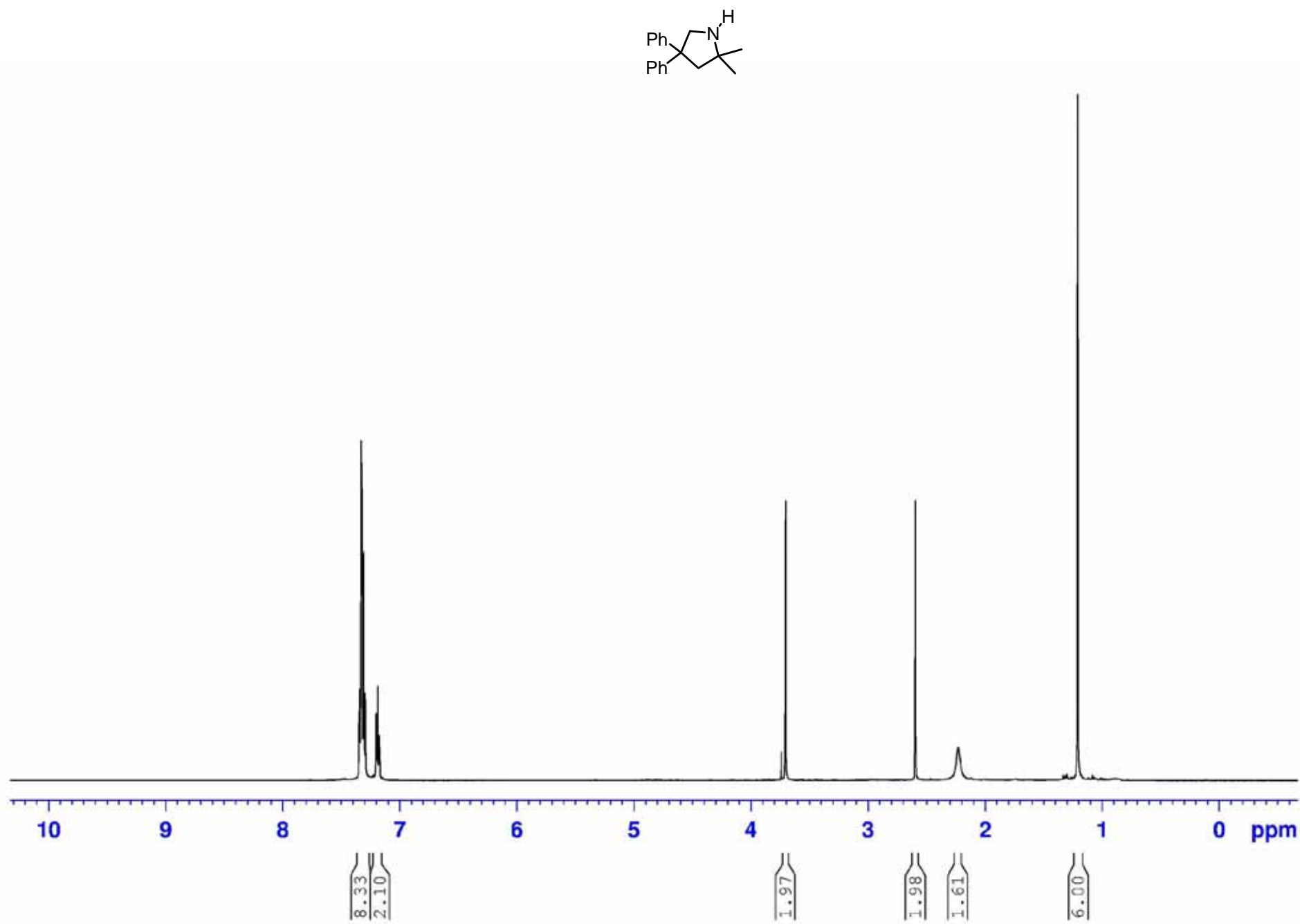
¹H NMR of 2-Methyl-5,5-diphenylpiperidine. (CDCl₃, 500 MHz, 300 K)



$^{13}\text{C}\{\text{H}\}$ NMR of 2-Methyl-5,5-diphenylpiperidine. (CDCl_3 , 126 MHz, 300 K)



¹H NMR of 2,2-Methyl-4,4-diphenylpyrrolidine. (CDCl₃, 500 MHz, 300 K)



$^{13}\text{C}\{\text{H}\}$ NMR of 2,2-Methyl-4,4-diphenylpyrrolidine. (CDCl_3 , 126 MHz, 300 K)

